AD-A205 772

CHARACTERIZATION OF SEMICONDUCTOR
DEVICE PROCESSING ETCHANT SOLUTIONS
FOR GaAs AND p^+ GaAs LAYERS EMPLOYED
IN $Al_xGa_{1-x}As$/GaAs MODFETS AND RELATED
HETEROJUNCTION DEVICES

THESIS

Brett F. Mayhew, BSEE
Captain, USAF

AFIT/GE/ENG/88D-26

DEPARTMENT OF THE AIR FORCE

AIR UNIVERSITY

AIR FORCE INSTITUTE OF TECHNOLOGY

Wright-Patterson Air Force Base, Ohio

89 3 29 021

DTIC
ELECTED
MAR 2 9 1989
S   D
D

CHARACTERIZATION OF SEMICONDUCTOR
DEVICE PROCESSING ETCHANT SOLUTIONS
FOR GaAs AND p^+ GaAs LAYERS EMPLOYED
IN $Al_xGa_{1-x}As$/GaAs MODFETS AND RELATED
HETEROJUNCTION DEVICES

THESIS

Brett F. Mayhew, BSEE
Captain, USAF

AFIT/GE/ENG/88D-26

AFIT/GE/ENG/88D-26

CHARACTERIZATION OF SEMICONDUCTOR DEVICE PROCESSING ETCHANT SOLUTIONS FOR GaAs AND p^+ GaAs LAYERS EMPLOYED IN $Al_xGa_{1-x}As$/GaAs MODFETS AND RELATED HETEROJUNCTION DEVICES

THESIS

Presented to the Faculty of the School of Engineering

of the Air Force Institute of Technology

Air University

In Partial Fulfillment of the

Requirements for the Degree of

Master of Science in Electrical Engineering

Brett F. Mayhew, BSEE

Captain, USAF

30 November 1988

A-1

Table of Contents

Preface

The etch rates of GaAs, $p^{\pm}$ GaAs, $Al_xGa_{1-x}As$ and $n\text{-}Al_xGa_{1-x}As$ were examined with respect to solution composition and pH in an effort to determine a solution that will selectively etch only GaAs from the area between the gate-and-source and gate-and-drain of a $p^{\pm}GaAs/Al_xGa_{1-x}As/GaAs$ Modulation-Doped Field-Effect Transistor. The measurement of the etch rates for GaAs and $Al_xGa_{1-x}As$ was approached from different perspectives. First, a method based upon corrosion testing, that determines etch rates from weight loss, was attempted. A second method involved the use of a Fischione Twin-Jet Electropolisher. Both techniques were verified against a known method of etch depth measurement using a profilometer. A selective etch would also be useful in the last step of the fabrication process of the (ES)MODFET.

I would like to acknowledge several people from the Air Force Avionics Laboratory who provided assistance during this research. Cole Litton, who sponsored the research and provided encouragement and insight, Ed Stutz and Keith Evans, for the MBE-growth on the GaAs substrates, and the help of the staff in the Clean Room Facility (Mr. Larry Callahan for dicing the samples, Lt. Paul Cook for operating the Chemical Vapor Deposition System, and Belinda Johnson for operation of the plasma etching).

I would like to recognize Captain Ron Beyers who contributed his technical knowledge toward the modification of the Fischione Electropolisher. The modifications improved the operation of the equipment and allowed successful

completion of this research. I am also grateful to Scott Apt, from the Air Force Materials Laboratory, for dimpling the GaAs and $Al_xGa_{1-x}As$ samples and providing spare parts for the Fischione Electropolisher.

Special thanks are reserved for Major Donald Kitchen, my thesis advisor, who provided insight and guidance for this project. He helped to keep me focused on the light at the end of the tunnel during the long days spent in the laboratory. I would also like to thank Major Edward Kolesar for the perspective that often exposed the missing piece of information I needed. A word of appreciation goes to Captain Bill Hodges for critical review of my manuscript.

I am deeply indebted to my wife, Anita and daughter, Ashley who provided their love, support and encouragement that allowed me to complete this project. They also endured extended periods of my "absence" from the family.

Finally, I would like to acknowledge Jesus Christ, my Lord and Savior. This project was completed through His will, unfailing grace, mercy, and power. May his name be glorified forever and ever.

Abstract

The purpose of this study was to characterize the etch rate of p^+ GaAs, GaAs, $Al_xGa_{1-x}As$ and $n-Al_xGa_{1-x}As$ in order to find a suitable etchant for the last step of the fabrication process of an (ES)MODFET (i.e., removal of the p^+ GaAs layer between the gate-and-drain and the gate-and-source). The effects of solution composition and pH on the etch rates of GaAs, p^+ GaAs, $n-Al_xGa_{1-x}As$, and $Al_xGa_{1-x}As$ (for $x = 0.30$ and $x = 0.15$) were investigated. Three different techniques were used to measure the etch rates of the material. The first technique used was based upon established procedures for determining the bulk corrosion rates of metals. This technique was applied to etching semiconductor materials. The second method was a variation of a technique used for thinning metals in transmission electron microscopy. It was also applied to etching the semiconductor materials. The third technique, step height measurement with a Sloan Dektak profilometer, was used to verify the results of the first two methods.

The corrosion method of etching yielded etch rates consistent with those reported in the literature. For a solution of $NH_4OH:H_2O_2:H_2O$ (20:7:973 by volume) an average etch rate of 16 Å/sec (or 0.10 μm/min) for a (100) GaAs substrate material was measured. This data compares favorably with the published result of 0.12 μm/min (or 20 Å/sec) for (100) GaAs. The Fischione Electropolisher produced an etch rate of 72 Å/sec for a solution composition of $NH_4OH:H_2O_2$ (1:200 by volume); and an etch rate of 17 Å/sec for the $NH_4OH:H_2O_2:H_2O$ (20:7:973 by volume) etchant. The Dektak profilometer was used to establish etch

rates for the $Al_xGa_{1-x}As$ (x = 0.15 and 0.30). For a solution of $NH_4OH:H_2O_2:H_2O$ (1:1:100 by volume) the etch rate for $Al_{0.15}Ga_{0.85}As$ and $Al_{0.3}Ga_{0.7}As$ was 23 Å/sec and 16 Å/sec, respectively. The etch rate for p^+ GaAs in $NH_4OH:H_2O_2$ (1:100 by volume) was 68 Å/sec, approximately 30 times faster than the etch rate for $Al_{0.3}Ga_{0.7}As$ in $NH_4OH:H_2O_2$ (1:100 by volume). This etchant displays the desirable characteristics that are required in the final fabrication step of an (ES)MODFET.

List of Tables

CHARACTERIZATION OF SEMICONDUCTOR DEVICE PROCESSING ETCHANT SOLUTIONS FOR GaAs AND p^+ GaAs LAYERS EMPLOYED IN $Al_xGa_{1-x}As$/GaAs MODFETS AND RELATED HETEROJUNCTION DEVICES

I. Introduction

Background

It has been forecast that faster computers with more computational power will be needed in future Air Force fighter aircraft to aid the pilot in assimilating all the necessary data to make a split second decision during combat. The technological advances in the semiconductor industry have enhanced the speed of computers at an exponential rate (16:8). The speed of digital computers rests upon the ability of logic circuits to change states quickly. Typically, transistors are used as switching devices that propagate logic states through a computer. To increase the speed of a computer, the movement of charge through the transistor must be as quick as possible. The propagation delay, τ_d, or time needed to transition between off- and on-states, and the power dissipated, P_d, during the switching of the transistors are conventional figures of merit in digital circuits that comprise computers (6:774).

1

The speed of a computer system can be increased if the time the transistor needs to charge and discharge the capacitances of the interconnected logic gates is minimized. The higher the current capacity, and the shorter the transit time of charge carriers through the device, the faster the capacitances can be charged and discharged (6:776). Silicon metal-oxide field-effect transistors (MOSFETS) display carrier saturation velocities on the order of 0.8-1.0 x 10^7 cm/s (44:1017). This limit is attributable to the fundamental electron mobility in silicon, which is 1500 cm^2/V-s (47:851). A material with superior transport properties is undoped GaAs. It possesses a higher electron mobility, 8500 cm^2/V-s (47:851), and a higher peak drift velocity, 2.0 x 10^7 cm/s (6:808). These characteristics translate into short transit times in metal-semiconductor field-effect transistors (MESFETS) that are on the order of 50 ps (6:776; 44:1020). When dopants are added to GaAs to enhance its current carrying capacity, the drift velocity decreases because of the large population of impurity scattering centers. Impurity scattering results from the interaction of the ionized donors and the charge carriers (6:776; 44:1017). To minimize the detrimental side effects of slower propagation times relative to the advantage of increased current capacity in GaAs, heterostructures have been investigated (32:28).

Heterostructures or heterojunctions are composed of "two dissimilar semiconductor materials" (48:144) which have the same crystal structure, but different bandgap energies. Molecular beam epitaxy (MBE) facilitates the growth of these dissimilar semiconductor materials on an atomic scale. The difference in

the bandgap energies causes a discontinuity in the conduction band edges at the heterojunction interface (44:1016; 6:777). Figure 1 shows a multiple $Al_xGa_{1-x}As$/GaAs heterojunction and the corresponding conduction band energy
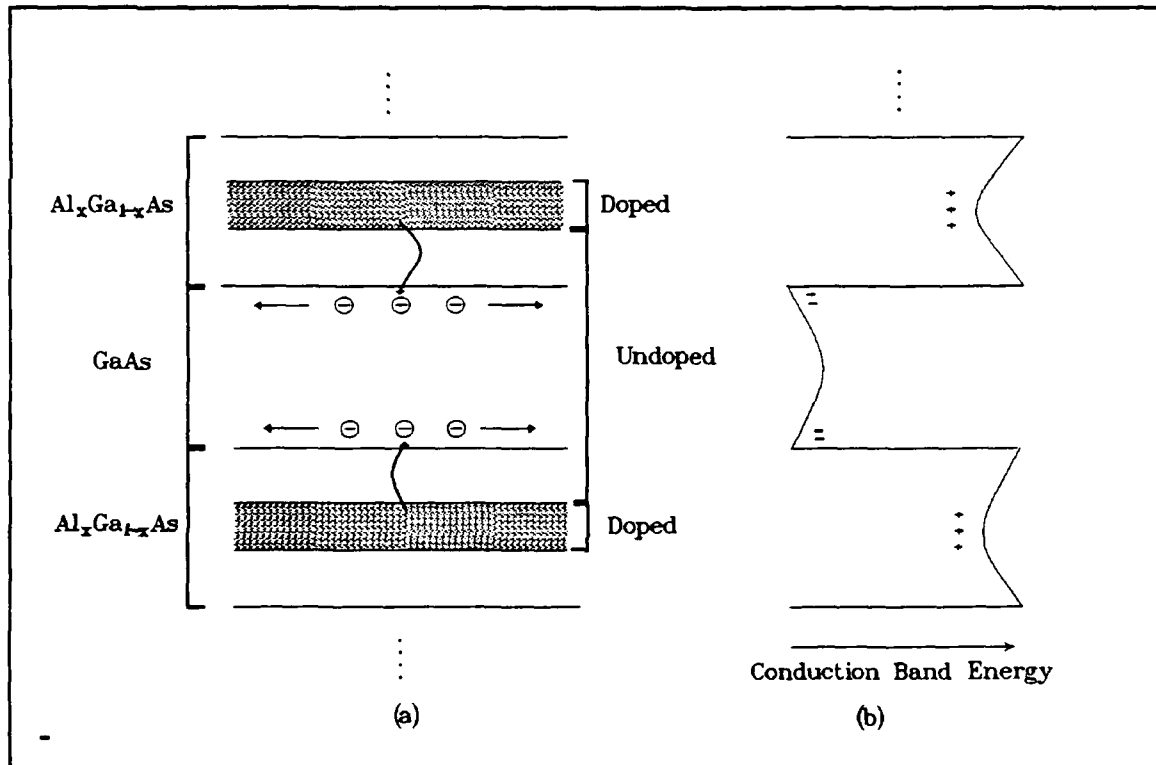
Figure 1. (a) Multiple $Al_xGa_{1-x}As$/GaAs Heterojunction With the Center Region of the $Al_xGa_{1-x}As$ Doped and (b) the Corresponding Energy Bandgap Diagram (44:1016).

diagram. To attain equilibrium, the electrons in the doped $Al_xGa_{1-x}As$ semiconductor diffuse to the smaller energy bandgap GaAs material, where they are confined by the energy barrier (44:1017). Heterojunctions permit an increased carrier concentration in GaAs, without the detrimental effects of impurity scattering

resulting from high donor concentrations (44:1017; 6:776). The operation of the heterojunction will be discussed in Chapter II.

The Modulation-Doped Field-Effect Transistor (MODFET)

The Modulation-Doped Field-Effect Transistor (MODFET) is a device that utilizes heterostructures (or modulation doping) to achieve superior propagation delay times. Possessing a 10 ps propagation delay time, it qualifies as "the fastest logic switching device" (44:1015). The fast switching times of the MODFET also imparts its advantages into microwave applications. The MODFET possesses a small noise figure (NF) and high transconductance (g_m) at microwave frequencies (6:790). Figure 2 depicts the noise figure vs gate length for a MODFET and a GaAs MESFET. Researchers have fabricated MODFET devices with transconductances as large as 310 millisiemens/millimeter of gate (mS/mm) at 300°K (33:434) and 400 mS/mm at 77°K. The best GaAs MESFETs operate with transconductances of 230 mS/mm (44:1024). An operating frequency of 230 GHz has been reported for a modulation-doped field-effect transistor (MODFET), the highest ever, for a transistor (46:107). The MODFET is a member of the field-effect transistor (FET) family, and thus, consists of a source, a drain, and a gate contact. Similar to other FETs, the gate controls the flow of charge carriers between the source and drain. A typical $Al_xGa_{1-x}As$/GaAs MODFET structure (with appropriate dimensions) resulting from a molecular beam epitaxy fabrication process is shown in Figure 3.

The initial MODFET devices have displayed outstanding speed and low power consumption, which are ideal characteristics for the next generation of

4
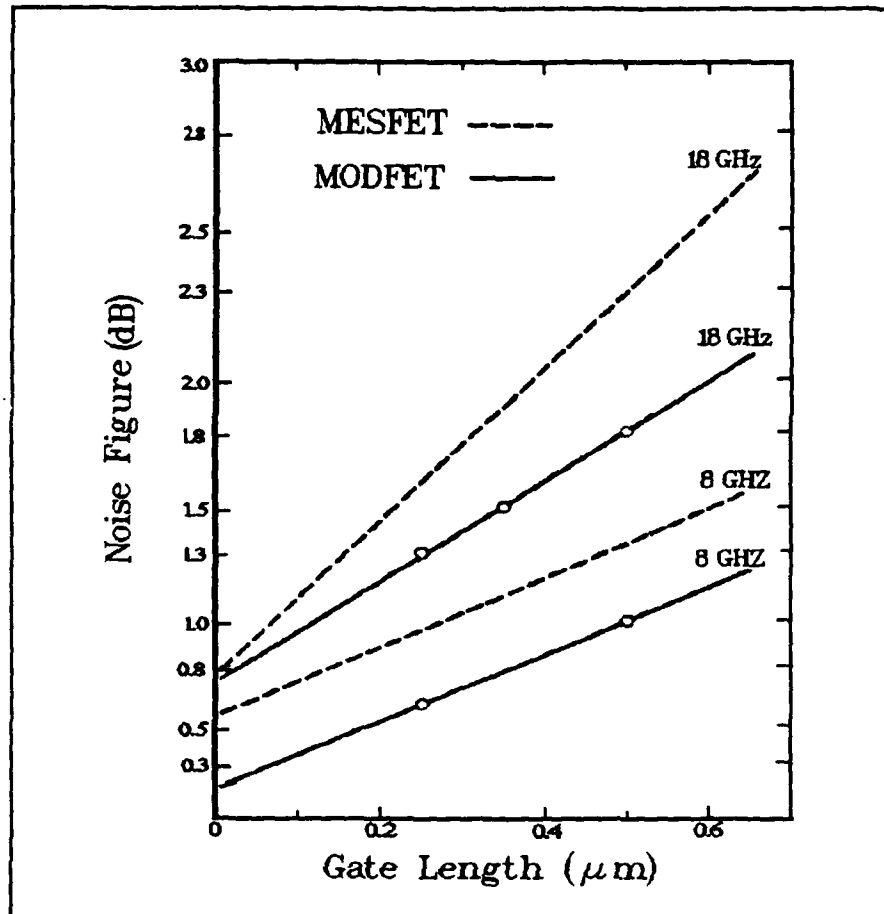
Figure 2.   Noise Figure vs Gate Length for the MODFET and
             GaAs MESFET (6:777).
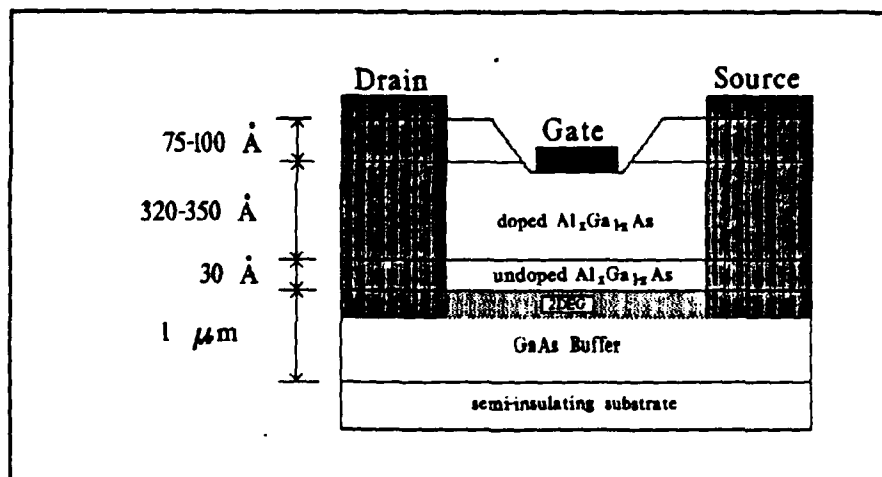
Figure 3. Typical MODFET (cross-sectional view) with
           Heterostructure Dimensions (3:1399).

5

computers. They are however, not without their limitations. The maximum allowable gate voltage is only 0.8 volts. The resulting noise margin is not adequate in high-noise environments with this small gate bias. Moreover, small voltage spikes, if not properly filtered, could prematurely switch the device. The small applied gate voltage also limits its use as a power amplifier (44:1017). This limitation is a result of the low breakdown voltage of the Schottky-barrier gate (44:1020). The usual advantages of cooling devices to decrease the propagation delay times has not been consistently applied to the initial MODFET devices because of peculiar drain I-V relationships at cryogenic temperatures. "In particular, when the device is cooled to 77°K without exposure to light, the drain I-V characteristics become distorted (i.e., they collapse) ..." (11:1028). A related problem also observed at cryogenic temperatures is referred to as persistent photoconductivity (PPC) (7:1238; 4:644). At temperatures below 100°K, the electron concentration in the $Al_xGa_{1-x}As$ layer increases upon exposure to light. The additional charge produced may persist for several days after the illumination source is removed (4:645). The effect is more pronounced at higher mole fractions (x) of Al in $Al_xGa_{1-x}As$ (4:645).

The shortcomings of the initial MODFET designs led researchers to investigate ways to improve the device's performance. Studies have focused on the maximum allowable gate voltage which yields larger noise margins in digital circuits and improved microwave amplifier performance. These investigations have shown that one method of raising the allowable gate voltage is to increase the mole fraction of Al in $Al_xGa_{1-x}As$ (44:1020). However, if the mole fraction of Al reaches a value

6

of approximately 0.36, the semiconductor changes from a direct bandgap material to an indirect bandgap structure. The corresponding change in the effective mass of the carriers reduces the mobility of the electrons (7:1239). In order to avoid the adverse effects of increasing the Al concentration, an extra layer is added to the MODFET heterostructure. This device is known as the enhanced Schottky-barrier (ES)MODFET (30:10; 38:5).

The Enhanced Schottky-Barrier MODFET [(ES)MODFET]

The distinguishing feature of an (ES)MODFET is a thin (≈ 100 Å) layer of beryllium-doped GaAs grown on the doped $Al_xGa_{1-x}As$ (or n^+ GaAs) layer before the Schottky-barrier gate is deposited (30:12; 38:5). The maximum allowable applied gate voltage increases from 0.8 volts to 1.6 volts when the p^+ GaAs layer is present (37:ii). The (ES)MODFET utilizes the same properties of the heterojunction for fast propagation delay times, lower power dissipation and high transconductances. An (ES)MODFET structure with appropriate dimensions resulting from a MBE fabrication process is shown in Figure 4. The problem with low gate voltages is corrected with a device fabricated in this manner. However, several problems exist with fabricating this device. If the unwanted p^+ layer is not removed between the source-and-gate and drain-and-gate regions, a parasitic metal-semiconductor field-effect transistor (MESFET) is formed. The parasitic MESFET establishes an alternative conduction path for electrons from the source to the drain and compromises the maximum operating efficiency of the (ES)MODFET. Also, if a portion of the doped $Al_xGa_{1-x}As$ layer is removed, it will affect the maximum
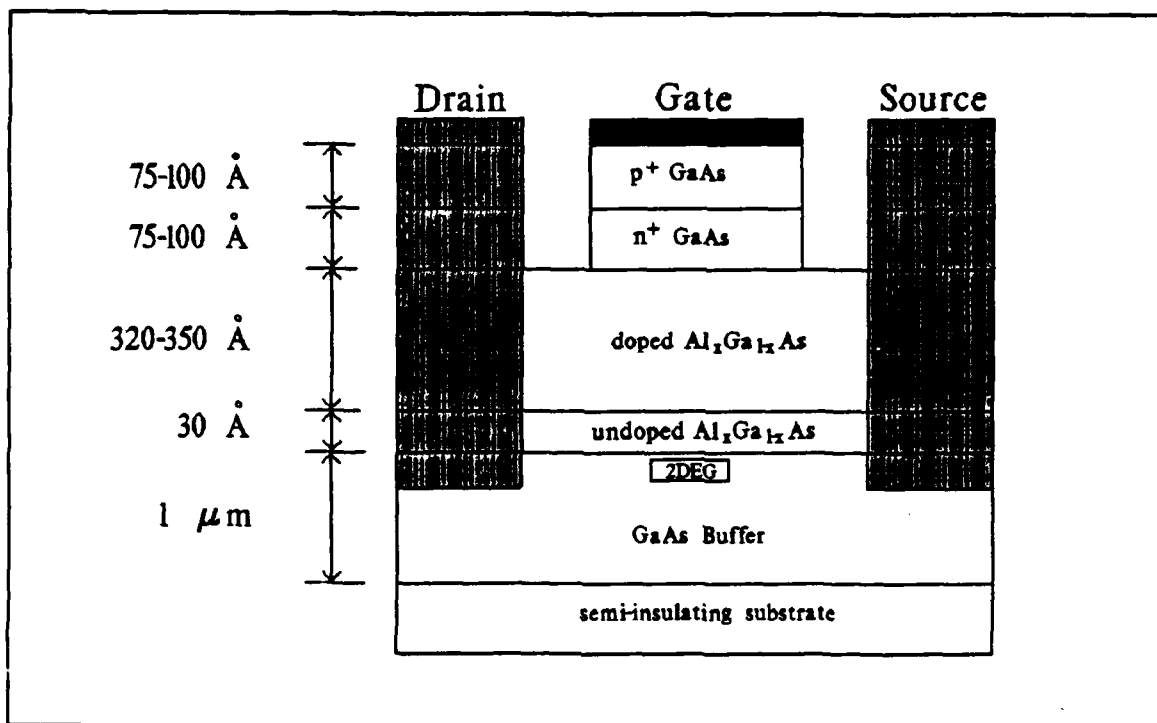
Figure 4. Typical (ES)MODFET (cross-sectional view) with Heterostructure Dimensions (33:434).

transconductance $(g_m)_{max}$ (6:783) and the maximum operating frequency, f_{max}, of the device (3:1400; 6:788).

Problem Statement

In order to realize higher operating frequencies and higher maximum applied gate voltages, investigations have'led to the addition of a p^+ GaAs layer beneath the gate region of a MODFET. However, a problem encountered with this technique occurs during the fabrication of the device.

Both McLaughlin, and Lott fabricated (ES)MODFETs in previous studies (29; 30). While both realized working devices, there was some question

regarding the effectiveness of the etchant used to remove the unwanted p^+ layer. The etchant employed by Lott to remove the p^+ layer of the (ES)MODFETs was a solution composed of ammonium hydroxide, hydrogen peroxide and deionized water ($NH_4OH:H_2O_2:DIW$) with a volume ratio of 3:1:150 (29). An etch rate of 30 Å/sec was assumed, but not verified (29).

To fabricate the (ES)MODFET with consistent and reproducible operating characteristics, the removal of the p^+ layer must be precisely controlled. In order to determine the best method of etching the p^+ layer without adversely affecting the $Al_xGa_{1-x}As$ layer, a detailed investigation of the etching properties of $Al_xGa_{1-x}As$ was conducted. In addition, since silicon doped $Al_xGa_{1-x}As$, beryllium doped GaAs and GaAs are affected during the etching procedure, the etching properties of these materials were also studied.

Scope

The primary focus of this study was to etch GaAs, p^+ GaAs, $Al_xGa_{1-x}As$ and silicon-doped $Al_xGa_{1-x}As$, and $Al_xGa_{1-x}As$. The effects of solution concentration and pH on the etch rates of these materials (GaAs, p^+ GaAs, n-$Al_xGa_{1-x}As$, and $Al_xGa_{1-x}As$ (for $x = 0.30$ and $x = 0.15$)) was investigated. One technique used to determine the etch rates was based upon established procedures utilized to characterize the bulk corrosion rates of metals. This technique was applied to the etching semiconductor materials. Also, a variation of the technique used by Schoone

9

and Fischione (40:1351) for thinning metals for transmission electron microscopy examination was applied to etching the semiconductor materials.

Neither the formulation of chemical reaction equations, nor the kinetics (rate equations) of the chemical reactions were investigated. These concepts are beyond the scope of this study. However, appropriate chemical equations, when available, are presented. Examination of the effects of doping concentration (silicon in $Al_xGa_{1-x}As$ or beryllium in GaAs) on the etch rates was not investigated.

Assumptions

It is assumed that the bulk corrosion testing procedures are applicable to etching semiconductor materials. A linear etch rate was assumed for all etch methods. For the corrosion method, it was assumed that the silicon nitride cap was resistant to the etchants under investigation. It was also assumed that the MBE grown heterostructures provided by the Air Force Avionics Laboratory were defect free and grown to the specified thickness.

Major Results

Fontana's method of bulk corrosion testing produced etch rates for GaAs that agree with the results published in the literature. For Gannon's solution of $NH_4OH:H_2O_2:H_2O$ (20:7:973 by volume), an average etch rate of 16 Å/sec (or 0.10 μm/min) for an undoped (100) GaAs substrate material was found. This data compares favorable with Gannon's published result of 0.12 μm/min (or 20 Å/sec) for p-doped (100) GaAs. Problems with the lifting of the SiN mask prevented extremely

accurate measurements of etch rates using the bulk corrosion method. However, the Fischione Electropolisher provided more accurate etch rates for GaAs. Using the Fischione Electropolisher, the etch rate for an undoped (100) GaAs substrate material was measured and found to be 0.10 μm/min (or 17 Å/sec), an etch rate previously reported. Attempts to measure the etch rate for n-$Al_xGa_{1-x}As$ were not accomplished. The Fischione Electropolisher test methodology did not work as expected with the $Al_xGa_{1-x}As$ epitaxial layers grown on GaAs. Measurements using a Dektak profilometer further confirmed the validity of the bulk corrosion and Fischione Electropolisher methods.

Results also showed that reducing the etchant solution pH, with the addition of H_2SO_4, reduced the etch rate. The etchant composition of $NH_4OH:H_2O_2:H_2O$ (3:1:150 by volume), which was pH adjusted to 7.3, resulted in an etch rate of 0.8 Å/sec for p^+ GaAs, 0.07 Å/sec for $Al_{0.15}Ga_{0.85}As$ and virtually zero for $Al_{0.3}Ga_{0.7}As$. For a nominal pH of 10.8, the etch rates for p^+ GaAs, $Al_{0.15}Ga_{0.85}As$ and $Al_{0.3}Ga_{0.7}As$ were 24, 15 and 18 Å/sec, respectively. The selectivity is defined as the ratio of the GaAs etch rate to $Al_{0.3}Ga_{0.7}As$ etch rate. The etchant that displayed the highest selectivity was the $NH_4OH:H_2O_2$ (1:100 by volume) solution. The etch rate for p^+ GaAs was 68 Å/sec, and the etch rate for $Al_{0.3}Ga_{0.7}As$ was 2 Å/sec, resulting in selectivity of 34. This etchant displays the desired characteristics required for the final fabrication step of an (ES)MODFET.

Plan of Development

Chapter II describes the structure and operation of the MODFET and (ES)MODFET. The fabrication procedures and associated problems realizing the (ES)MODFET are discussed. A brief description of wet chemical etching and its application to the (ES)MODFET fabrication procedures are introduced. Chapter III discusses the special equipment required, and the experimental procedures used to accomplish the study. The results of the experiments are compared to the literature and analyzed in Chapter IV. Chapter V contains the major results of the study along with appropriate conclusions and recommendations for further study.

II. Background

This Chapter reviews the literature and discusses the operation and fabrication of the MODFET and (ES)MODFET with a focus concerning the wet chemical etching process. The physical structure, operation and performance limitations of the MODFET will be presented. To correct the limitation imposed by the small gate voltage swings, a p^+ GaAs layer is added to the device structure. This change does not affect the basic transistor action of the device, but it does lead to fabrication difficulties for the (ES)MODFET. The removal of the p^+ GaAs layer with wet chemical etching techniques represents an opportunity for correcting this fabrication problem. This Chapter also discusses the status of etching $GaAs/Al_xGa_{1-x}As$ epitaxial layers.

Modulation-Doped Field-Effect Transistors

The pursuit of faster devices with shorter propagation times has forced device designers to examine different structures and materials. From the first junction field-effect transistor (JFET) designed by Shockley in 1952 (42:1524), to the latest advance, the modulation-doped field-effect transistor (MODFET), the field-effect transistor (FET) family has advanced the interest in producing faster integrated circuits (IC's). The MODFET has demonstrated a propagation delay time of 10 picoseconds (ps), making it "the fastest logic switching device" (44:1015). The MODFET, also known as the high electron mobility transistor (HEMT), a two-dimensional electron gas FET (TEGFET) or selectively doped heterojunction

13

transistor (SDHT) (44:1015), also can be used for low noise microwave frequency amplifiers (33:434). The first functional MODFET reported in the open literature was fabricated in 1980 by Fujitsu Ltd. (6:775). That same year, a device with "reasonable microwave characteristics" (44:1015) was produced at the University of Illinois. Because the processing technology of a MODFET is similar to a GaAs MESFET, development of the device proceeded rapidly (6:775). By 1983, MODFET logic devices displayed delay times of 12.2 ps with a power delay product of 13.7 femto-joules (fJ) at 300°K when configured in a ring oscillator circuit (6:775). In addition, microwave MODFET devices have demonstrated transconductances as large as 500 mS/mm at 77°K (350 mS/mm at 300°K) for a 0.5 μm gate length that same year (6:775; 26:29). By comparison, the GaAs MESFET displays a transconductance of 230 mS/mm, and the MOSFET 80 mS/mm, both at room temperature (32:28). The MODFET can also exhibit low noise figures. In 1984, Ohata (33:434) built a 0.5 μm gate length MODFET that operated at 12 GHz with a gain of 11.7 dB and a noise figure of 1.2 dB. Typical GaAs MESFETs have gain and noise figures of 5.6 watts and 7 dB at 6 GHz, respectively (43). An operating frequency of 230 GHz has been documented, the highest ever for a three terminal transistor (46:139).

Research on this innovative device has led to investigating various structures of the basic MODFET to optimize the maximum applied gate voltage swing and noise figures at high frequencies. The primary thrust has been to change the materials employed in the device (29; 30). Before considering these changes, the initial structure and operation of the device is described.

14

Structure of the MODFET

Molecular beam epitaxy (MBE) is used to grow the field-effect transistor heterostructures (44:1018). The MBE process uses ultra-low pressures ($\sim 10^{-10}$ Torr) to precisely control the thickness and chemical composition of the epitaxial layers (48:333). A semi-insulating GaAs wafer is used as the substrate for the epitaxial layers of the MODFET. The first layer to be grown is an undoped GaAs buffer layer, usually 1 μm thick. This buffer layer provides a near defect-free, high quality surface for the growth of the subsequent epitaxial layers (29). A heterojunction is formed next by growing an undoped layer of $Al_xGa_{1-x}As$ deposited on the GaAs buffer layer. A heterojunction is produced from "two dissimilar semiconductors" (48:144) with the same crystal structure but different bandgap energies. The $Al_xGa_{1-x}As$ is typically 20 - 60 Å thick (44:1018). Next, an n-type, silicon-doped $Al_xGa_{1-x}As$ layer is grown on the heterojunction. This layer is nominally about 600 Å thick (44:1018). The final layer is a n^+ GaAs cap layer which is used to form the devices's ohmic contacts (33:434). The final MBE structure with the nominal material thicknesses is shown in Figure 5.

MODFET Device Operation

The basic operation of the MODFET is similar to a Si/SiO_2 metal-oxide-semiconductor field-effect transistor (MOSFET) (44:1021; 6:779). The gate voltage controls the concentration of electrons in the channel (or two-dimensional electron gas (2DEG)) in the same manner as it controls the concentration of carriers in the channel of a MOSFET (44:1021, 32:30). The channel for the MODFET is formed

n+ GaAs	75-100 Å
doped Al$_x$Ga$_{1-x}$As	320-350 Å
undoped Al$_x$Ga$_{1-x}$As	30 Å
GaAs Buffer	1 μm
semi-insulating substrate	
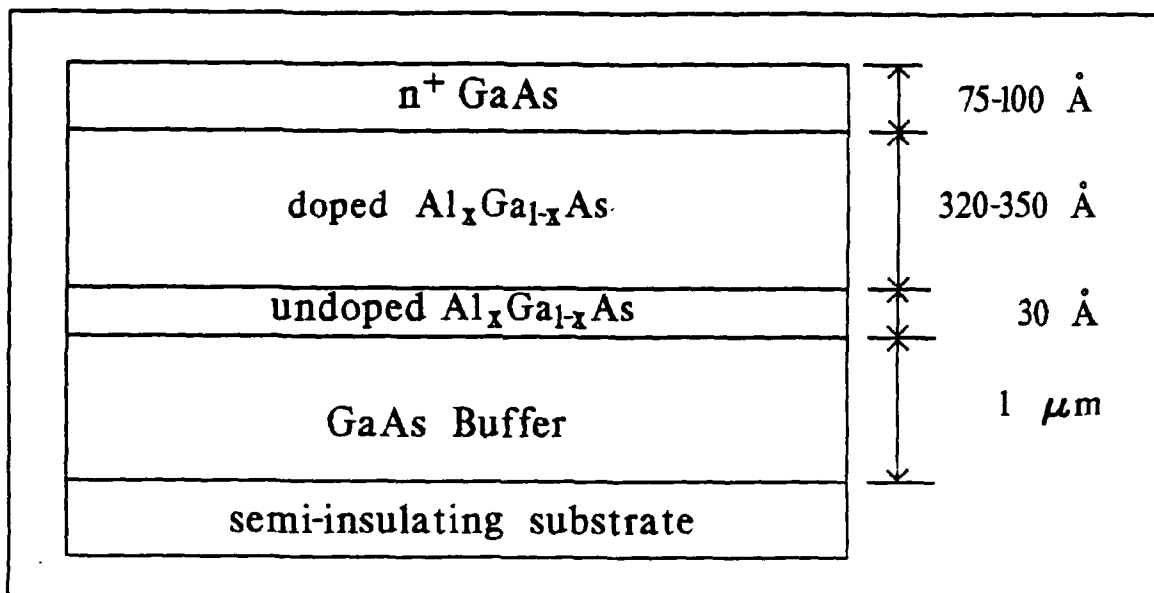
Figure 5.   Molecular Beam Epitaxially Grown Heterostructure with Typical Dimensions Used to Realize the MODFET (44:1015).

in the undoped GaAs buffer layer of the heterostructure. In an undoped GaAs layer, electrons demonstrate higher mobilities and drift velocities when compared to doped GaAs layers (6:778; 44:1020). The undoped GaAs buffer layer is part of the heterojunction. The discontinuity in the conduction band at the heterointerface is caused by the difference in the bandgap energies of the GaAs and Al$_x$Ga$_{1-x}$As materials. A triangular-shaped well (or quantum well) develops as the result of the band discontinuity and the electric field formed between the ionized donors (positive charge) and the 2DEG (negative charge). The generated field at right angles to the heterojunction interface causes "severe band bending particularly in GaAs" (44:1018). Figure 6 shows the conduction band discontinuity in a typical MODFET. The energy bandgap difference of the heterojunction discontinuity (ΔE) must be greater

16
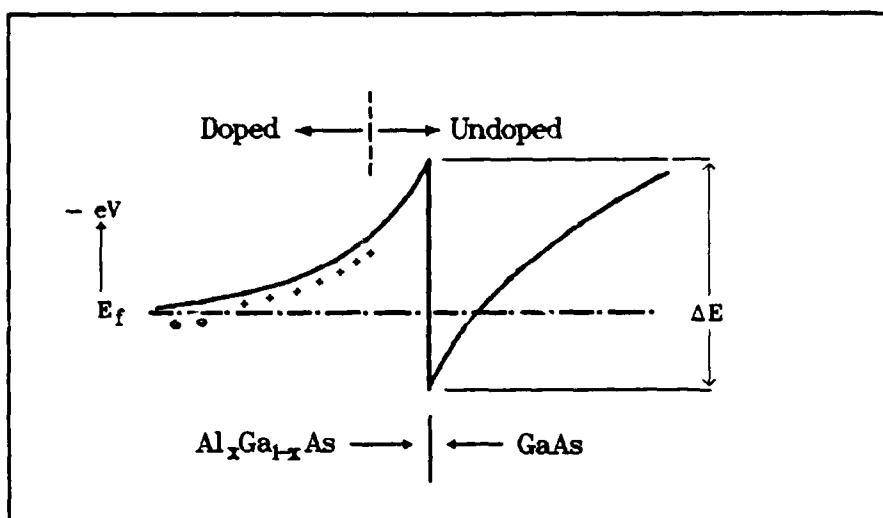
Figure 6. Conduction Band Discontinuities of a Heterojunction (44:1015).

than 0.3 eV to adequately contain the electrons (32:30; 44:1019). Free electrons introduced by doping the $Al_xGa_{1-x}As$ material diffuse into the GaAs buffer layer and form the two-dimensional electron gas (2DEG) just below (to the right in Figure 6) the AlGaAs/GaAs interface. The conduction band discontinuity at the heterointerface causes the diffused electrons to remain in the quantum well. Once trapped in the quantum well, the electrons normally will not overcome the energy barrier (ΔE) formed at the $Al_xGa_{1-x}As$/GaAs heterojunction and will remain in the GaAs buffer layer or channel (6:775; 44:1019). This behavior is equivalent to the case of a "electrons confined to the oxide interface in a SiO_2/Si MOS capacitor biased into inversion" (6:776). The 2DEG formed is about 80 Å thick (44:1019; 6:776). If the n-doped $Al_xGa_{1-x}As$ extends to the $Al_xGa_{1-x}As$/GaAs interface, the ionized donors (positively charged) in the $Al_xGa_{1-x}As$ material interact

17

with the 2DEG (negatively charged) in the GaAs buffer layer according to Coulomb's Law. This "Coulombic scattering" (44:1019) does not allow the electrons in the 2DEG to achieve their maximum mobility or saturation velocity. A thin undoped $Al_xGa_{1-x}As$ layer provides a partition between the 2DEG and the ionized donors, reducing the effects of the Coulombic attraction (44:1020). This setback-layer reduces impurity scattering and allows higher electron mobilities and saturation velocities (32:29). The large transit velocity through the device is a "critical parameter" (5:1164) in determining the maximum frequency of operation.

The excitement over the speed and power dissipation advantages of the MODFET are not without some shortcomings. Even though projections for the MODFET have shown chip and system propagation delays to be at least twice that for GaAs MESFETs, the peculiar I-V relationships, and in particular, the small applied gate voltage limitation, must be resolved (32:33).

MODFET Limitations

A concern regarding the ability of a MODFET to handle large gate voltages has prompted further study of this device. The limitation of a small applied gate voltage is a result of the low breakdown voltage of the Schottky-barrier gate (44:1020), and the fact that "too high a voltage on the gate will cause current leakage at the gate and allow conduction" (32:33) in the doped $Al_xGa_{1-x}As$ material. To increase the voltage handling capabilities of the MODFET gate, different structures have been proposed and evaluated. The first approach attempted to increase the mole fraction of Al (x) in the $Al_xGa_{1-x}As$ layer. An increased mole

fraction of Al increases the energy bandgap of the $Al_xGa_{1-x}As$ material (29). As a result, the larger energy bandgap increases the Schottky-barrier height of the gate (38). The larger energy bandgap, in turn, permits higher applied gate voltages (44:1022). However, a disadvantage of this approach is that the mole fraction of Al cannot be increased without bound. If the concentration of Al gets to large, the semiconductor changes from a direct bandgap to an indirect bandgap structure ($x \approx 36$ at the transition). Changing to an indirect bandgap structure increases the effective mass of the electrons, thereby reducing their mobility (7:1238). Another disadvantage of a large Al concentration is referred to as persistent photoconductivity (PPC) (7:1238; 4:644). PPC appears when the material is exposed to light at temperatures below 100°K. The electron concentration increases upon exposure to light, and persists for several days after the light is removed (4:645). This effect is attributed to deep trap states in the $Al_xGa_{1-x}As$ (11:1029). The PPC effect is most pronounced when $0.2 \leq x \leq 0.4$, and it reaches a maximum at $x = 0.32$ (4:644). To overcome the small applied gate voltage limitations of the MODFET, and the negative affects of increasing the mole fraction of the Al, another layer has been added to the MBE grown structure resulting in a modified MODFET.

The Enhanced Schottky-Barrier MODFET [(ES)MODFET]

The (ES)MODFET structure is distinguished from a MODFET by a p^+ GaAs layer grown on the n^+ GaAs cap layer before the Schottky gate is deposited (33:434). This thin layer is approximately 100 Å thick, and it is typically

19

doped with beryllium. Figure 7 depicts the MBE grown heterostructure associated with the (ES)MODFET. In addition, Shannon (41:537) demonstrated that the Schottky-barrier height can be modified by adding a thin layer ($\approx$ 100 Å) between the semiconductor and metal. For an n-type substrate, a p^+ layer increases the barrier height, and an n^+ layer will decrease the barrier height (41:537). Devices using the enhanced Schottky-barrier, increase the maximum allowable applied gate voltage.

p^+ GaAs	75-100 Å
n^+ GaAs	75-100 Å
doped $Al_xGa_{1-x}As$	320-350 Å
undoped $Al_xGa_{1-x}As$	30 Å
GaAs Buffer	1 μm
semi-insulating substrate	

Figure 7. Molecular Beam Epitaxially Grown Heterostructure with Typical Dimensions Used to Realize an (ES)MODFET (33:434).

20

(ES)MODFET Device Operation

Operation of the (ES)MODFET is identical to that of the MODFET. The 2DEG is formed by trapping diffused free electrons from the doped $Al_xGa_{1-x}As$ material in the two-dimensional quantum well created at the $Al_xGa_{1-x}As$/GaAs interface. The applied gate voltage modulates the carriers in the channel. Another conduction band discontinuity is introduced at the p^+ GaAs/n-$Al_xGa_{1-x}As$ layer in the (ES)MODFET structure (29). This discontinuity is shown in Figure 8. The enhanced Schottky-barrier modulation doped field-effect transistor (ES)MODFET
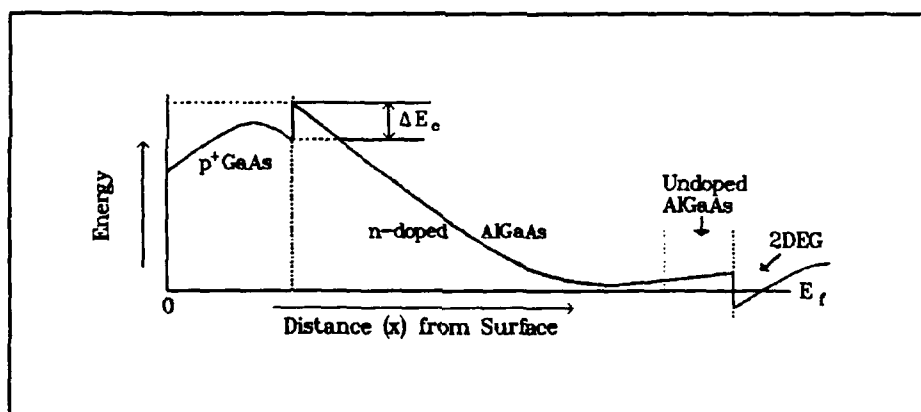
Figure 8.   Conduction Band Discontinuities in the (ES)MODFET Heterostructure (29).

studied by Priddy (37) and Ohata, Hida, and Miyamoto (33:434) increased the Schottky-barrier height of the gate and allowed higher applied gate voltages to be used. Priddy demonstrated that the maximum allowable applied gate voltage increased from 0.8 volts to 1.6 volts when the p^+ GaAs layer was added (37:175).

While the (ES)MODFET shows promise for increasing the maximum allowable applied gate voltage, and does not present the same limitations of increasing the mole fraction of Al, there is one fabrication process step that presents some difficulties in realizing optimized devices.

Fabrication of the (ES)MODFET

Once the layers have been grown using MBE, fabrication of the device's active regions can be accomplished. The fabrication steps are illustrated in Figure 9. The first step is to isolate the device (6:775; 44:1022). Ion milling, ion implantation or wet chemical etching forms a mesa in the semi-insulating GaAs layer, electrically isolating the active device areas (6:775; 44:1022). Then the source and drain contacts are defined using a positive photoresist process. Next, metal is evaporated (typically AuGe/Ni/Au) (44:1022). A lift-off process is used to remove unwanted metal except for the source and drain contacts. After the lift-off procedure is completed, a rapid thermal anneal process is accomplished at approximately 400°C for one minute to form ohmic contacts. During the annealing process, the Ge atoms diffuse from the surface to the heterojunction interface to make contact with the 2DEG (44:1022). The next step is gate definition. Positive photoresist defines the gate region. Another lift-off process is used to remove the unwanted metal-coated photoresist. Al is commonly used to form the Schottky-barrier gate (29). The final step is the removal of the p^+ GaAs layer between the source-and-gate and the drain-and-gate. The standard method of removal is wet chemical etching (33:434; 29; 30). The finished device is illustrated in Figure 4.
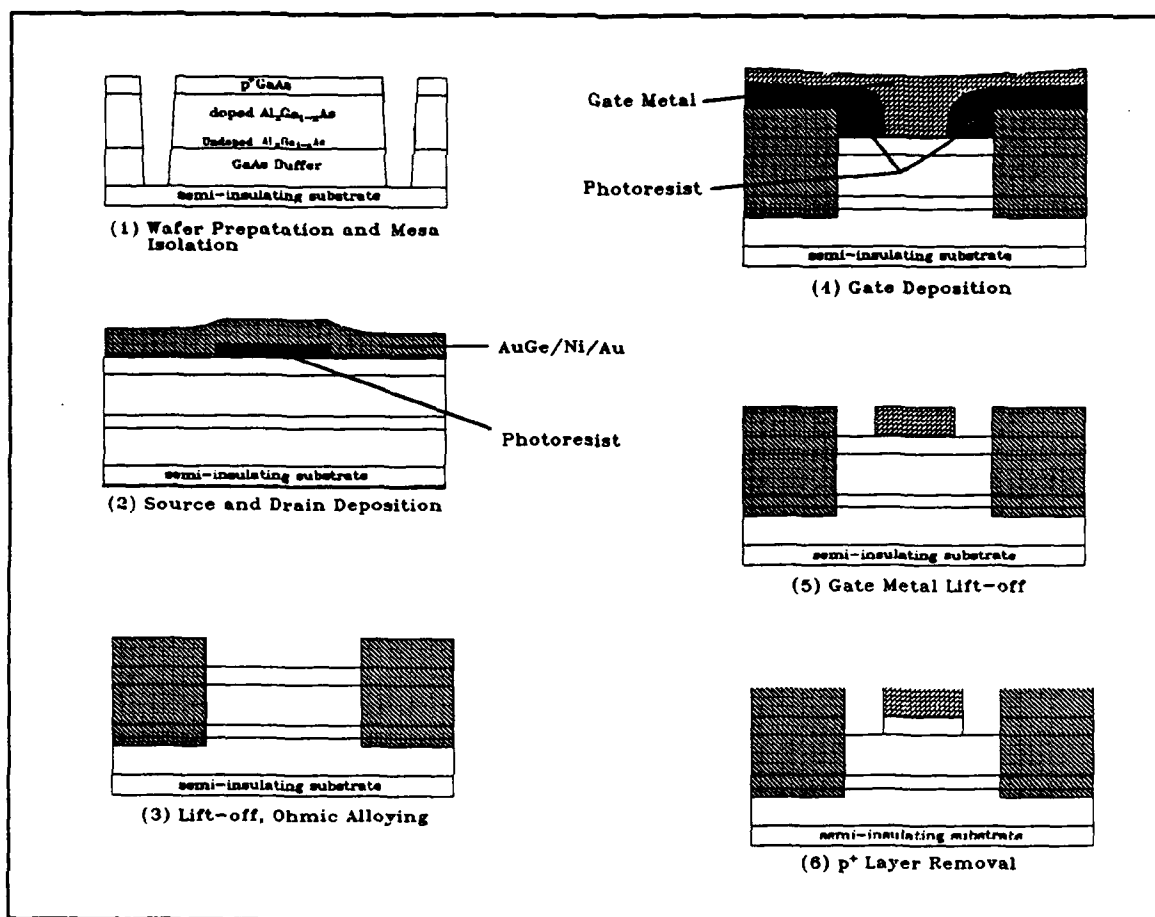
Figure 9. Fabrication Procedures of the (ES)MODFET (30).

The removal of the p^+ GaAs layer during the fabrication of the (ES)MODFET "is the only [additional] step to the conventional fabrication process for planar Schottky-barrier gate GaAs FETs" (33:434). The removal of that layer presents some complications in the fabrication of the (ES)MODFET. Care must be exercised in the removal of the p^+ layer between the gate-and-drain and the source-and-gate. If the p^+ layer is not completely removed, a parasitic conduction path is formed between the source-and-drain which can reduce the device's transconductance (26:29). On the other hand, if a portion of the doped $Al_xGa_{1-x}As$

23

layer between the source and drain is etched, the source and drain resistance (R_s and R_d, respectively) will be increased, and the maximum frequency (f_{max}) is decreased (3:1399). There are many techniques available that can be used to remove unwanted layers from a semiconductor surface (48:451; 15:480). Removal of material is accomplished by plasma etching, ion milling, reactive ion etching or wet chemical etching. Wet chemical etching is one method often used. The next section discusses this method as applied to GaAs device fabrication.

Wet Chemical Etching

Etching can be described as "techniques by which material can be uniformly removed from a wafer" (15:476). Chemical etching is used in many different processing steps during the fabrication of integrated circuits. A host chemical solutions are available to clean, polish, and highlight surface defects and remove selected areas of the wafer's surface. The opened areas can then be exposed to other device processes, such as diffusion, ion implantation or metal deposition (48:451; 15:476).

Wet chemical etching facilitates the reduction of the semiconductor's surface material into compounds (solutes) that are soluble in the etchant solution. After their formation, agitating the etchant solution will accelerate the removal of the compounds (solutes) from the semicondutor's surface (15:476). The three processes associated with wet chemical etching are portrayed in Figure 10. They are: (1) transportation of the chemical reactants to the wafer's surface (by diffusion); (2) chemical reaction at the semiconductor's surface (formation of soluble products or

24

solutes); (3) transportation of the solutes formed by the reaction away from the surface (by diffusion) (48:451). When the diffusion rates of the reactants control the
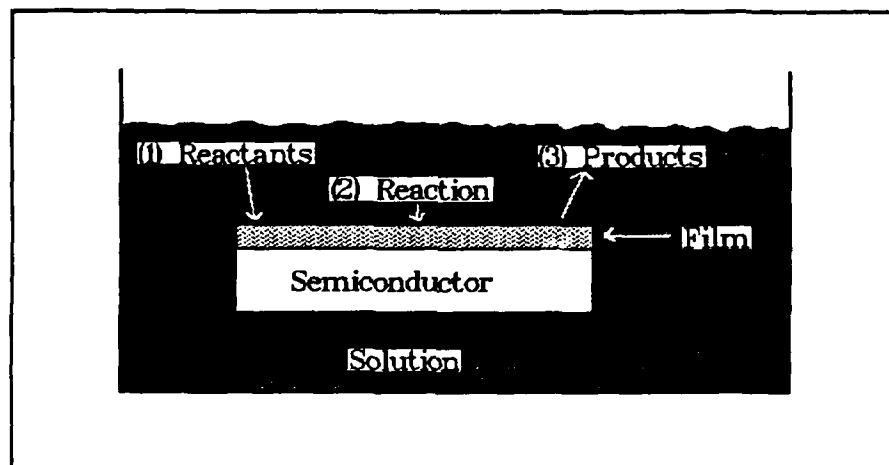
Figure 10. The Three Processes of Wet Chemical Etching (48:451).

speed of the process, the etching is said to be diffusion limited. For a reaction limited process, the regulating factor is the surface reaction rate (15:477; 25).

To precisely control the small dimensions needed for electronic devices, most semiconductor etching procedures require slow, reproducible etch rates (25:505; 15:477). Selectivity is also a desirable characteristic. Selectivity is defined as the ratio of the etch rate of one material with respect to the etch rate of a different material. This property leads to "rapid selective removal of a part of the crystal with a given chemical composition without damage or removal to the rest of the crystal" (27:6441). In order to achieve the desired result of the etching process, the effects of the crystalline structure (i.e. atomic planar density), solution composition (i.e., pH and concentration) and solution environment (i.e., agitation) must be considered.

25

Crystalline Structure

Most etching is performed on crystalline structures. The etching of these structures can either be isotropic, which is characterized as having an equal etch rate in all directions, or anisotropic, which is characterized by different etch rates in different directions (15:478). Most etches for GaAs are not isotropic because of the asymmetrical crystal structure of GaAs (13:1215; 15:484).

The crystal structure of GaAs is a zincblende structure. Figure 11 depicts a zincblende structure, which can be visualized as being composed of two separate interpenetrating face-centered-cubic (fcc) lattices that are offset with respect to each other by 1/4 of the length of an internal diagonal of the unit cell The Ga atoms
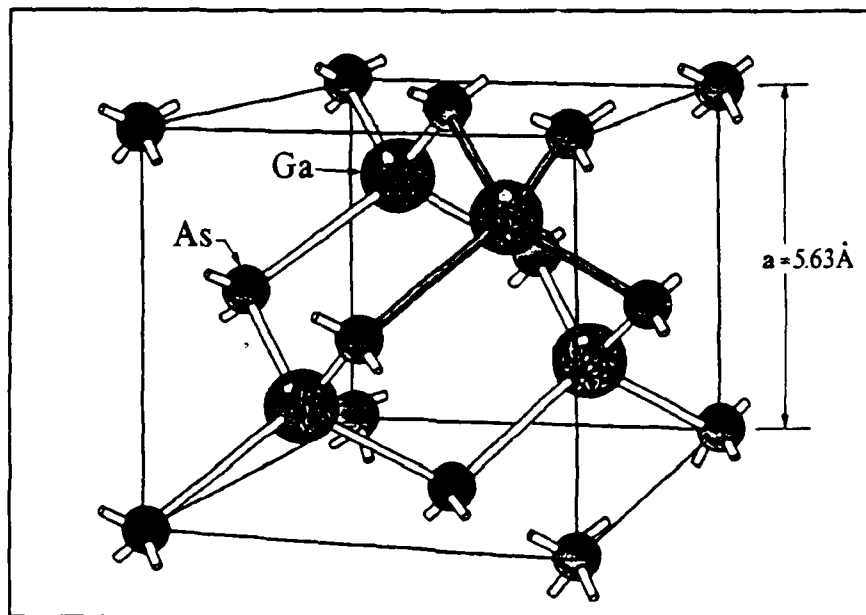
Figure 11. The Zincblende Crystalline Structure of GaAs (48:5).

26

have coordinates of: 1/4 1/4 1/4; 1/4 3/4 3/4; 3/4 1/4 3/4; 3/4 3/4 1/4 in the unit cell, while the As atoms have the coordinates: 0 0 0; 0 1/2 1/2; 1/2 1/2 0 (23:20). Figure 12 shows the (111) plane of the zincblende structure. Examining the {111} set of planes reveals that only one type of atom (Ga or As) is present in a given
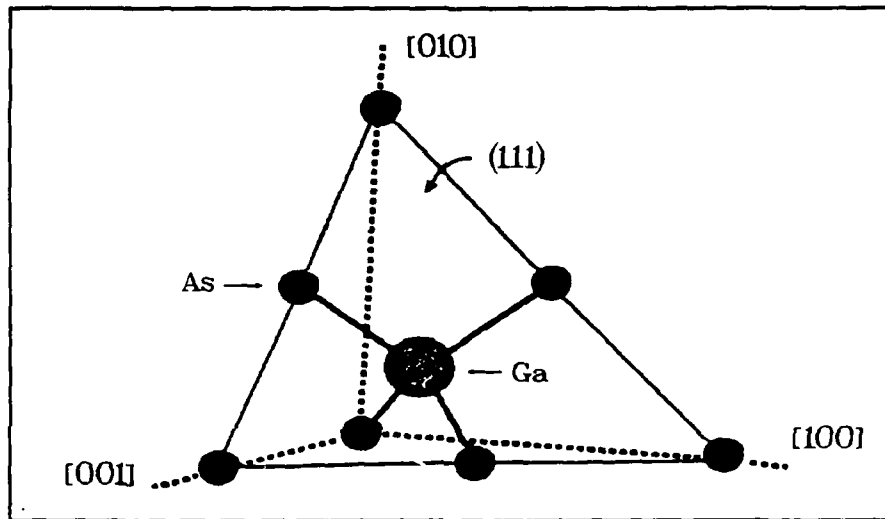
Figure 12. Exposed (111) Plane of the GaAs Unit Cell (53).

plane. Four of the eight planes contain only Ga atoms, sometimes referred to collectively as the (111)A plane. The other four planes contain only As atoms, and they are collectively known as the (111)B plane (53:24; 15:13).

The zincblende structure is not symmetrical in all directions. The anisotropic (or preferential) etching behavior is a result of the asymmetrical lattice. In examining the atoms of the Ga (111) plane, all of the valence electrons (3 each) are involved in covalent bonds with the arsenic atoms in the next lower layer. The As

atoms have five valence electrons for each atom. Two valence electrons are not involved in bonds with the next layer of Ga atoms. Propagating this arrangement to the surface of the crystal results in two free electrons on the surface of the (111)B plane, and they are available to participate in a (cathodic) chemical reaction (15:13; 53:105). Figure 13 shows a three-dimensional view of alternating planes of Ga and As atoms joined by single and triple bonds, respectively. Figure 14 depicts the bonds in two dimensions. The increased electrical activity of the As face results in faster etch rates. The faster etch rate of the (111)B plane has been verified in studies by several researchers (13:1215; 31:1510; 49:118; 20:768).
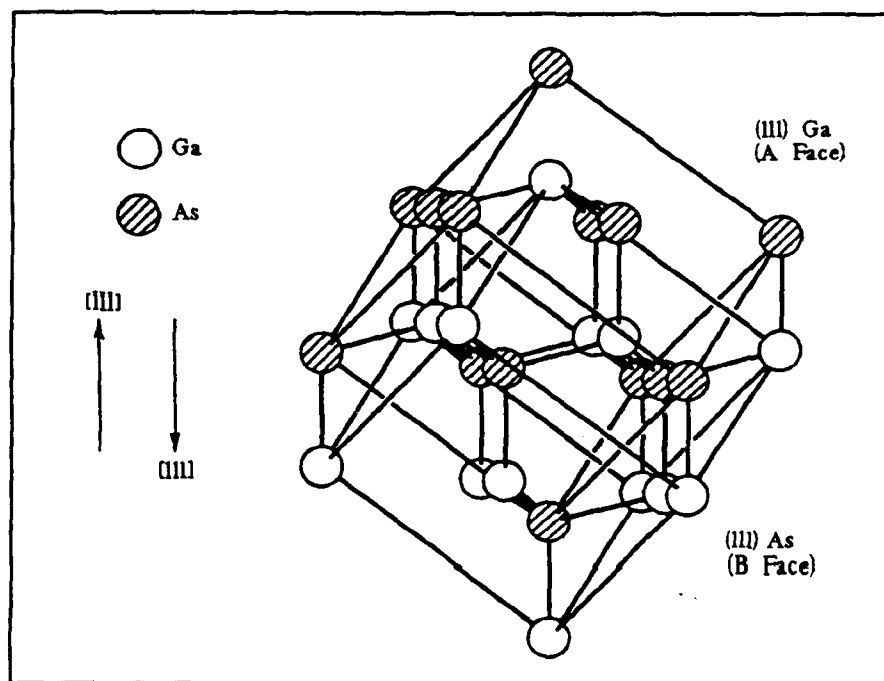
Figure 13. Three-Dimensional View of Alternating Planes of Ga
and As Atoms in the Crystal Structure (15).
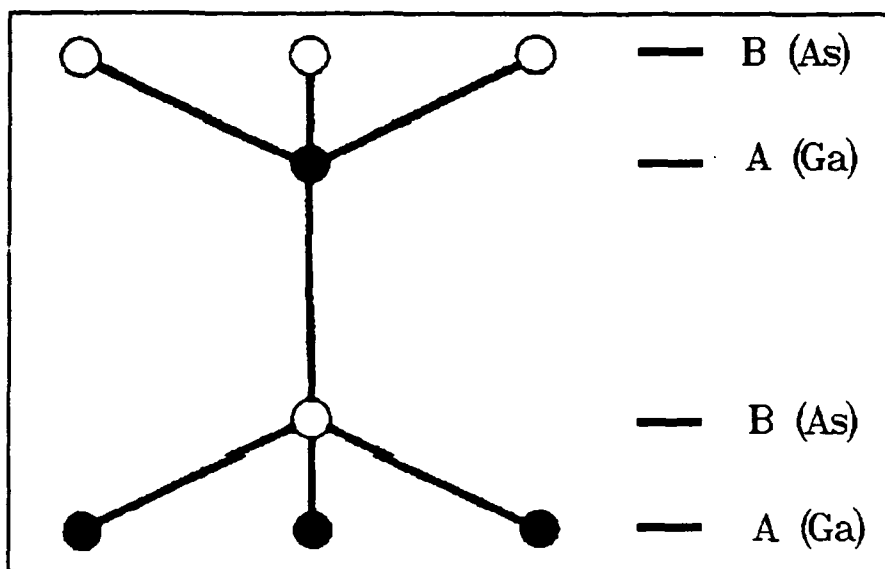
Figure 14. Two-Dimensional View of Alternating Planes of Ga and As Atoms (53).

Surface Reaction

Many different etchant have been investigated to accomplish the selective etching of GaAs (53:120). The basic reaction for several of these etch solutions is the same (25:505). A brief explanation of the surface reaction follows. The reaction at the surface of gallium arsenide involves the formation of gallium and arsenic oxides. The oxides formed are soluble in the etch solution and transported from the semiconductor's surface. The anodic reaction (represented by "a production of electrons" (12:10)) for GaAs as noted by Ghandhi is (15:404):

$$GaAs + h^+ \rightarrow Ga^{3+} + As^{3+} \tag{1}$$
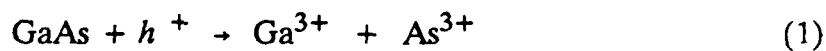
Once the GaAs is ionized, the Ga and As ions form compounds which are soluble in the etchant. Ghandhi presents the separate reaction for the formation of gallium oxide as follows (15:404):

$$3H_2O \rightleftharpoons 3H^+ + 3(OH)^- \qquad (2)$$

$$Ga^{3+} + 3(OH)^- \rightarrow Ga(OH)_3 \qquad (3)$$

$$2Ga(OH)_3 \rightarrow Ga_2O_3 + 3H_2O \qquad (4)$$
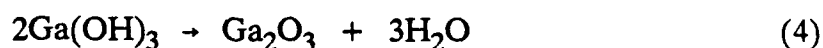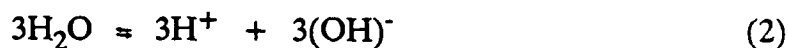
Similarly, the formation of arsenic oxide proceeds as follows (15:404):

$$2H_2O \rightleftharpoons 2H^+ + 2(OH)^- \qquad (5)$$

$$As^{3+} + 2(OH)^- \rightarrow AsO_2^- + 2H^+ \qquad (6)$$

$$2AsO_2^- + 2H^+ \rightarrow As_2O_3 + H_2O \qquad (7)$$
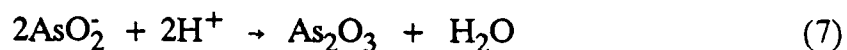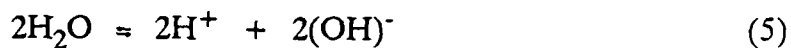
The combination of the above chemical equations as reported by Ghandhi results in the following overall reaction (15:404):

$$2GaAs + 12h^+ + 10H_2O \rightarrow Ga_2O_3 + As_2O_3 + 4H_2O + 12H^+ \qquad (8)$$
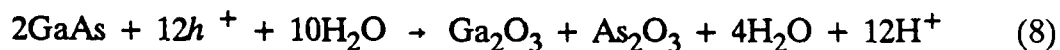
For many etching solutions the hydroxide ion (OH^-) is supplied by hydrogen peroxide (H_2O_2) (25:505).

An example of the preferential nature of GaAs etching is observed when one side of a rectangular patterned window is parallel to the <110> direction on a (100) oriented substrate. The cross-sections of the adjacent walls are shaped

30

differently. Figure 15(a) depicts that the cross-section of one side-wall is trapezoidal in shape with its short side on the bottom. However, the adjacent side-wall is trapezoidal with its long side on the bottom. If the window's edge is parallel to the
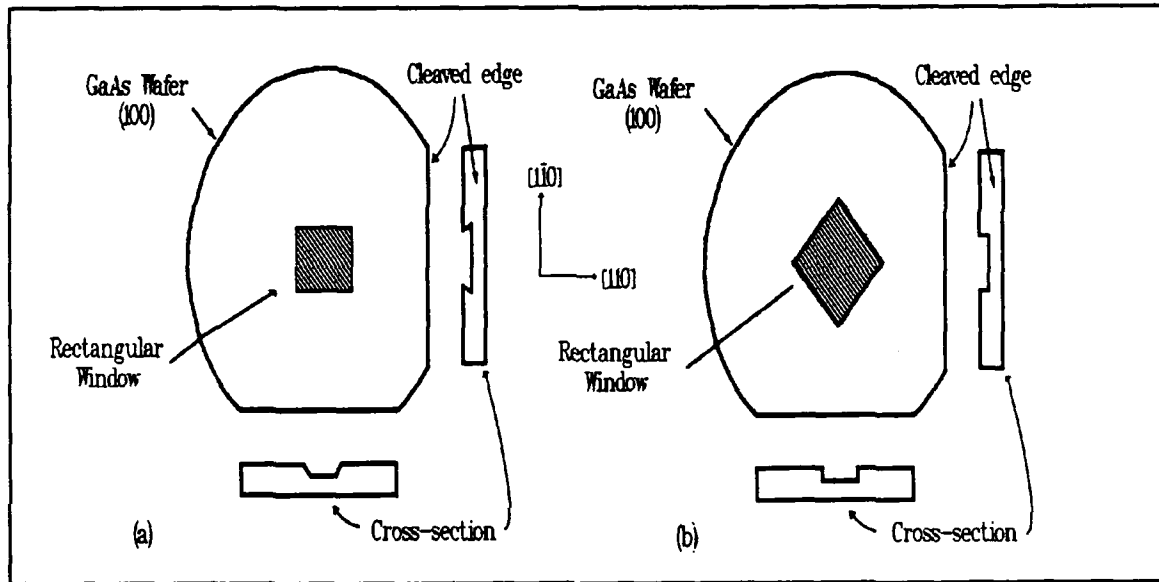
Figure 15.   Examples of Etched Walls for Rectangular Windows Patterned on a (100) GaAs Substrate (53; 20).

<100> direction, the etched walls are identical on adjacent sides and are mutually perpendicular. This situation is depicted in Figure 15(b) (20:768; 53:24).

Result of Previous Etching Studies

In order to fabricate devices that take advantage of the properties of GaAs, several researchers (28:4172; 13:1215; 31:1510) have studied a number of different chemical solutions. The results of these studies that are pertinent to the fabrication

of (ES)MODFETs are now considered. Some of the less exotic etchants for GaAs are summarized in Table 1. All of these etchants exhibit some degree of preferential etching of GaAs surfaces as described above. Some GaAs etchants have the undesirable characteristic of an enhanced etch rate at the edge of the mask (25:505). The reason for this effect has been attributed to a H_2O_2 diffusion limited

Table 1.   Common Etchant Solutions and Etch Rates for GaAs

Etchant Solution	Composition (by volume)	Etch Rate (μm/min)	Reference
1. $NaOH + H_2O_2 + H_2O$	1:1:10	0.38	(53)
2. $NH_4OH + H_2O_2 + H_2O$	1:1:5	1.8	(53)
3. $NH_4OH + H_2O_2$	1:160	0.3	(27)
4. $H_2SO_4 + H_2O_2 + H_2O$	4:1:1	0.5	(15)
5. $H_2SO_4 + H_2O_2 + H_2O$	1:1:1	5.0	(53)
6. $H_3PO_4 + H_2O_2 + H_2O$	1:1:1	4.0	(53)
7. $H_3PO_4 + H_2O_2 + H_2O$	7:3:3	1.4	(31)
8. $HNO_3 + H_3PO_4$	1:1	10.0	(53)

reaction, with additional hydrogen peroxide being provided from the protected area (25:505).

The phosphoric acid + hydrogen peroxide + deionized water (DIW) (H_3PO_4 + H_2O_2 + H_2O) system studied by Mori and Watanabe (31:1510) exhibited reproducible etch rates within specific composition ranges. Agitation of the etchant was not addressed in the study. The temperature was varied from 0 to 40°C. Figure 16 shows an isoetch curve. The dashed lines represent different solution compositions for which the etch rate remains constant. The graph can be
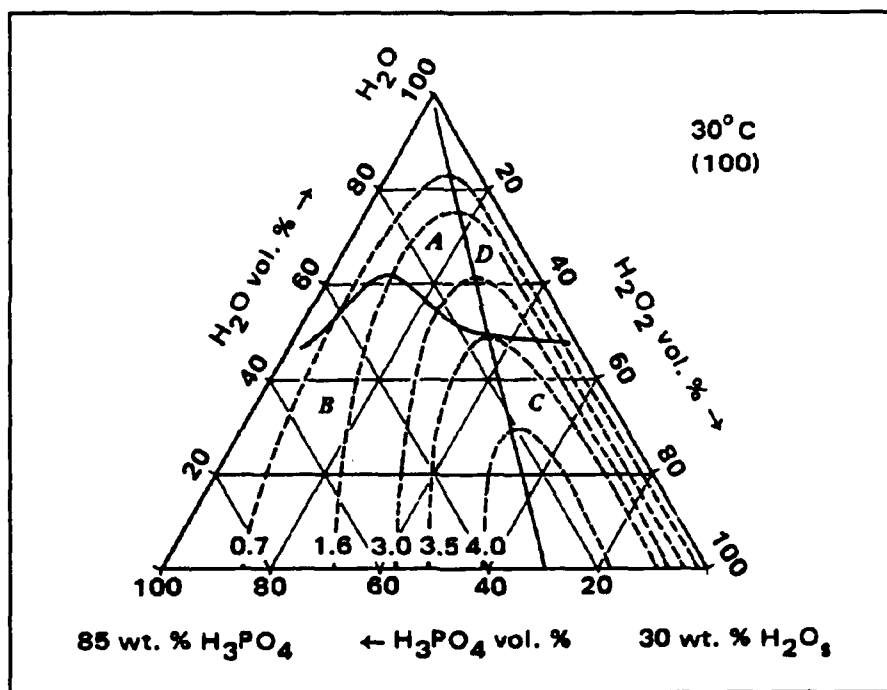
Figure 16. Isoetch Curves for (100) GaAs Using the H_3PO_4+H_2O_2+H_2O System at 30°C (31:1512).

broken in to four regions: **A, B, C,** and **D.** For solution compositions in the **A** region of the isoetch curves, the etch rate "is determined by and proportional to the H_2O_2 (minority reactant) concentration" (31:1511). In region **A,** the etched surface is flat

33

and there is no enhanced etch rate at the edge of the mask. The etch rate was also found to be independent of wafer doping and resistivity. This system also displays the preferential etching characteristics discussed above. For a solution composition of H_3PO_4 + H_2O_2 + H_2O (3:1:150 by volume), the etch rate for the (111)Ga plane is 0.4 μm/min and 0.8 μm/min for the other planes (31:1510).

The sulfuric acid + hydrogen peroxide + DIW (H_2SO_4 + H_2O_2 + H_2O) etchant studied by Iida and Ito (20:768) can be used as a process step in the fabrication of Gunn oscillators and millimeter wave diodes. Their research demonstrated that the concentration of sulfuric acid in the etchant solution influenced the smoothness of the etched surface. A non-planar hole resulted from high H_2SO_4 concentrations, whereas a planar etched surfaces resulted from low concentrations of H_2SO_4 (20:768). For example, H_2SO_4 + H_2O_2 + H_2O in a volume ratio of 1:1:8 results in etch rates of 3 μm/min, 8 μm/min, 8 μm/min and 12 μm/min for the (111)Ga, (100), (110) and (111)As planes, respectively. The surfaces remaining are smooth (20:768). This system also displays preferential etching characteristics.

Another useful etchant solution for the removal of GaAs is the ammonium hydroxide + hydrogen peroxide + DIW (NH_4OH + H_2O_2 + H_2O) mixture (used in varying ratios). This etchant solution was first proposed by Sayko of Bell Laboratories, and it was reported in the open literature by Dyment and Rozgonyi (8:1346) as a replacement for the bromine-methanol (BM) solutions. BM solutions, used as polishing agents, show undesirable aging characteristics and result

in non-reproducible etch rates. Gannon and Nuese (13:1215) demonstrated the utility of the $NH_4OH:H_2O_2:H_2O$ mixture for GaAs bipolar transistor fabrication. It "provides relatively low etching rates for both n- and p-type <100> GaAs, and a flat etching plane ..." (13:1215). This etchant will not attack a SiO_2 mask or metallic contacts, as will most alkaline etches and acid etches. The etchant will attack photoresists after etching to a depth of approximately 1 μm (17; 52). A solution of 20 ml of NH_4OH, 7 ml of 30% H_2O_2 and 973 ml of DIW produce an etch rate of 0.12 - 0.14 μm/min on p-type <100> orientated GaAs wafers (13:1215). Temperature and agitation were not considered in Gannon and Nuese's study. A study by Kohn, who investigated Gannon's etchant (25:505), states that:

> ... in solutions with low H_2O_2 and high H_2O content the etching rate is roughly proportional to the mole percentage of H_2O_2 content and thus determined by the H_2O_2 - GaAs reaction. [Eqs (2 - 7)] [25:506]

Again the <111>A direction demonstrates the slowest etch rate (0.037 μm/min), while the <111>B direction has the fastest etch rate (0.20 μm/min). The corresponding etch rate of the <100> direction is 0.12 μm/min (13:1215). This etch rate order, {111}B > {100} > {111}A, is expected from the zincblende structure because of the density of atoms in the different planes and the higher electrical activity associated with the As atoms (53:105).

The etchant solutions presented thus far have not been investigated with respect to their selectivity. Selectivity, the ability to remove one semiconductor material (e.g., GaAs) while not affecting any other material (e.g., $Al_xGa_{1-x}As$), or

"the ratio of GaAs to $Al_xGa_{1-x}As$ etch rate" (21:2381), can greatly aid the device fabrication engineer when designing a fabrication procedure for a particular device. With the advent of heterostructure devices, research has been initiated regarding the selective etching of $Al_xGa_{1-x}As$/GaAs systems.

The ammonium hydroxide + hydrogen peroxide (NH_4OH + H_2O_2) or Peroxide Alkaline (P/A) solution, a modification of the NH_4OH:H_2O_2:H_2O system, has also been investigated for potential application in the fabrication of heterostructure devices (21:2380; 28:4172; 2:2602; 27:6441). Logan and Reinhart (28:4172) determined a new method of fabricating optical waveguides in GaAs/$Al_xGa_{1-x}As$ heterostructures using the H_2O_2:NH_4OH mixture. By varying the pH (between 1 and 6) of the 30% H_2O_2 (superoxol) component with the addition of NH_4OH or H_3PO_4, the solution can be used to grow an oxide on GaAs (or $Al_xGa_{1-x}As$). When the pH of this solution is raised above pH 6 it also etches GaAs, while $Al_xGa_{1-x}As$ (where x > 0.1) layers appear unaffected (28:4172). With a solution pH greater than 7, the surface roughness increases during the etching of the GaAs. When the pH is approximately 8, pitting of the GaAs surface occurs. The etch rate for GaAs was 1.8 μm/hr (0.03 μm/min) for a solution with a pH equal to 7.02. Agitation increased the etch rate to approximately 5 μm/hr (28:4172).

Kenefick (21:2380) demonstrated a P/A etchant solution suitable for fabricating light emitting diodes and semiconductor lasers. Etch rates of 1.4 to 4.1 μm/min for GaAs, and 0.12 to 0.15 μm/min for $Al_{0.16}Ga_{0.84}As$ were observed. The selectivity, defined as the ratio of the etch rate of GaAs to the etch

36

rate of $Al_{0.16}Ga_{0.84}As$, was also determined (21:2381). When the samples were placed in a teflon holder, the selectivity varied from approximately 3 to 32 over a pH range of 7.2 to 8.4. A greater selectivity was noted using a teflon sample holder versus a stainless steel sample holder. The highest selectivity, of 32, was obtained at a pH of 8.4. Kenefick postulates that a "galvanic action" (21:2382) is responsible for the faster etch rate of $Al_{0.16}Ga_{0.84}As$ in the stainless steel sample holders. In these experiment the solution was stirred, and the temperature was constant.

LePore modified the etching technique described above by using a Jet Thinning Instrument (27:6441) and reducing the temperature to 0°C. With the same P/A solution, he achieved selectivities as large as 30 by varying the volume ratio (γ) of the solution ($\gamma = Vol(H_2O_2)/Vol(NH_4OH)$). For $\gamma = 80$ and $x = 0.30$, the selectivity was approximately 30. This feature translates to an etch rate of 0.085 μm/min for $Al_{0.30}Ga_{0.70}As$, and 2.0 μm/min for GaAs. When $x = 0.80$, a selectivity of 30 was achieved for $\gamma = 60$. LePore's motivation for using this etching procedure was to form a window in a GaAs wafer for the spectroscopic analysis of $Al_xGa_{1-x}As$ epitaxial layers (27:6441).

Summary

The modulation-doped field-effect transistor is a proven technology for high frequency, low noise, low power consumption and fast switching applications (44). The behavior of the electrons in the 2DEG channel is the key to the electrical performance advantages displayed by the MODFET. These advantages are higher transconductance, lower noise figure and higher operating frequencies comOpared

to the state of the art GaAs metal-semiconductor field-effect transistor (6). In order to optimize the maximum applied gate voltage of the device, researchers have added a p^+ GaAs layer beneath the gate, drain and source. This device, known as the (ES)MODFET, allows the maximum applied gate voltage to be increased from 0.8 volts to 1.6 volts (37). During fabrication of the (ES)MODFET, the p^+ layer must be removed between the drain-and-gate and the source-and-gate. The removal of the unwanted p^+ layer is normally accomplished using wet chemical etching techniques (29; 30).

Wet chemical etching allows the controlled removal of unwanted material from the semiconductor's surface. The removal of GaAs occurs by the formation of gallium and arsenic oxides, and their subsequent dissolution in the etchant solution (15). The common oxidizing agent in many GaAs etching solutions is the hydroxide ion (OH^-) which is often provided by H_2O_2 (25). The zincblende structure of GaAs causes preferential etching of the different planes. The order of decreasing etch rate is {111}B, {100}, and {111}A (53). For a low concentration of H_2O_2 and high water content, the etch rate is roughly proportional to the mole percent of H_2O_2 (25:506). A peroxide-alkaline solution developed by Logan was used to selectively etch GaAs layers from GaAs/$Al_xGa_{1-x}As$ heterostructures (28). Selectivities as high as 30 have been reported. The selectivity feature is advantageous when the fabrication process of a heterostructure device requires the selective removal of GaAs (28; 27). The fabrication problems associated with the removal of the p^+ layer from between the gate-and-drain and the gate-and-source

of the (ES)MODFET could possibly be eliminated with the high selectivity of the Peroxide Alkaline (P/A) etch. Chapter III describes the experimental procedures used to investigate the selectivity of several different etch solutions on $GaAs/Al_xGa_{1-x}As$ heterostructures.

III. Experimental Equipment and Procedures

This Chapter develops a brief description of the special equipment needed and the experimental procedures used in completing this investigation. The tests were completed in the class 100 clean room facility in the Air Force Avionics Laboratory, Wright-Patterson Air Force Base. Much of the equipment used is common to integrated circuit processing facilities (e.g., a spinner, a mask aligner, an oven, a profilometer, and a scanning electron microscope (SEM)). The operation of these instruments will not be explained. Two special instruments used, whose basic operation will be discussed, were a Fischione Electropolisher and an Orion pH meter.

Three experiments were used to characterize the etch rates of GaAs, p^+ GaAs, $Al_xGa_{1-x}As$ and $n-Al_xGa_{1-x}As$. The first experiment sought to establish an etch rate for GaAs using an established method that has been applied to the corrosion testing of metals since the early 1950's (12). The variable solution concentrations were considered. The solution(s) from this experiment that displayed an etch rate slow enough to consistently and accurately etch 100 Å of GaAs were used in the second experiment. The second experiment used these solution(s) to investigate the affect(s) on GaAs and $n-Al_xGa_{1-x}As$ using a Fischione electropolisher. The variables of solution concentration and pH were examined. The third experimental method measured the etch depth versus time. The etch depth was measured with a Dektak profilometer after the sample was exposed to the etchant

for a specified time. This method is well-established and verified the validity of the first two experiments.

Special Equipment

The Fischione Automatic Twin-Jet Electropolisher and the Orion pH meter are not extraordinary complex pieces of scientific equipment. However, they are not always associated with the standard equipment used to fabricate ICs. The basic operation of this special equipment is discussed below.

Fischione Automatic Twin-Jet Electropolisher. The Fischione Automatic Twin-Jet Electropolisher is typically used for thinning metal specimens for transmission electron microscopy (TEM) (40:1351). The operation of this equipment combines several simple principles (electrochemical reactions and light detection) to make the preparation of samples for TEM easier. This study used the Fischione Electropolisher as a tool to determine the etch rates of semiconductor materials. Figure 17 shows the basic components of the Fischione Electropolisher.

The operation of the Fischione Electropolisher relies on terminating the thinning process at the instant the sample is perforated. The thinning process is accomplished with or without a polishing current applied. A 1.4 mm diameter opening in the specimen holder exposes only a small area of a sample (i.e., the semiconductor) to the etchant (40:1351). The holder is then placed in the etchant along with a light source (transmitted through a "Light Wire (the Bausch & Lomb trade name for noncoherent bundles)") (40:1351) directed at the center of one side of the holder. The light source can be tuned (i.e., wavelength and intensity) such

that it will not transmit through the sample until perforation occurs. A photocell on the opposite side of the sample detects the transmitted light at the instant perforation occurs and it triggers an audible and visual alarm (40:1351).
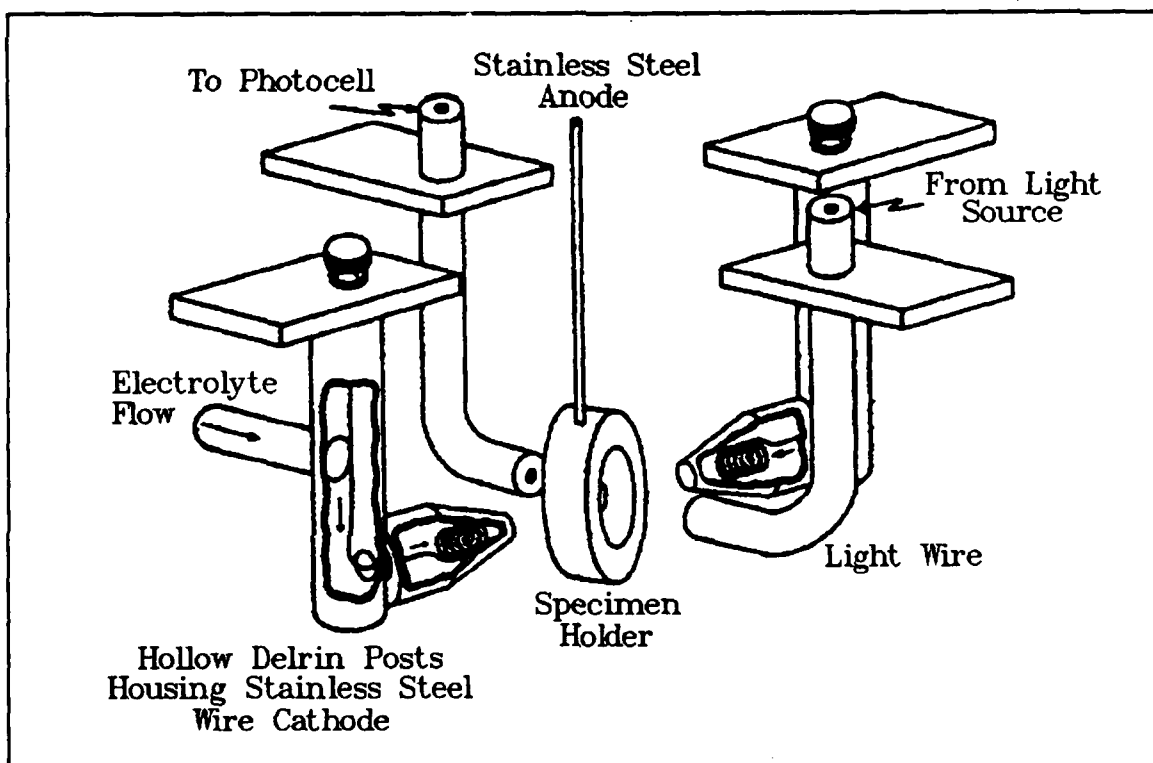
Figure 17. Components of the Fischione Twin-Jet Electropolisher (40:1351).

There are jet nozzles directed at the opening in the sample holder. The flow of the etchant impinging upon the sample can be controlled with a maximum flow rate of 600 ml/min (40:1352). Inside the jet nozzle is housed a "3 mm diameter ... stainless steel wire" (40:1352) that forms the cathode (See Figure 17). As Figure 18 illustrates, the anode rests inside the specimen holder and is connected to the sample
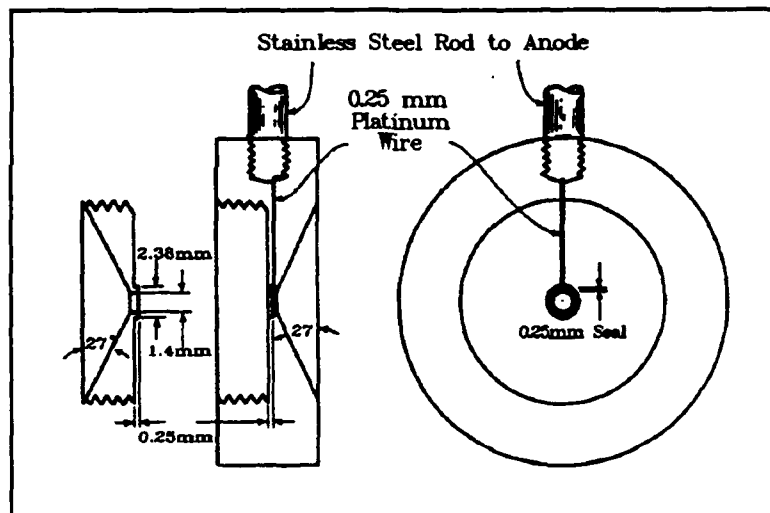
Figure 18.   Cross-Section of the Fischione Specimen
               Holder (40:1351).

via a 0.25 mm diameter platinum wire. When the alarm is triggered at sample

perforation, the motor controlling the jets and any applied current are turned off.

This feature allows removal of the sample at the exact time of perforation (40).

SA 520 Orion pH Meter. The Orion SA 520 is a "microprocessor controlled

pH/mV/temperature meter" (36). The term pH is a simplified "way of expressing

the concentration of hydrogen ions" (14).   It is defined by the relation,

pH = - log [H^+] (1). A solution with a high concentration of hydrogen ions is acidic

(pH < 7.0); a solution with a low concentration of hydrogen ions is basic

(pH > 7.0) (34). A pH = 7.0 indicates a neutral solution with equal concentrations

of hydrogen and hydroxyl ions.

In general a pH meter consists of "a pH measuring electrode, a reference

electrode, and a high input impedance meter" (34). The reference electrode typically

consists of a silver wire coated with silver chloride (AgCl), a filling solution (4M KCl saturated with AgCl) and a permeable junction which allows the filling solution to escape the electrode (34:A-6). "The pH measuring electrode is a hydrogen sensitive glass bulb, with a millivolt output that varies with the changes in the relative hydrogen ion concentration inside and outside of the bulb" (34:A-3). The potential that develops on the two sides of the glass bulb is a measure of the pH difference in the two solutions (39:648). Both of the electrodes (the reference and pH measuring electrodes) are placed in the solution whose pH is to be determined. "The reference electrode does not vary with the activity of the hydrogen ion" (34:A-4). "The potential difference between these two electrodes is measured and converted to a pH value" (39:648). "The pH meter is basically an amplifier that accurately measures the minute electrode voltages" and converts it to a pH reading (34:A-4). The Orion combination pH electrode contains an Ag/AgCl internal reference along with the pH measuring electrode (35). The combination electrode is shown in Figure 19.

The SA 520 also contains an automatic temperature compensation (ATC) probe. Temperature compensation is necessary because the pH of the solution is sensitive to temperature changes (34). Orion recommends the use of an ATC probe to eliminate the need for manual temperature compensation (36).

Experimental Procedures

The experimental procedures in this investigation were focused toward the goal of precisely etching a 100 Å thick p^+ GaAs epitaxial layer from between the

44
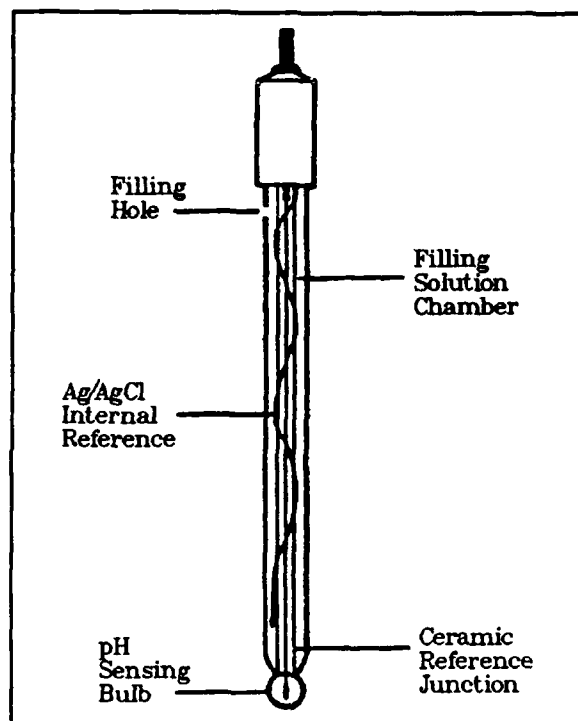
Figure 19.   Orion   Ag/AgCl   Glass
Combination pH Probe (35).

gate-and-drain and the gate-and-source of an (ES)MODFET. The removal of this

layer is the final fabrication step for an (ES)MODFET. Three experiments were

performed to achieve this goal. The first is a "new approach" in determining etch

rates in semiconductors which was beneficial toward identifying the different etchants

to be investigated. The second experiment utilized an established technique for

thinning materials, but extends it to accurately determine etch rates of semiconductor

materials. The final experiment verified the accuracy of the previous two methods.

It involved the established procedure of measuring the step height versus etch time

with a Dektak profilometer.

<u>Establishment of an Etch Rate Baseline.</u> The first experiment utilized the experimental procedure devised by Fontana (12) to determine the corrosion rates in metals. Fontana demonstrated that penetration/time (i.e., mils/year) could be determined from a sample of known area and density that has been placed in a corrosive environment. Next the weight loss of the sample was determined after a specified time (12). Combing these factors yields a penetration/time parameter. Fontana's method has been used since the early 1950's to study the corrosive properties of many metals on a bulk level.

An outline of the procedure for determining the GaAs etch rate using Fontana's method follows (A detailed step-by-step procedure is described in Appendix A). First the GaAs semi-insulating substrate has a known area masked on its surface, and then it is weighed. Next, it is immersed in the etch solution for a pre-determined time. The sample is then removed from the solution, rinsed in DIW, blown dry with nitrogen and re-weighed to determine the weight loss. The weight loss in milligrams (W), density of the specimen in g/cm^3 (D), area of exposure in cm^2 (A) and time exposed to the solution in seconds (t) can be combined to yield an etch rate as follows (12):

$$\text{etch rate} = \frac{100,000 \cdot W}{D \cdot A \cdot t} \quad (\text{Å/sec}) \tag{9}$$

Two etchants from the literature were chosen to verify the application of Fontana's method to semiconductor etching. The solutions are: 20:7:973 of $NH_4OH:H_2O_2:DIW$ by volume with an etch rate of 0.18 μm/min (33 Å/sec) (13), and 1:200 of $NH_4OH:H_2O_2$ by volume (without agitation) with an etch rate of approximately 1.6 μm/hr (5 Å/sec) (27; 28). Both solutions were evaluated at room temperature. The pH for each solution was also recorded.

A different, widely used technique verified the etch rates established by the weight loss method. GaAs wafers were masked and placed in the etchant solution for a specified amount of time based upon the etch rate determined by the weight loss method. Afterwards the etch profile was measured and recorded with a Dektak profilometer. The step height versus the time in solution was used as a method to confirm the etch rate results of the weight loss experiment. The results of the first experiment are presented in Chapter IV, and they were used as a guideline for further investigation in the second experiment.

<u>Wafer Etching with the Fischione Electropolisher.</u> The most appropriate etchant(s) from the first experiment were carried forward to etch MBE grown layers of n-$Al_xGa_{1-x}As$ (silicon doped) and GaAs substrate material. The wafers used for this experiment were prepared using the GEN II MBE system at the Air Force Avionics Laboratory. The samples and layer thicknesses are summarized in Table 2. All substrates were (100) and 2° off axis, measured with respect to the nearest (110) flat. The temperature of the substrates during the MBE growth process was 650°C. The Fischione electropolisher was used to achieve precise etch rates (40). (The

Table 2.   Thickness of Epitaxial Layers Grown Using the GEN II MBE System

Specimen Designator	Layer	Material	Thickness (cm^{-3})	Doping[1]	Percent Al X [2]
MBE F40	1	GaAs	0.25 μm[3]	none	N/A
	2	$Al_xGa_{1-x}As$	2 μm[3]	none	30
	3	p^+ GaAs	100 Å[5]	$1.0x10^{19}$	N/A
MBE F51	1	GaAs	0.25 μm[3]	none	N/A
	2	$Al_xGa_{1-x}As$	2 μm[3]	none	15
	3	p^+ GaAs	100 Å[5]	$1.0x10^{19}$	N/A
MBE F97	1	GaAs	0.5 μm[3]	none	N/A
	2	$n-Al_xGa_{1-x}As$	0.5 μm[4]	$3.0x10^{18}$	15
MBE F98	1	GaAs	0.5 μm[3]	none	N/A
	2	$n-Al_xGa_{1-x}As$	0.5 μm[4]	$3.0x10^{18}$	15
	3	p^+ GaAs	500 Å[5]	$1.0x10^{19}$	N/A
MBE G01	1	GaAs	0.5 μm[3]	none	N/A
	2	$n-Al_xGa_{1-x}As$	0.5 μm[4]	$3.0x10^{18}$	15
	3	p^+ GaAs	0.5 μm[4]	$1.0x10^{19}$	N/A
MBE G02	1	GaAs	0.5 μm[3]	none	N/A
	2	$n-Al_xGa_{1-x}As$	0.5 μm[4]	$3.0x10^{18}$	30

NOTE:
(1) Tolerances on doping concentration were ±0.1 (i.e. $3.0\pm0.1 \times 10^{18}$ cm^{-3}).
(2) Tolerances on mole fraction were ±0.1
(3) Tolerances on thickness were ±0.01 μm
(4) Tolerances on thickness were ±0.001 μm
(5) Tolerances on thickness were ±5 Å
(6) Tolerances on thickness were ±10 Å

detailed procedures are discussed in Appendix B. Appendix C describes the modifications made to Fischione Electropolisher for this research) A sample of known thickness was then placed in the specimen holder and immersed in the etchant. The sample was etched until the alarm sounded which indicated perforation. For a given layer thickness and the time needed for perforation, a precise etch rate was determined. The twin-jets were used to provide agitation. The polishing current used for thinning metallic samples was not used for etching the semiconductor samples.

During the MBE growth process, the material was only deposited on one side of the wafer. Therefore, a window must be opened in the GaAs substrate, so that only the MBE layer under investigation was etched. Lepore demonstrated a technique for opening a window on a GaAs/$Al_xGa_{1-x}As$ heterostructure to prepare the $Al_xGa_{1-x}As$ epitaxial layer for spectroscopic analysis (27). His method utilized a red light emitting diode on one side of the sample and a photo-detector on the other. Gallium arsenide is opaque to the red light source, while the $Al_xGa_{1-x}As$ will transmit the red light (27). This situation arises because of the difference in the energy bandgap of GaAs and $Al_xGa_{1-x}As$. The relation $\lambda_c = h \cdot c/E_g$, where h is Planck's constant, c is the speed of light and E_g is the bandgap energy in eV, determines the long-wavelength cutoff (47:744). "For wavelengths shorter than λ_c , the incident radiation is absorbed by the semiconductor, and hole-electron pairs are generated" (47:744). For GaAs, λ_c is 0.873 μm, and it is 0.690 μm for $Al_{0.3}Ga_{0.7}As$. Therefore the wavelength of the light source must be tuned such that

$0.690 \mu m < \lambda < 0.873 \mu m$ for the GaAs to be opaque and the $Al_{0.3}Ga_{0.7}As$ to be transparent. Because the Fischione Electropolisher uses an incandescent light bulb, a filter combination was used to achieve the same affect as a red LED. Figure 20 shows an example of a window that was used to expose only the epitaxial layer to the etching process. The glass slide was used as a platform to provide structural support for the epitaxial layers. After the epitaxial layer has been exposed and the thickness of the layer measured, the filter combination can be removed and the etch rate for the epitaxial layer determined. The pH for different solutions was varied to find an etchant suitable for removing the p^+ GaAs without affecting the $Al_xGa_{1-x}As$.
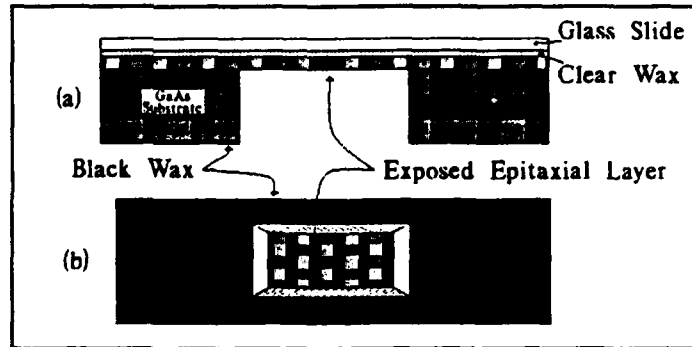
Figure 20. Exposed Window of an Epitaxial Layer on a GaAs Substrate (a) Cross-Sectional view, (b) Top view.

The goal of finding an etchant that will etch the p^+ GaAs layer between the gate-and-drain and the gate-and-source of an (ES)MODFET without attacking the

$Al_xGa_{1-x}As$ should result from theses procedures. The results obtained using these experimental procedures are presented and discussed in the next Chapter.

IV. Experimental Results and Discussions

This Chapter discusses the results of the experiments described in Chapter III. First, the results of the bulk corrosion test for GaAs is presented and compared to the literature and Dektak profilometer results. Next, the data collected from the Fischione Electropolisher method for GaAs and n-$Al_xGa_{1-x}As$ material are discussed. Finally the etch rates obtained using the Dektak profilometer method for p^+ GaAs, $Al_{0.15}Ga_{0.85}As$ and $Al_{0.3}Ga_{0.7}As$ are examined.

Baseline Etch Rate Determination

Fontana's method of bulk corrosion testing yielded etch rates consistent with those reported in the literature, and measurements accomplished using a Dektak profilometer. For Gannon's solution of $NH_4OH:H_2O_2:H_2O$ (20:7:973 by volume), an average etch rate of 16 Å/sec (or 0.10 μm/min) for an undoped (100) GaAs substrate material was found. This data compares favorably with Gannon's published result of 0.12 μm/min (or 20 Å/sec) for p-doped (100) GaAs (13:1215). Figure 21 shows the etch rate measured versus the etching time in the solution. As shown, the etch rate dose not appear to be constant. The weight loss method appears to illustrates a decreasing slope or etch rate as the time in the etchant solution increases. Gannon noted that the etch depth had "a slightly sub-linear dependence on etching time" (13:1216). The Dektak profilometer method confirmed the results of the weight loss method. Samples were masked, placed in the etchant, removed after a specified length of time, and the etch depth measured. The etch rate was
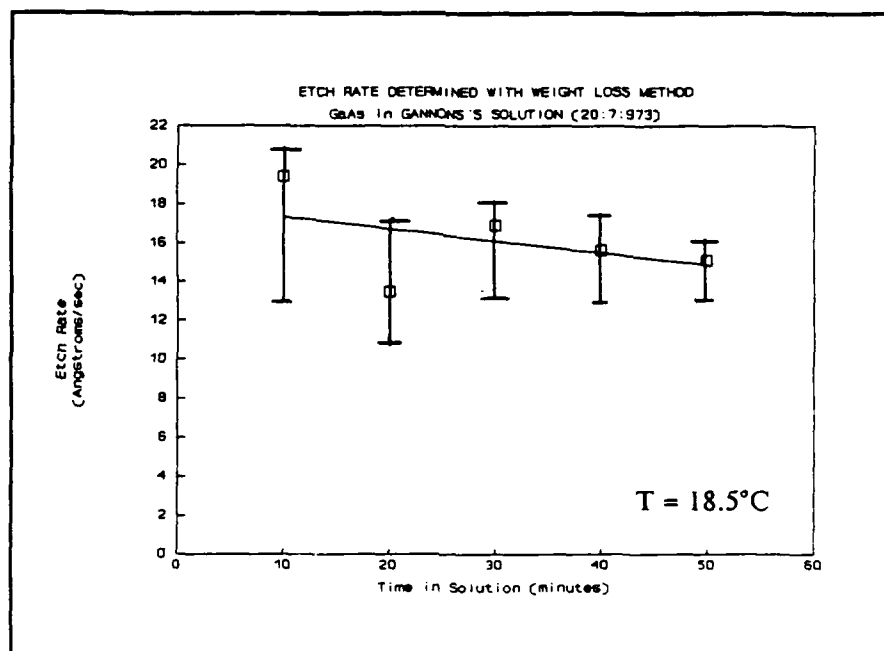
Figure 21. Etch Rate vs Time for GaAs in Gannon's Etchant
Using the Weight Loss Method.

43 Å/sec after 25 seconds, 27 Å/sec after 50 seconds and 23 Å/sec after 250 seconds.

Figure 22 plots the etched depth versus time for Gannon's etchant. A straight line

(linear regression) is drawn through the data points on the assumption of a linear

etch rate. The linear assumptions is made to simplify the etch rate determination

using the slope of the line. Three measurements were made at each pointed plotted

for the weight loss method and corresponding Dektak profilometer measurements.

The slope of the line indicates an average etch rate of 23 Å/sec. The data illustrates

that the etch rate decreases the longer the sample is in the solution. This average

etch rate similarly agrees with the weight loss method result and previously published

results (13:1215).

ETCH DEPTH VS TIME FOR GaAs IN GANNON'S SOLUTION

T = 18.5°C
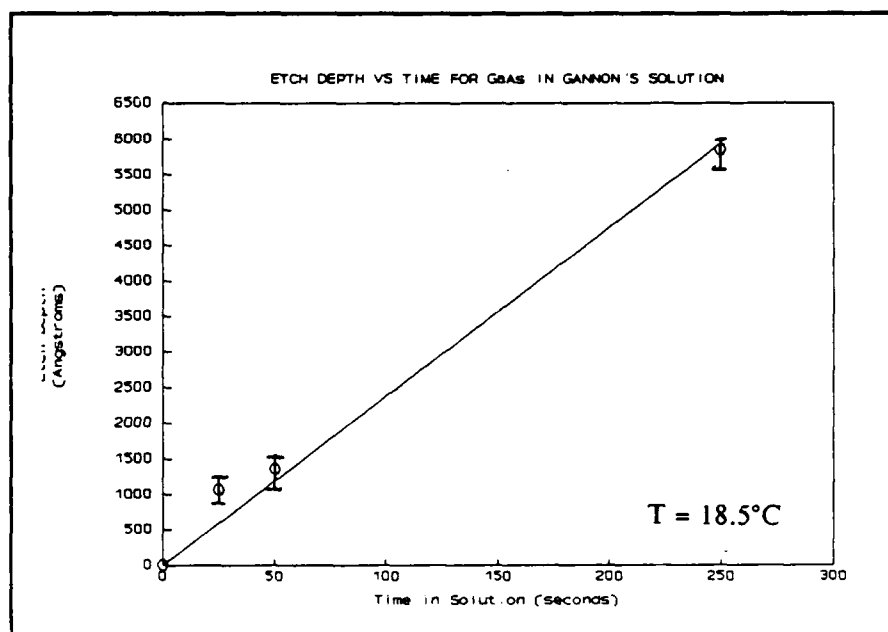
Figure 22. Etch Depth vs Time for GaAs in Gannon's Etchant
Using the Dektak Profilometer Method.

The second etchant tested with the weight loss method was the $NH_4OH:H_2O_2$

(1:200 by volume) solution used by LePore. The pH was measured and found to be

7.3. An average etch rate of approximately 1 Å/sec or (0.01 μm/min) was measured.

LePore, with his Jet Thinning technique, established an etch rate of 0.14 μm/min (or

23 Å/sec). Logan, who also used the $NH_4OH:H_2O_2$ etchant (pH = 7.3) without

agitation, demonstrated an etch rate of approximately 1 μm/hr (or 2.7 Å/sec). The

etch rate measured versus time in etchant solution is shown in Figure 23. The

weight loss method correlates well with Logan's results, but not with LePore's results.

The discrepancy in the weight loss method versus Lepore's results can be attributed

to the jet spray agitation used (27:6442). The Dektak profilometer method reveals

etch rates of 0.8 Å/sec after 100 seconds, 2.2 Å/sec after 150 seconds and 1.2 Å/sec
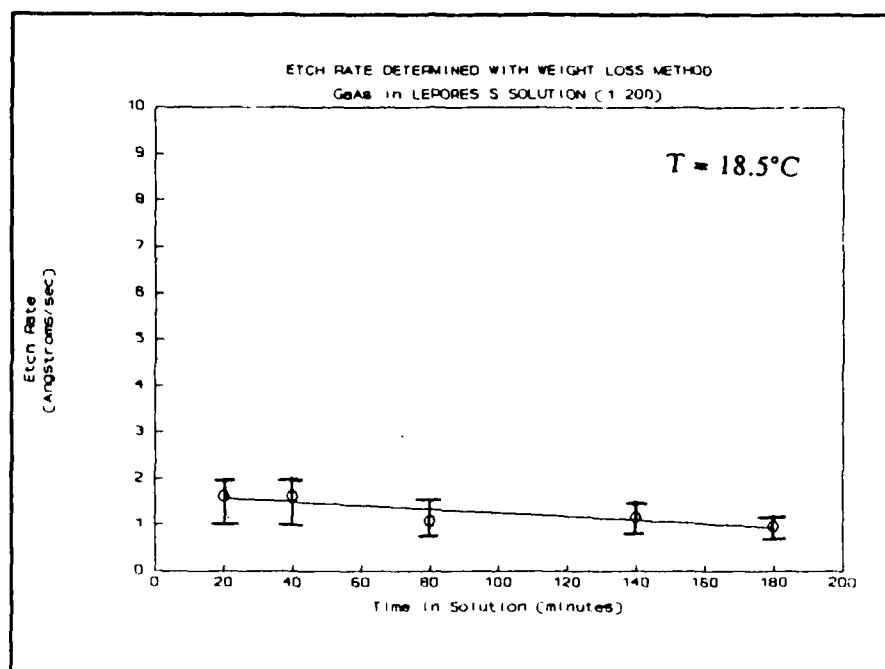
Figure 23. Etch Rate vs Time for GaAs in Lepore's (1:200, pH = 7.3) Etchant Using the Weight Loss Method.

after 250 seconds. Figure 24 shows the etch depth vs time for LePore's etchant. Comparing the weight loss data to the Dektak profilometer measurements shows that on the average, approximately the same etch rate, 1 Å/sec results. Examining the data points of the Dektak profilometer measurements shows that the etch rate is not linear, but more like a stair step process. Logan noted the formation and removal of "oxide sheets" (28:4172). It is hypothesized that the oxides (gallium oxide and arsenic oxide) build up slowly then are dissolved in large layers. During the formation of the oxides, the etch rate is slower and while the oxide layers dissolve, the etch rate is faster. Figure 25 shows the surface of the GaAs wafer after being exposed to the etchant ($NH_4OH:H_2O_2$) for 250 seconds. The surface of the exposed area is left rough and uneven.
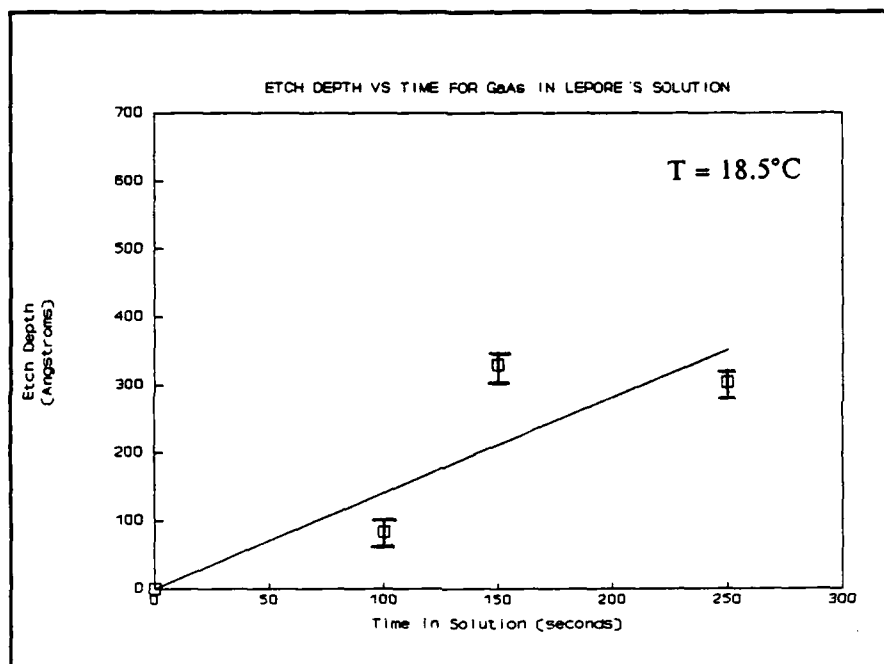
Figure 24. Etch Depth vs Time for GaAs in LePore's (1:200, pH = 7.3) Etchant Using the Dektak Profilometer Method.

The weight loss method provides an etch rate for GaAs and a means for determining an approximate etchant solution composition. For example, if the solution etches away GaAs in a matter of minutes it could be discarded as too fast, and if it took days to detect any weight loss, the etchant would be considered too slow.

Examining the samples under an optical microscope during the procedure showed the silicon nitride (SiN) mask was not completely resistant to the etchants used. There appeared to be some pitting on the surface of the SiN. In some areas the film actually lifted from the substrate. One sample, whose SiN film lifted, was examined with a Scanning Electron Microscope (SEM). Figure 26 is an SEM
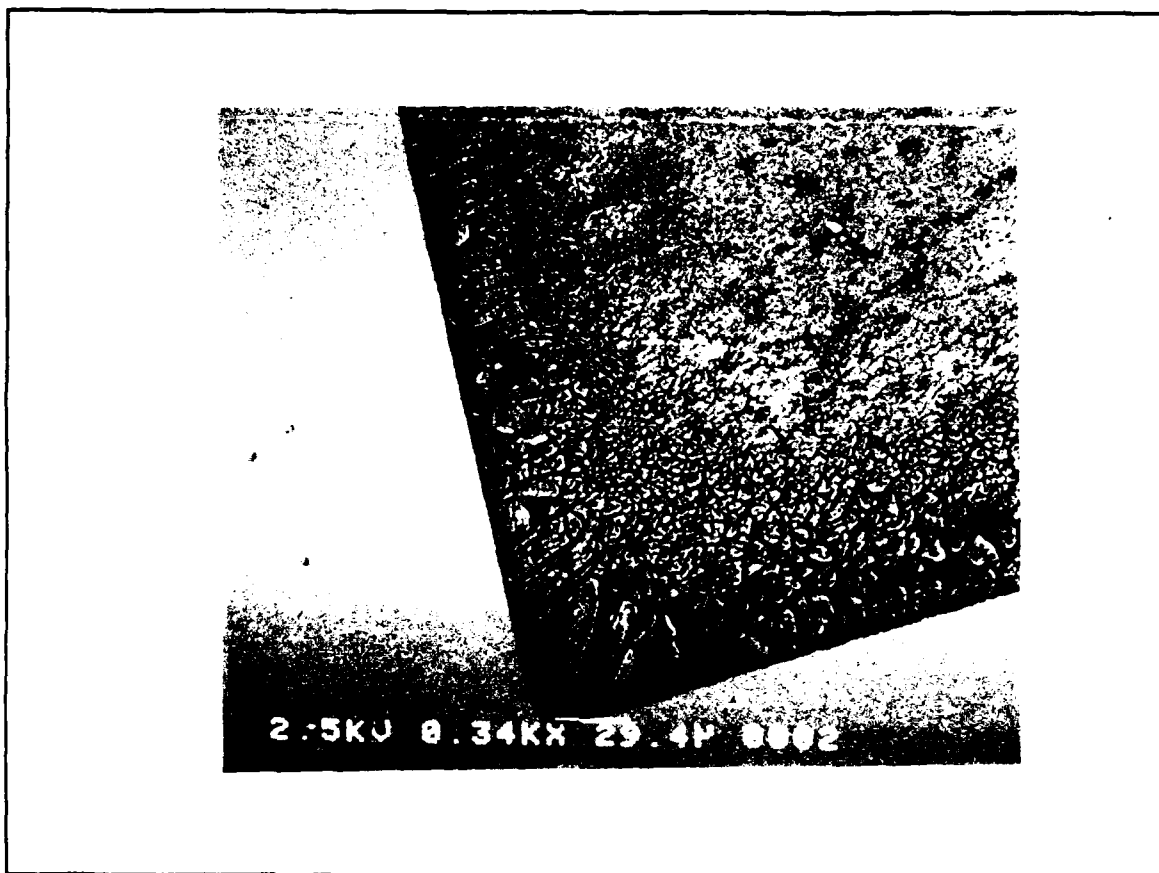
Figure 25.   SEM Photograph of the Surface of GaAs Sample After Being Exposed
to the Lepore (1:200) Etchant for 250 seconds.

photograph that illustrates the GaAs surface and the SiN mask that were exposed

to the etchant. The lower portion of the photograph shows the GaAs surface, and

the upper portion of the photograph shows the blistered SiN mask.

The pitting, blistering and lifting of the silicon nitride prevents high accuracy

measurements of the etch rate of GaAs using the weight loss method. The lifting

of the silicon nitride causes more of the GaAs surface to be exposed to the etchant.

An increased area, (A) in the denominator of Eq (9), results in a slower etch rate.

The pitting of the silicon nitride mask manifests itself as an increased weight loss
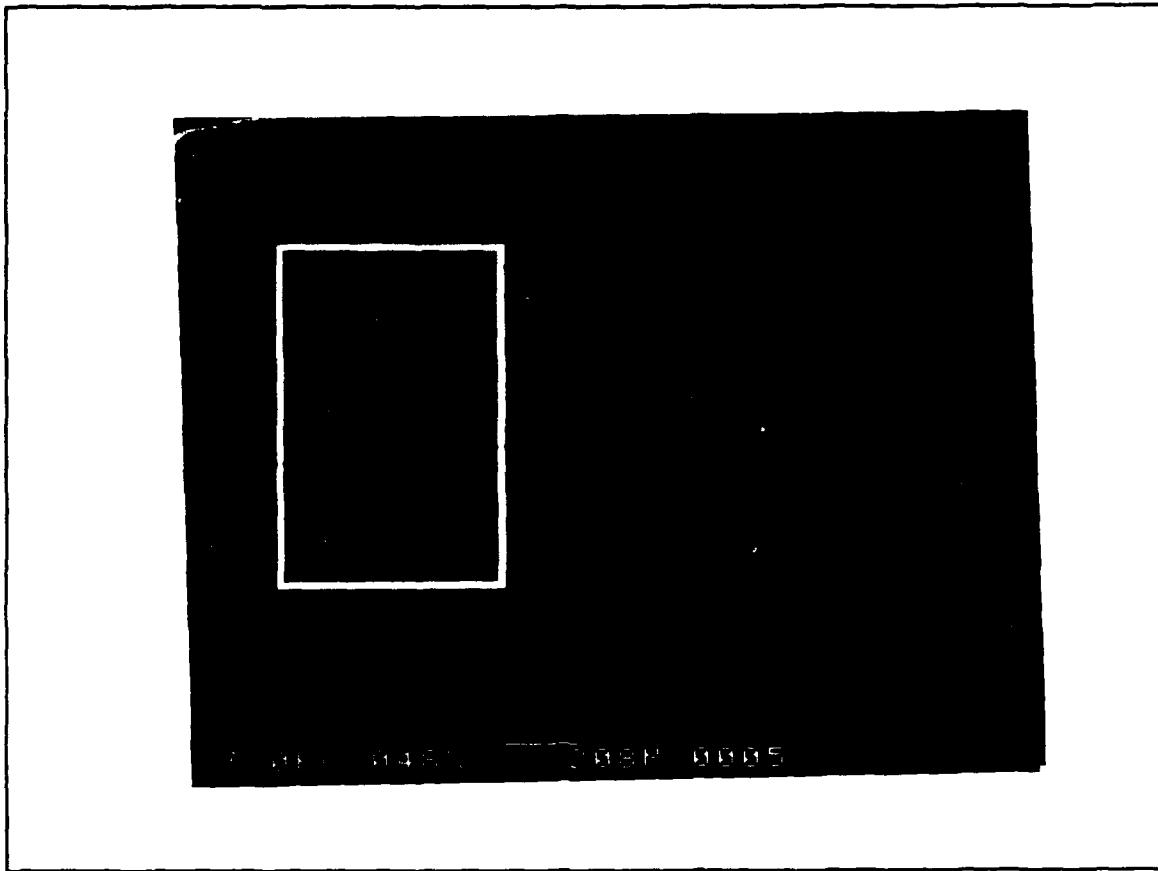
Figure 26.   SEM Photograph of a Blistering and Lifting SiN Mask on a GaAs
             Sample.

(W) in the numerator of Eq (9). The density of SiN is smaller, 2.4 to 2.8 g/cm^3

(48:361) versus 5.32 g/cm^3 (47:849) for GaAs. An increased weight loss would

increase the etch rate. Examining both of these characteristics implies that they

offset each other. Assuming the increased area is on the order of $400 \cdot 10^{-24}$ cm^2

(the approximate blistered area in the SEM photograph), the effect on the etch rate

is insignificant when compared to a large surface area purposely opened in the

silicon nitride (0.484 cm^2 is the area of the mask made in Appendix A). The same

analysis applies equally to the pitting. Because of these effects, the weight loss

58

method is not particularly useful in determining the precise etch rate of GaAs. If a mask could be found that is more resistant to the etchant, a precise etch rate could be obtained. The weight loss method was, however, an adequate tool which identified $NH_4OH:H_2O_2:H_2O$ as a suitable etchant to be used with the Fischione Electropolisher.

Wafer Etching with the Fischione Electropolisher

Etch rates for GaAs were obtained with the Fischione Electropolisher as expected using four different etchant solutions. The solutions investigated were: Gannon's $NH_4OH:H_2O_2:H_2O$ (20:7:973 by volume) solution, LePore's $NH_4OH:H_2O_2$ (1:200 by volume) solution, a composition composed of $NH_4OH:H_2O_2:H_2O$ (1:1:100 by volume) (Test solution), and a composition composed of $NH_4OH:H_2O_2:H_2O$ (3:1:150 by volume) (Lott's solution). The results of each solution are now covered individually and then compared.

Gannon's etchant was used as a control in this portion of the testing. The average etch rate of 0.10 μm/min (or 17 Å/sec) measured for undoped (100) GaAs material using the Fischione Electropolisher compares well to the published etch rate of 0.12 μm/min (or 20 Å/sec) for p-doped (100) GaAs (13:1215) and the etch rate determined in the first experiment (16 Å/sec). Figure 27 depicts time in solution versus the thickness etched. Again a linear etch rate is assumed to simplify etch rate determination. For the Fischione Electropolisher method only two data points were collected for each solution. The data points illustrates some variance of the data; however, the Fischione data correlates satisfactorily with Gannon's published result.
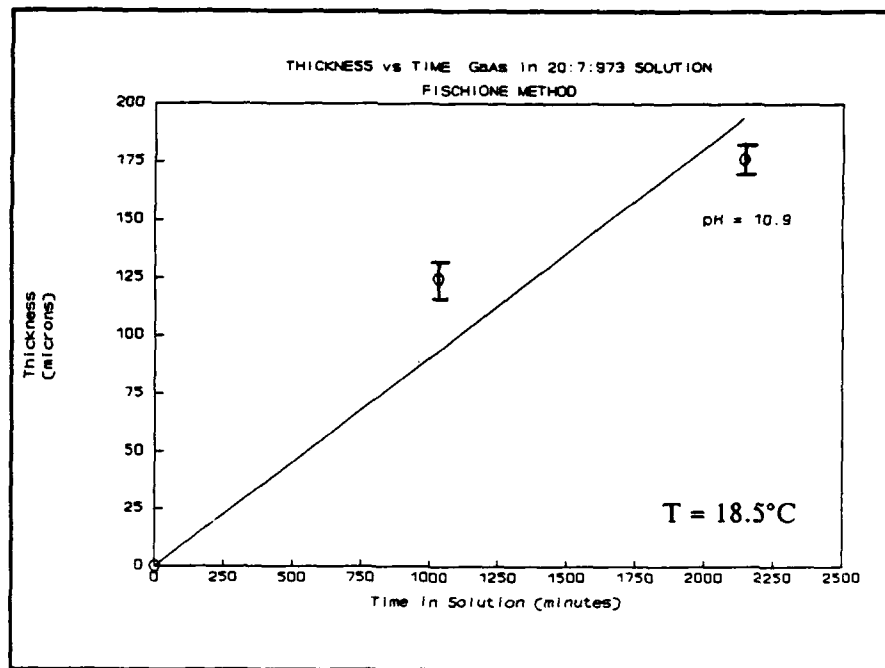
Figure 27. Thickness Etched vs Time for GaAs in Gannon's
Etchant Using the Fischione Method.

The possible reasons for the variance of the data points are discussed at the end of this section.

The next etchant investigated was LePore's $NH_4OH:H_2O_2$ with a volume ratio of 1:200. The resulting pH of the etchant was 7.5. The measured etch rate for this solution was 0.43 μm/min. This measured value is about 3 times faster than the value published by LePore (0.15 μm/min). Figure 28 reveals that the etch rate of this solution is easily reproduced. The difference in etch rate can be accounted for in the temperature differences between the two processes. LePore's published measurements were conducted at 0°C, and this study examined etch rates at 18.5°C. The reduced temperature "slow[s] down the etch rate" (27:6441).

THICKNESS vs TIME GaAs In LEPORES'S SOLUTION
FISCHIONE METHOD
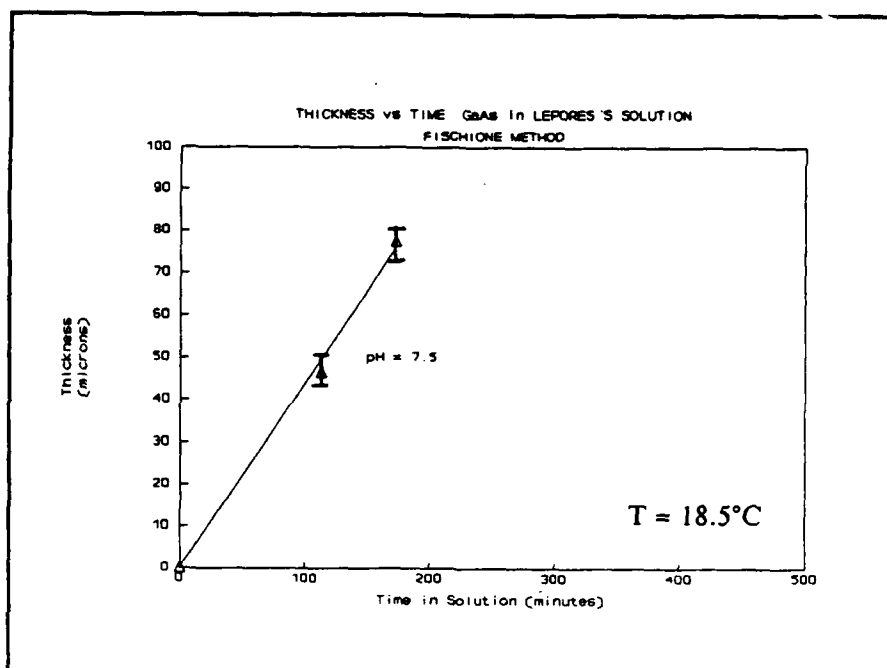
Figure 28. Thickness Etched vs Time for GaAs in LePore's
(1:200) Etchant Using the Fischione Method.

The Test etchant (NH_4OH:H_2O_2:H_2O 1:1:100 by volume) is based upon a composition of 1:1:Z (variable H_2O content) studied by Kohn (25:505). Kohn varied the H_2O component between 16 and 50 and demonstrated an increasing etch rate with a decreasing H_2O component (25:505). The etch rates measured with the Fischione Electropolisher are displayed in Figure 29. For a solution pH of 10.6 (normal solution composition), an etch rate of 0.115 μm/min was measured. With the solution pH lowered to 10.0 (by the addition of H_2SO_4), the etch rate determined was 0.092 μm/min. The solution with the lower pH value produced a slower etch rate.

The final solution investigated was the NH_4OH:H_2O_2:H_2O (3:1:150 by volume) etchant used by Lott in a previous study (29). The etch rate for GaAs was
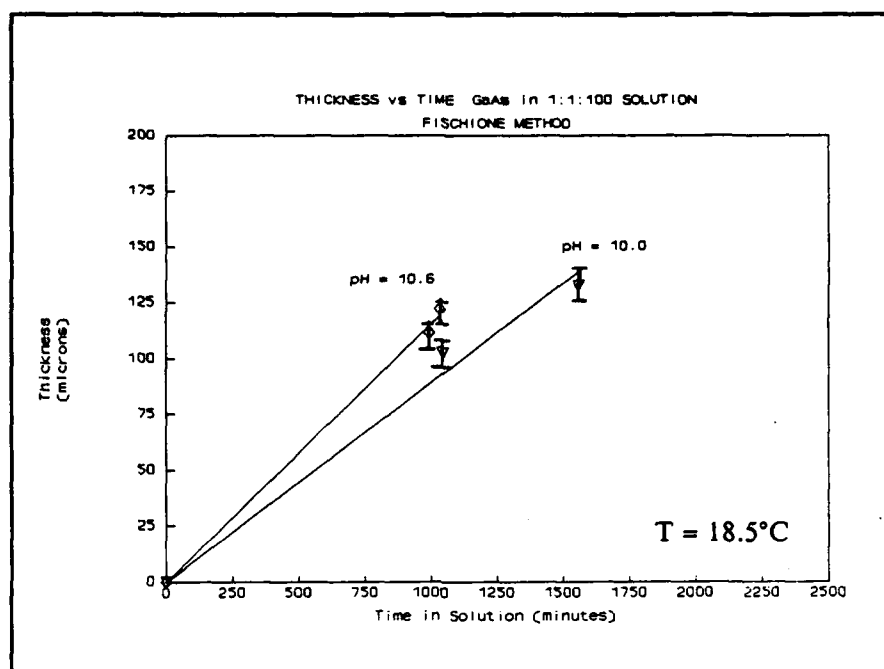
Figure 29. Thickness Etched vs Time for GaAs in the Test NH₄OH:H₂O₂:H₂O (1:1:100 by volume) Etchant Using the Fischione Method.

determined at 3 different pH values of the solution. Figure 30 shows the etch rates for the different pH values of the etchant. The unaltered pH of the 3:1:150 solution is 10.8. An etch rate of 0.11 μm/min (or 18Å/sec) was measured for this pH. The measured value differs with the value of 30 Å/sec assumed by Lott. With addition of H_2SO_4 the pH was lowered to 10.2. The etch rate measured at this pH was 0.076 μm/min. Reducing the pH to 7.2, correspondingly decreased the measured etch rate to 0.051 μm/min. The reduction in the pH value produces a parallel reduction in the etch rate. Examination of the Test etchant and Lott's etchant (both with the composition $NH_4OH:H_2O_2:H_2O$) reveal a trend of decreasing etch rate with the reduction of pH.
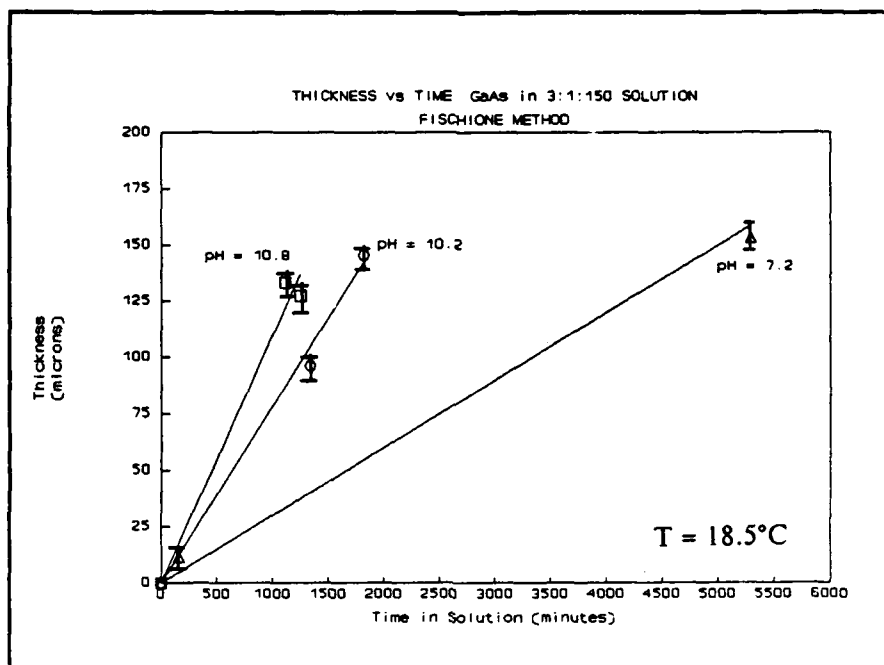
Figure 30. Thickness Etched vs Time for GaAs in Lott's
NH$_4$OH:H$_2$O$_2$:H$_2$O (3:1:150 by volume) Etchant
Using the Fischione Method.

A comparison of the different etchants studied using the Fischione
Electropolisher is shown in Figure 31. The fastest etch rate was produced by
Lepore's NH$_4$OH:H$_2$O$_2$ (1:200, pH = 7.5) solution. Reduction of the pH slowed
the etch rate in both the 1:1:100 and the 3:1:150 (NH$_4$OH:H$_2$O$_2$:H$_2$O) solution
compositions. Lepore also noted a decreased etch rate with a reduced pH value.
The Fischione Electropolisher is an adequate means for determining etch rates of
semiconductor materials. However, the configuration of the system prevents
extremely accurate determination of etch rates which result in a error associated with
the measured data.
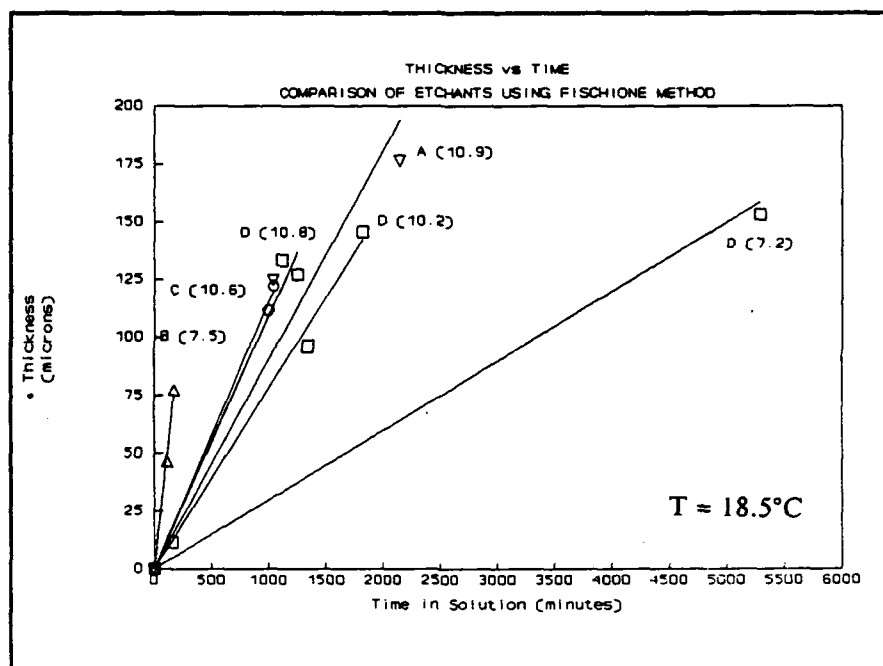
Figure 31. Comparison of Etchants Using Fischione Method.
A: Gannon's Etchant; B: LePore's (1:100) Etchant;
C: Test NH$_4$OH:H$_2$O$_2$:H$_2$O (1:1:100); D: Lott's
3:1:150 Etchant. Numbers in Parentheses indicate
pH.

The errors associated with the measurement of etch rates centers on the

ability to accurately determine the thickness of the material to be etched and proper

alignment of the sample in the Fischione Electropolisher specimen holder. The

Bausch & Lomb optical gauge used to evaluate the thickness of the GaAs samples

had an accuracy of ±1.2 μm. The determination of the thickness of the dimpled

area added even more chance for error. Because of the arc of the dimpled area the

smallest thickness may not have been measured. Another factor that adds a source

of error is the alignment of the sample in the specimen holder. The dimpled area

of the samples is approximately 4 mm in diameter. The opening in the specimen

64

holder is only 1.4 mm in diameter. There exists a possibility that improper alignment could prevent the thinnest area of the sample from being exposed to the etchant.

Determination of the etch rates of n-$Al_xGa_{1-x}As$ with the Fischione Electropolisher was attempted, however no valid results were obtained. The samples tested had a 0.5 μm thick silicon doped $Al_xGa_{1-x}As$ layer grown by MBE on a GaAs substrate. Calculations revealed that light with the wavelength between 689 nm and 873 nm would not pass through the GaAs, but would pass through the $Al_xGa_{1-x}As$, for $x \geq 0.3$. LePore's $NH_4OH:H_2O_2$ etchant (1:100) demonstrated a selectivity of approximately 30 (27:6441). It was used in an attempt to remove the GaAs substrate so that etch rates for the n-$Al_xGa_{1-x}As$ could be determined. The first trial utilized a No. 29 red Kodak Wratten gelatin filter having a peak spectral response at 750 nm. The sample was removed from the Fischione Electropolisher when the alarm sounded and examined under a microscope. The examination revealed that perforation of both the GaAs and the $Al_xGa_{1-x}As$ had occurred. Figure 32 shows a SEM photograph of a sample etched using the red Kodak filter. The small dark area in the lower right is the spot of perforation. Light could be seen through the hole with the eye. Another sample was attempted with identical results. The Kodak filter was characterized and the actual cutoff of the filter was about 650 nm. This value is outside the calculated wavelength. To achieve a much more narrow spectral response, a diffraction filter centered at 700 nm was attempted. The result was the same; both layers were perforated.

Figure 32.   SEM Photograph of $Al_{0.3}Ga_{0.7}As/GaAs$ Sample Removed From LePore's (1:100) Etchant Immediately After the Alarm Triggered.

Two possible explanations are offered.   First, the silicon doping of the $Al_xGa_{1-x}As$ epitaxial layer introduces an additional allowed energy state in the energy bandgap of the material.   Assuming the ionization energy for silicon in $Al_xGa_{1-x}As$ is the same for GaAs, 0.0058 eV (48:32), the effective λ_c must be recalculated.   The recalculated λ_c is 692 nm.   The diffraction filter passed wavelengths between 698 and 711 nm with the peak at 700 nm.   It is possible that the energy of the light was absorbed by the silicon dopant, which would occupy an energy state the energy bandgap.   The other reasonable explanation centers on the thickness of the film and

66

the actual etch rate of the solution. The preferential etching of GaAs could work against the process. If the surface of the sample exposed to the etchant was not removed uniformly (e.g., the (111)As face, which etches at a faster rate than the (111)Ga face), a small area of the $Al_xGa_{1-x}As$ could be exposed to the etchant and be removed before the area was large enough to trigger the alarm. This process would continue until enough photons of light source passed through the film and trigger the alarm. The etch rate of the 1:100 $NH_4OH:H_2O_2$ solution is 1.5 μm/min. Assuming a selectivity of 30, the etch rate of $Al_xGa_{1-x}As$ would be 0.05 μm/min. This implies that 10 minutes are needed to remove 0.5 μm of $Al_xGa_{1-x}As$. If the (111)As face is the area exposed to the etchant, it follows that an even larger etch rate could be expected. It is also possible that the epitaxial layer was not grown to a thickness of 0.5 μm as specified. The thinner the layer the more pronounced the above effect would be. Figure 33 shows a cross-sectional view of the sample MBE G02. The epitaxial layer is the shaded area just above the distance marker. It appears to be approximately 0.35 μm, less than 0.5 μm. It is possible that a combination of two mechanisms proposed above prevents an accurate measurement of the etch rate of n-$Al_xGa_{1-x}As$ with the Fischione Electropolisher.

Etch Depth Measurements

To complete the study of etching $Al_{0.15}Ga_{0.85}As$, $Al_{0.30}Ga_{0.70}As$ and p^+ GaAs, step height measurements using a Dektak profilometer were accomplished. The results of these measurements are now presented. Figure 34 compares the etch depths for $Al_{0.15}Ga_{0.85}As$, $Al_{0.30}Ga_{0.70}As$ and p^+ GaAs in the
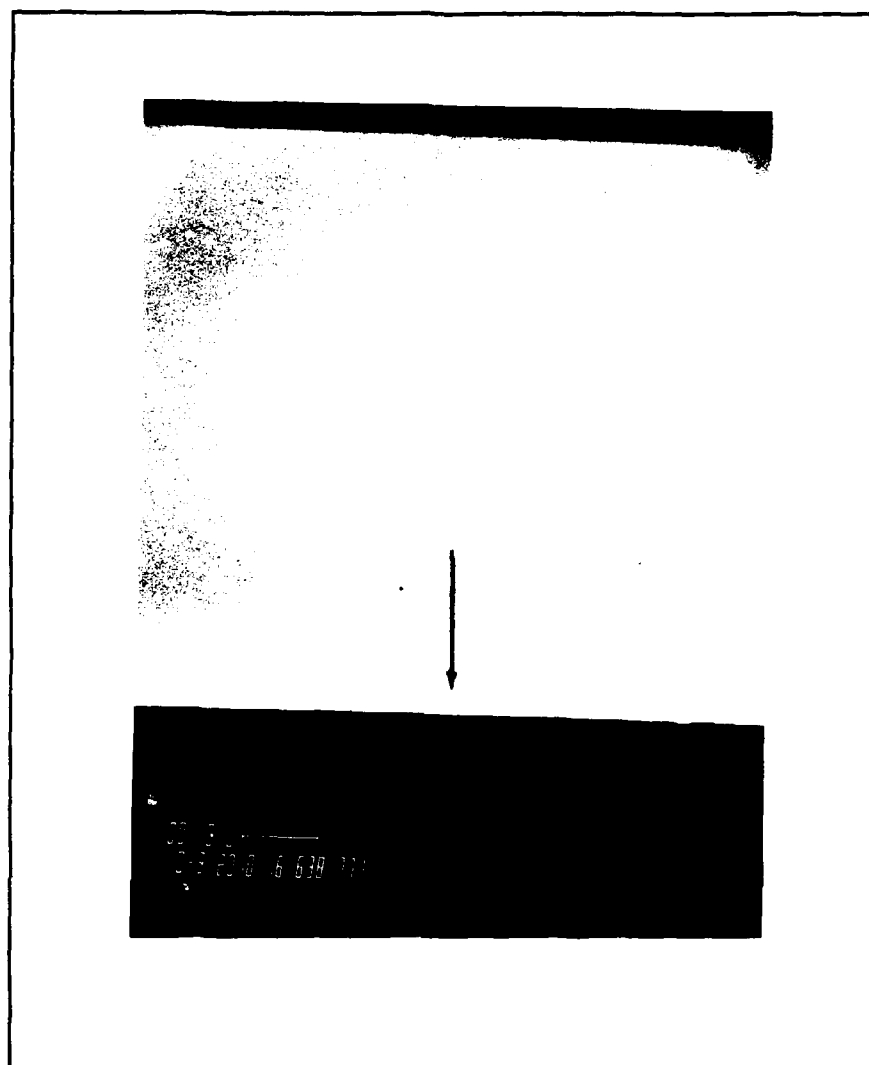
Figure 33. SEM Photograph of Specimen MBE G02 illustrating the Epitaxial Layer Thickness of $Al_{0.3}Ga_{0.7}As$ on GaAs.

$NH_4OH:H_2O_2:H_2O$ (3:1:150 by volume). The pH of the etchant was 10.8. As the graph shows, the etch rate does not significantly change for the various materials. Measured etch rates were 24, 15 and 18 Å/sec for p^+ GaAs, $Al_{0.15}Ga_{0.85}As$ and $Al_{0.3}Ga_{0.7}As$, respectively.
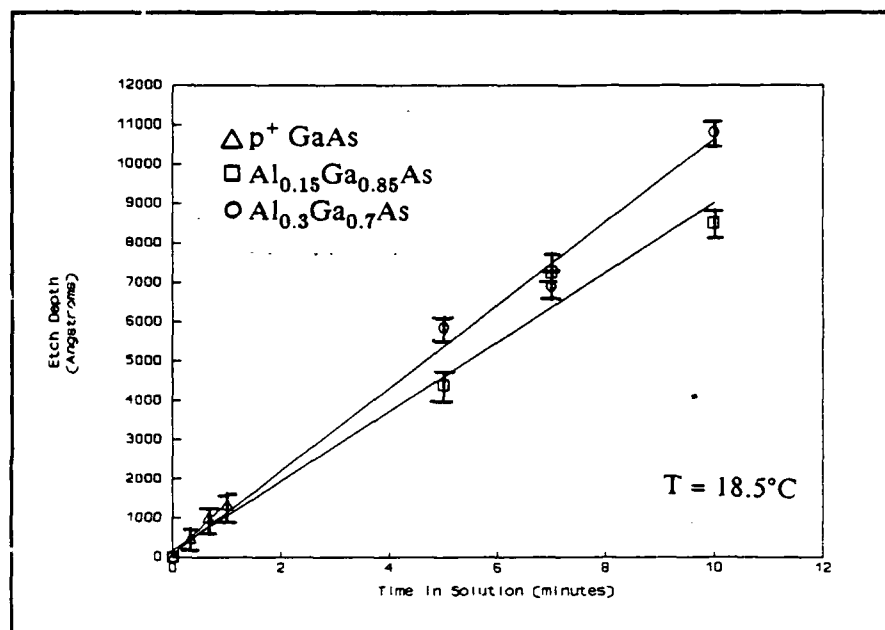
Figure 34. Etch Depth vs Time in Lott's $NH_4OH:H_2O_2:H_2O$
(3:1:150) Etchant for p^+ GaAs, $Al_{0.15}Ga_{0.85}As$ and
$Al_{0.3}Ga_{0.7}As$ Using the Dektak Profilometer Method.

Figure 35 shows a comparison of the etch depths for p^+ GaAs,
$Al_{0.15}Ga_{0.85}As$ and $Al_{0.3}Ga_{0.7}As$ in the $NH_4OH:H_2O_2:H_2O$ (1:1:100 by volume)
etchant. The measured pH of the solution was 10.6. Again, the graph shows the
etch rate for does not significantly change for the various materials. Measured etch
rates were 35, 23 and 16 Å/sec for p^+ GaAs, $Al_{0.15}Ga_{0.85}As$ and $Al_{0.3}Ga_{0.7}As$,
respectively. Neither of these etchants would be suitable for the selective removal
of a GaAs layer from a $GaAs/Al_xGa_{1-x}As$ interface.

When both of these solutions had their pH reduced to 7.2 ± 0.1, the etch
rates for the three materials decreased. Figure 36 shows the etch depth versus time
for the 3:1:150 pH adjusted etchant. The measured etch rate for p^+ GaAs was
approximately 1 Å/sec. For the $Al_{0.15}Ga_{0.85}As$ no step height was discernable until

69
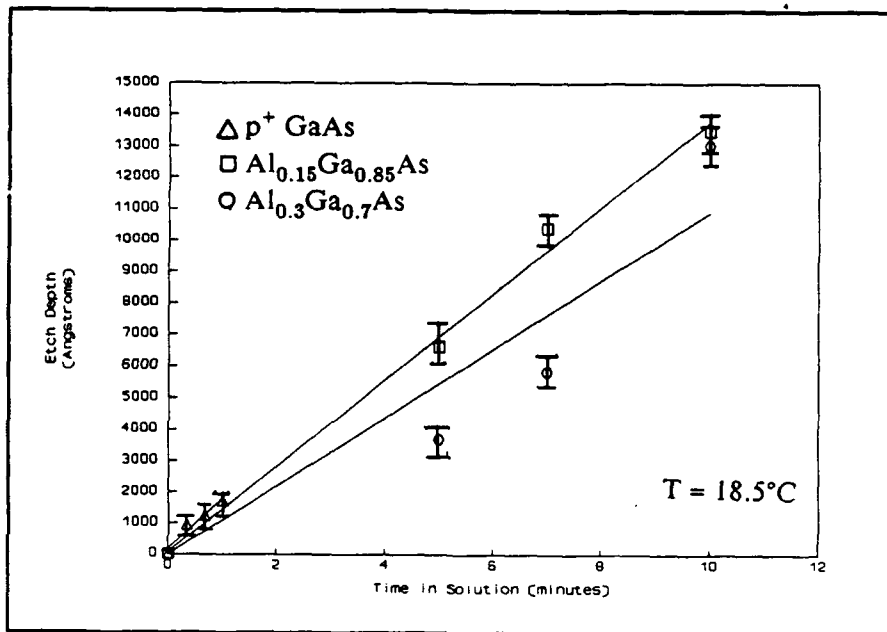
Figure 35. Etch Depth vs Time in the Test $NH_4OH:H_2O_2:H_2O$ (1:1:100) Etchant for p^+ GaAs, $Al_{0.15}Ga_{0.85}As$ and $Al_{0.3}Ga_{0.7}As$ Using the Dektak Profilometer Method.
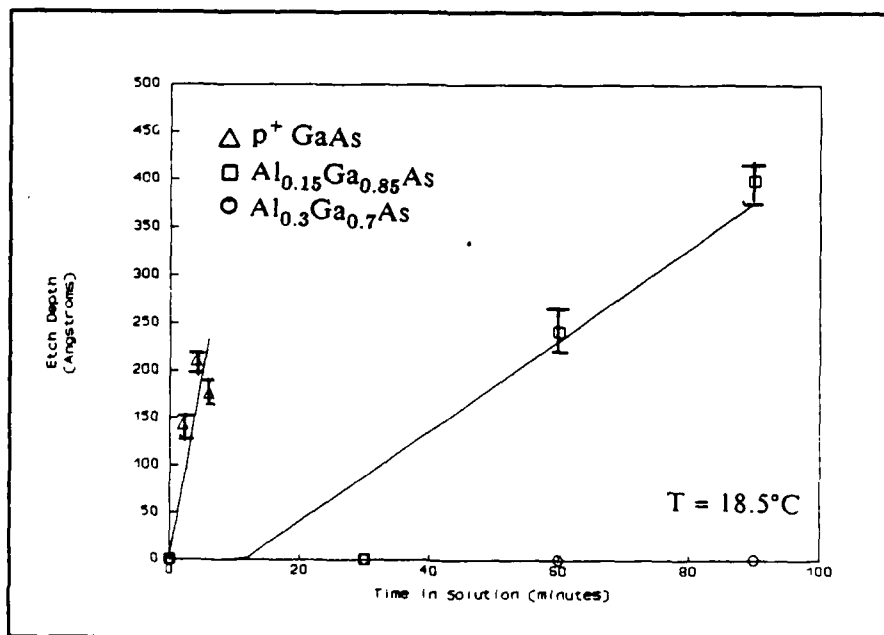
Figure 36. Etch Depth vs Time in $NH_4OH:H_2O_2:H_2O$ (3:1:150, pH = 7.3) Etchant for p^+ GaAs, $Al_{0.15}Ga_{0.85}As$ and $Al_{0.3}Ga_{0.7}As$ Using the Dektak Profilometer Method.

70

the sample had been exposed to the etchant for 60 minutes. The average etch rate for $Al_{0.15}Ga_{0.85}As$ was about 0.1 Å/sec. When the $Al_{0.3}Ga_{0.7}As$ samples were placed in the etchant for up to 90 minutes, no measurable step was observed. The etch rate is effectively zero. That is, the $Al_{0.3}Ga_{0.7}As$ appears to act as a etch-stop in a p^+ GaAs/$Al_{0.3}Ga_{0.7}As$ heterojunction structure.

The etch depth vs time for p^+ GaAs, $Al_{0.15}Ga_{0.85}As$ and $Al_{0.3}Ga_{0.7}As$ in the $NH_4OH:H_2O_2:H_2O$ (1:1:100 pH adjusted to 7.3) is illustrated in Figure 37. The pH adjusted 1:1:100 etchant displayed results similar to Lott's pH adjusted solution. The etch rate of the p^+ GaAs was faster than that of either the $Al_{0.15}Ga_{0.85}As$ or the
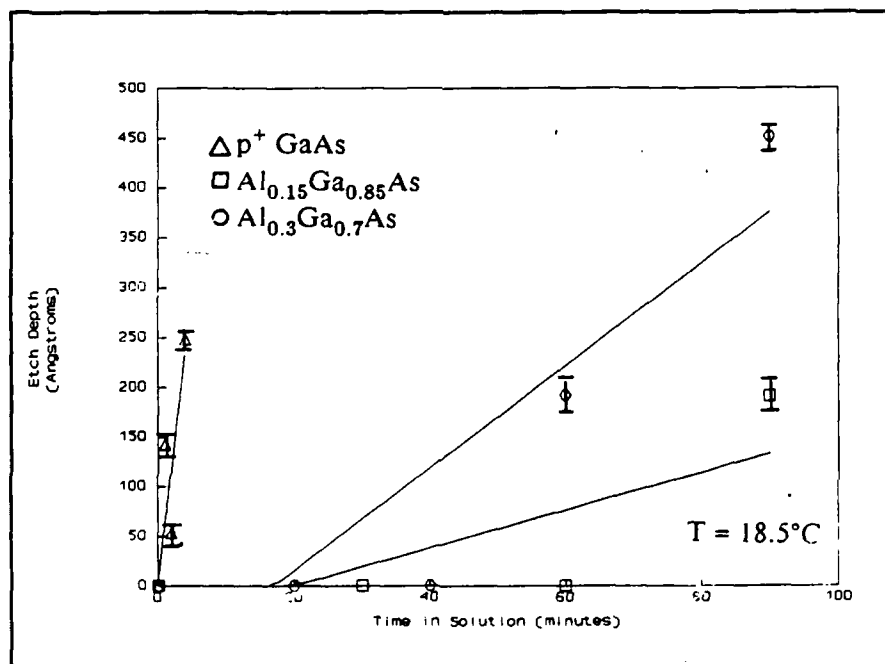
Figure 37. Etch Depth vs Time in the Test $NH_4OH:H_2O_2:H_2O$ (1:1:100   pH = 7.2)   Etchant   for p^+ GaAs, $Al_{0.15}Ga_{0.85}As$ and $Al_{0.3}Ga_{0.7}As$ Using the Dektak Profilometer Method.

$Al_{0.3}Ga_{0.7}As$ material. The measured etch rates for p^+ GaAs, $Al_{0.15}Ga_{0.85}As$ and $Al_{0.3}Ga_{0.7}As$ were approximately 1 Å/sec, 0.04 Å/sec and 0.07 Å/sec, respectively. The etch rates for the $Al_{0.15}Ga_{0.85}As$ and the $Al_{0.3}Ga_{0.7}As$ do not respond to pH adjustment in this solution as in the other solutions. Lepore showed that the higher the mole fraction of Al, the slower the etch rate (27:6442).

The etch depths vs time for Gannon's etchant is seen in Figure 38. It shows a slightly larger difference in the slopes (average etch rates) of the lines between p^+ GaAs and $Al_xGa_{1-x}As$, than Lott's etchant (pH = 10.8) and the Test etchant (pH = 10.6). The measured etch rates for p^+ GaAs, $Al_{0.15}Ga_{0.85}As$ and
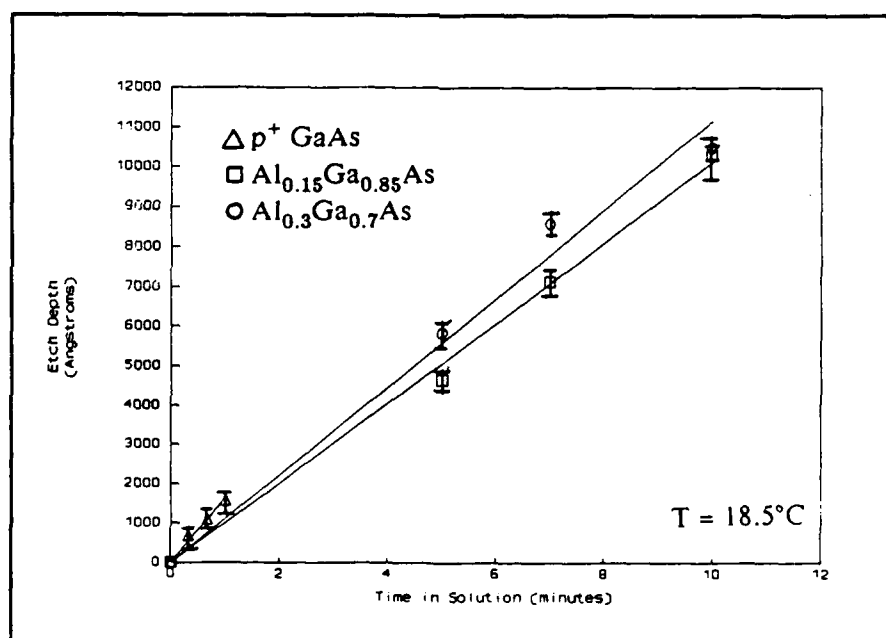
Figure 38. Etch Depth vs Time in Gannon's Etchant for p^+ GaAs, $Al_{0.15}Ga_{0.85}As$ and $Al_{0.3}Ga_{0.7}As$ Using the Dektak Profilometer Method.

$Al_{0.3}Ga_{0.7}As$ were 29, 17 and 19 Å/sec, respectively. However, the ratio of the p^+ GaAs etch rate to the $Al_{0.3}Ga_{0.7}As$ etch rate (or selectivity) is only 1.5.

LePore's (1:100) etchant shown in Figure 39 displays the largest difference in etch rates for p^+ GaAs and $Al_xGa_{1-x}As$. The etch rate for p^+ GaAs is 68 Å/sec. For $Al_{0.15}Ga_{0.85}As$ it is 5 Å/sec and for $Al_{0.3}Ga_{0.7}As$, 2 Å/sec. The selectivity of the etchant for p^+ GaAs relative to $Al_{0.3}Ga_{0.7}As$ is 34. This behavior illustrates that the p^+ GaAs etches much faster than the $Al_xGa_{1-x}As$.
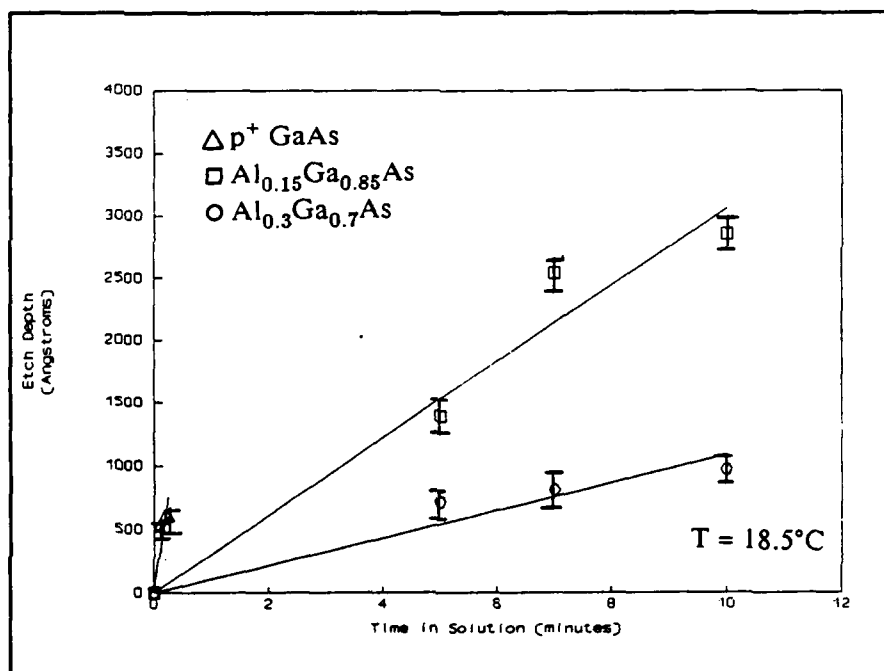
Figure 39. Etch Depth vs Time in LePore's (1:100) Etchant for p^+ GaAs, $Al_{0.15}Ga_{0.85}As$ and $Al_{0.3}Ga_{0.7}As$ Using the Dektak Profilometer Method.

Summary

Table 3 presents a summary of the different etchants studied, the etch rates of the different materials, the methods used and calculated selectivities. The etch rates are accurate within ±15 percent. The weight loss method provided etch rates for GaAs and an easy method for narrowing the selection of an etchant. Problems with the lifting of the SiN mask prevented an accurate measurement of the etch rates for GaAs. The Fischione Electropolisher also provided etch rates for GaAs. The results revealed that reducing the pH of the etchants containing water reduced the etch rate. The inability of the Fischione Electropolisher to determine etch rates for n-doped $Al_xGa_{1-x}As$ is thought to be caused by a combination of the $Al_xGa_{1-x}As$ layer thickness (too thin) and the absorbing effect of the silicon doping. The etch depth measurements revealed the selectivity of the different etchant(s). Figure 40 summarizes the etch rates of the different etchants and the different materials. From this graph, the selectivity of each etchant can be calculated with the ratio of the etch rate of p^+ GaAs to the material in question (i.e., $Al_{0.3}Ga_{0.7}As$). The selectivity is lowest, approximately 1, for GaAs/$Al_xGa_{1-x}As$ using the 3:1:150 and the 20:7:973 compositions of the $NH_4OH:H_2O_2:H_2O$ etchant, and highest approximately 34, for the p^+ GaAs/$Al_{0.3}Ga_{0.7}As$ in Lepore's (1:100, pH =7.8) etchant. The 3:1:150 pH adjusted etchant reveals a slow etch rate for p^+ GaAs and virtually no etching of the $Al_{0.3}Ga_{0.7}As$ material, which indicates a very high selectivity.

To simulate the removal of the p^+ GaAs layer as required in the last fabrication step of an (ES)MODFET, several samples of the MBE F98 specimen

74

Table 3.   Etch Rates, Etch Methods and Selectivities for Etchants Investigated.

Etchant Ratio (pH) $(NH_4OH:H_2O_2:H_2O)$	Material	Etch Rate (Å/sec)	Method	Selectivity $\dfrac{GaAs}{Al_{0.3}Ga_{0.7}As}$
20:7:973 (pH 10.9)	GaAs	16	WLM	
20:7:973 (pH 10.9)	GaAs	23	DP	1
1:200:0 (pH 7.3)	GaAs	1	WLM	
1:200:0 (pH 7.3)	GaAs	1	DP	
20:7:973 (pH 10.9)	GaAs	17	FEP	1
1:1:100 (pH 10.6)	GaAs	19	FEP	1
1:1:100 (pH 10.0)	GaAs	15	FEP	
3:1:150 (pH 10.8)	GaAs	18	FEP	1
3:1:150 (pH 10.2)	GaAs	13	FEP	
3:1:150 (pH 7.2)	GaAs	9	FEP	*
1:200:0 (pH 7.3)	GaAs	72	FEP	

Etchant Ratio (pH) $(NH_4OH:H_2O_2:H_2O)$	Material	Etch Rate (Å/sec)	Method	$\dfrac{p^+ GaAs}{Al_{0.3}Ga_{0.7}As}$
20:7:973 (pH 10.9)	$Al_{0.3}Ga_{0.7}As$	19	DP	1.5
3:1:150 (pH 10.8)	$Al_{0.3}Ga_{0.7}As$	18	DP	1.5
3:1:150 (pH 7.3)	$Al_{0.3}Ga_{0.7}As$	0	DP	*
1:1:100 (pH 10.6)	$Al_{0.3}Ga_{0.7}As$	16	DP	2
1:1:100 (pH 7.2)	$Al_{0.3}Ga_{0.7}As$	0.1	DP	10
1:100:0 (pH 7.8)	$Al_{0.3}Ga_{0.7}As$	2	DP	34

Etchant Ratio (pH) $(NH_4OH:H_2O_2:H_2O)$	Material	Etch Rate (Å/sec)	Method	$\dfrac{p^+ GaAs}{Al_{0.15}Ga_{0.85}As}$
20:7:973 (pH 10.9)	$Al_{0.15}Ga_{0.85}As$	17	DP	1.5
3:1:150 (pH 10.8)	$Al_{0.15}Ga_{0.85}As$	15	DP	1.5
3:1:150 (pH 7.3)	$Al_{0.15}Ga_{0.85}As$	0.07	DP	11.5
1:1:100 (pH 10.6)	$Al_{0.15}Ga_{0.85}As$	23	DP	1.5
1:1:100 (pH 7.2)	$Al_{0.15}Ga_{0.85}As$	0.04	DP	25
1:100:0 (pH 7.8)	$Al_{0.15}Ga_{0.85}As$	5	DP	13.5
20:7:973 (pH 10.9)	p^+ GaAs	29	DP	
3:1:150 (pH 10.8)	p^+ GaAs	24	DP	
3:1:150 (pH 7.3)	p^+ GaAs	0.8	DP	
1:1:100 (pH 10.6)	p^+ GaAs	35	DP	
1:1:100 (pH 7.2)	p^+ GaAs	1	DP	
1:100:0 (pH 7.8)	p^+ GaAs	68	DP	

* Selectivity undefined (division by 0)   WLM - Weight Loss Method
DP - Dektak Profilometer   FEP - Fischione Electropolisher
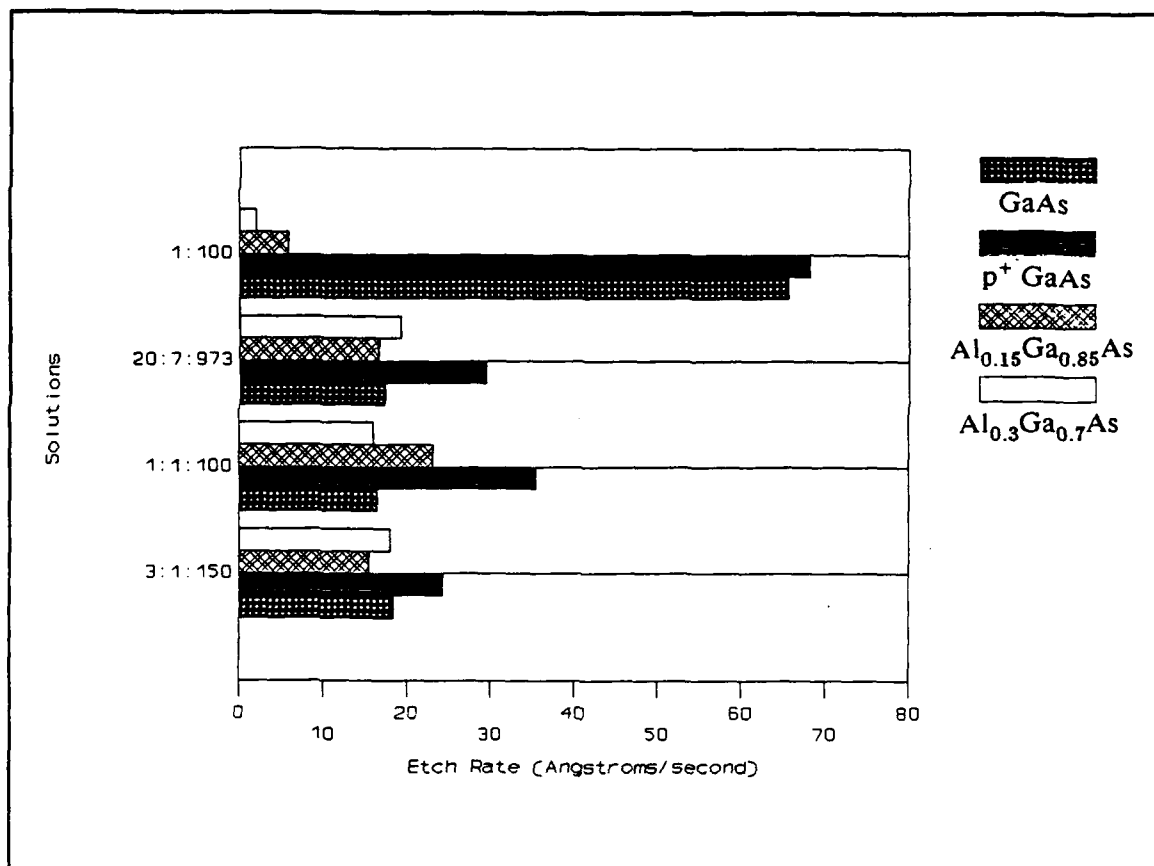
Figure 40. Comparison of Etch Rates for Different Etchant Compositions and Materials.

(500 Å of p^+ GaAs grown on 0.5 μm of $Al_{0.3}Ga_{0.7}As$) were masked and placed in LePore's 1:100 etchant. At specific times, samples were removed and the etch depth measured. Figure 41 displays the results of these measurements. As illustrated, the etch rate drastically changes after a depth of approximately 500 Å. This feature indicates that the p^+ GaAs is removed and there is minimal attack by the etchant on the $Al_{0.3}Ga_{0.7}As$ layer. The $NH_4OH:H_2O_2$ (1:100 by volume) and the pH adjusted $NH_4OH:H_2O_2:H_2O$ (3:1:150 by volume) etchants display the characteristics

76

required to efficiently remove the p^+ GaAs from between the gate-and-drain and the gate-and-source when fabricating an (ES)MODFET.
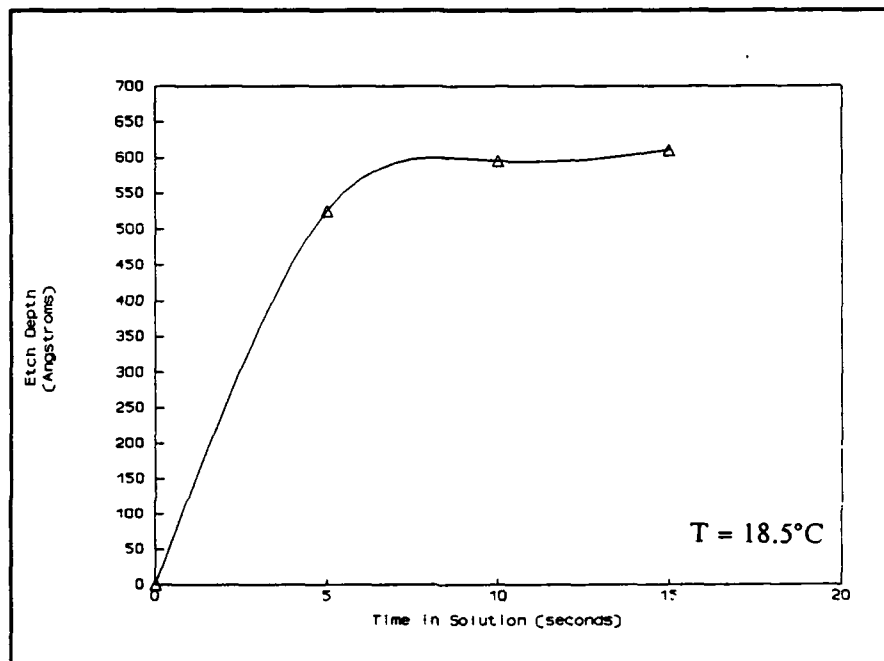
Figure 41. Removal of the 500 Å Thick Layer of p^+ GaAs From a p^+ GaAs/Al$_{0.3}$Ga$_{0.7}$As Heterointerface.

V. Conclusions and Recommendations

The purpose of this study was to determine the etch rate of p^+ GaAs, GaAs, $Al_xGa_{1-x}As$ and n-$Al_xGa_{1-x}As$ (x = 0.15 and x = 0.30) in various etchants to realize the removal of the p^+ GaAs layer between the gate-and-drain and the gate-and-source of an (ES)MODFET. Three different techniques were used to measure the etch rates of the materials. This Chapter contains a summary of the results and provides recommendations for further study.

Conclusions

1. The etchant that displayed the highest selectivity (GaAs etch rate divided by the $Al_xGa_{1-x}As$ etch rate), was the $NH_4OH:H_2O_2$ etchant solution (1:100 by volume). The etch rate for p^+ GaAs was 68 Å/sec and the etch rate for $Al_{0.3}Ga_{0.7}As$ was 2 Å/sec, resulting in selectivity of 34. All etch rates measured have an accuracy of ±20 percent. This etchant displays the characteristics required (removal of the p^+ GaAs layer without attacking the $Al_xGa_{1-x}As$ layer) in the final fabrication step of an (ES)MODFET.

2. The $NH_4OH:H_2O_2:H_2O$ etchant solution (3:1:150 by volume) was pH adjusted to 7.3 and resulted in an etch rate of 0.8 Å/sec for p^+ GaAs, and it virtually displayed a zero etch rate for $Al_{0.3}Ga_{0.7}As$. The selectivity for this etchant could not be determined from the experimental data. In addition this etchant displayed the added advantage of a slower etch rate for p^+ GaAs. It also should produce the desired results for the last fabrication step of an (ES)MODFET.

3. The $NH_4OH:H_2O_2:H_2O$ etchant solution (3:1:150 by volume) used by Lott in his study does not display a significant selectivity when etching GaAs versus $Al_xGa_{1-x}As$. This etchant should not be used for the removal of GaAs from a $GaAs/Al_xGa_{1-x}As$ interface. It is more suitable for a mesa etch, where it will remove both materials and achieve the objective of isolating the active device areas.

4. The weight loss method based on Fontana's corrosion testing of metals provided etch rates for the semiconductors materials as predicted by the theory. Problems with pitting, blistering and lifting of the SiN mask prevented precise measurement of etch rates. However, this technique did provide a means for narrowing the scope of perspective etchants for subsequent study. This method does not provide any insight in the preferential etching properties of the material or etchant being investigated.

5. The Fischione Electropolisher produced etch rates for the GaAs material. The inability of the Fischione Electropolisher to detect removal of GaAs from the $GaAs/n-Al_xGa_{1-x}As$ interface obstructed the measurement of the etch rate for $n-Al_xGa_{1-x}As$ epitaxial layers. The combination of an improper source wavelength and the layer's thickness (0.35 μm) is believed to be the cause for this failure. In addition the Fischione Electropolisher does not provide information on the preferential characteristics of the material or etchant under study.

6. It was determined that when the pH of an etchant (of the $NH_4OH:H_2O_2:H_2O$ composition) is decreased with the addition of H_2SO_4, the corresponding etch rate was also reduced. The reduced etch rate seem to be independent of the original volume ratio of the etchant.

Recommendations

The following list presents logical extensions of the work accomplished in this thesis. They are:

1. Investigate the characteristics of the $NH_4OH:H_2O$ etchant solution (1:100 by volume) and the etchant solution $NH_4OH:H_2O:H_2O$ (3:1:150 by volume) that are pH adjusted (i.e., Is there an enhanced etch rate at mask edges?) with respect to the small mask geometries (approximately 1 to 3 μm spacings) required for fabrication of the (ES)MODFET.

2. The affects of the above two etchants on the gate, drain and source metals (used as an etch mask for the last fabrication step) should be evaluated.

3. Examine the preferential characteristics, if any, of the $NH_4OH:H_2O_2:H_2O$ (3:1:150 by volume) and the $NH_4OH:H_2O_2$ (1:100 by volume) etchant solutions that are pH adjusted.

4. Investigate the etch rates of $Al_xGa_{1-x}As$ and n-$Al_xGa_{1-x}As$ with the Fischione Electropolisher using thicker epitaxial layers. A tunable monochromatic light source would aid the investigator in selectively removing the GaAs from a GaAs/$Al_xGa_{1-x}As$ interface.

5. Fabricate the (ES)MODFET with the previously mentioned etchants and compare the DC device characteristics of (ES)MODFETs versus different etch times on the p^+ GaAs layer between the gate-and-drain and the gate-and-source. The DC characteristics should aid the determination of the effectiveness of the etchants.

Appendix A

Etch Rate Baseline Experimental Procedures

This appendix describes the different procedures and processes used to determine the baseline etch rates utilizing the corrosion method described in Chapter III.

Mask Fabrication

To precisely control the area exposed to the etchant, a mask was fabricated at the AFIT Cooperative Electronic Materials and Processing Laboratory, Room 1065, Building 125. The final dimensions desired for the mask were approximately 7 mm x 7 mm. The following steps were accomplished to produce the mask.

1.0. A Coordinatograph table was used to prepare a mask pattern in Rubylith.

   1.1. Secure the Rubylith on the Coordinatograph table with tape.

   1.2. Cut the desired square area to three decimal place accuracy using the Micro/plotter cutting instrument.

   1.3. For a 10X reduction, the initial dimensions of the image was 2.755 in. x 2.755 in. (7 mm x 7 mm)

2.0. A photographic plate was then exposed to the pattern cut in Rubylith.

   2.1. Secure the Rubylith to the light table of the Decacon camera reduction system.

   2.2. For a 10X reduction, the camera required a 5 inch Wray lens and a rear box setting of 20.80. The front box was set, as required by the focus adjustment, to 0.20.

2.2.1. To focus the camera, an exposed High Resolution photographic Plate (HRP) with scratched emulsion was loaded in the camera. (NOTE: Insure HRP is loaded with the emulsion side facing toward the light box.)

2.2.2. A microscope was used to focus on the scratched emulsion of the HRP.

2.2.3. Without moving the microscope, the front box was moved to bring the Rubylith image into focus and then locked into position. (NOTE: The aperture was completely opened during the focusing operation)

2.3. Load an unexposed HRP in the camera (emulsion side facing toward the light box) and expose for 30 seconds with the aperture shut half-way.

3.0. The exposed HRP was developed using standard darkroom techniques.

3.1. Develop the HRP in Kodak HRP developer (1:4 dilution) for 2 minutes with ultrasonic agitation.

3.2. Place the HRP in the stop bath for 30 seconds.

3.3. Place the HRP in the fixer for 30 seconds.

3.4. Rinse the HRP in running water for 1 minute and blow dry with nitrogen. The mask produced is ready for use with a negative photoresist process.

To produce a mask for use with a positive photoresist process, an image reversal process is necessary. The process is the same up to the point of development and is presented as follows:

3.5. Develop the HRP in KODAK HRP Developer (1:2 dilution) for 5 minutes.

3.6. Wash the HRP in running water for 2 minutes.

3.7. Soak the HRP in the KODAK Bleach Bath R-9 for 2 minutes.

3.8. Then rinse the HRP in running water for 30 seconds.

3.9. Soak the HRP in the KODAK Clearing Bath CB-6 for 3 minutes.

3.10. Wash the HRP in running water for 4 minutes. (During the wash, the plate is exposed to a No. 212 or No. 302 enlarging lamp for 30 seconds at a distance of 2 feet.)

3.11. Develop the HRP in the KODAK HRP Developer (1:4 dilution) for 5 minutes.

3.12. Then soak the HRP in the KODAK Rapid fixer for 2 minutes.

3.13. Wash the HRP in running water for 5 minutes.

3.14. Finally, blow dry with nitrogen. [50:54]

4.0. The final dimensions of the reverse image plates were measured on the Micro/plotter with the cross-hair attachment. The dimensions of the three mask made were: 1) 6.96 mm x 6.96 mm, 2) 6.91 mm x 6.96 mm, 3) 6.99 mm x 6.93 mm.

Wafer Preparation

The GaAs wafers were cataloged and prepared for the Baseline Etch Rate experiment. The preparation of the wafers involved dicing, cleaning, capping with silicon nitride and exposing the substrate area.

5.0. The wafer was diced into approximately 1 cm square chips with a dicing saw. Some of the samples were then again diced in half with a dicer. The procedures are:

5.1. Secure the wafer to the vacuum chuck of the dicer.

5.2.   Lower the diamond tip stylus at the desired location.

5.3.   Pull the chuck towards the operator.

5.4.   Raise the stylus and repeat the process to form a checkerboard pattern on the wafer's surface.

5.5.   Remove the wafer from the dicer and cleave using a small amount of pressure applied with a cotton swab.

6.0. The following cleaning process was used to remove the organic contaminants and the native oxide from the wafer's surface.

6.1.   Soak the wafer in acetone for 1 minute. (NOTE: If only one side of the wafer needs to be cleaned, it can be placed on a spinner and sprayed with acetone.)

6.2.   Soak the wafer in methanol for 1 minute. (NOTE: If only one side of the wafer needs to be cleaned, it can be placed on a spinner and sprayed with methanol.)

6.3.   Soak the wafer in isopropyl alcohol for 1 minute. (NOTE: If only one side of the wafer needs to be cleaned, it can be placed on a spinner and sprayed with isopropyl alcohol.)

CAUTION: Do not let the acetone or the methanol dry on the wafer's surface.

6.4.   Blow the wafer dry with nitrogen.

6.5.   Dip the wafer in a 1:1 HCl:DIW solution for 30 seconds

6.6.   Then rinse it in DIW.

6.7.   Blow dry the wafer with nitrogen.

7.0. A chemical vapor deposition (CVD) unit was used to deposit a silicon nitride film on the surface of the wafer. A SemiGroup CVD System 1000 CC with a pre-mixed bottle of silane/nitrogen (5% silane) was used. The procedures are:

84

7.1. Press the run button on control panel.

7.2. Wait a few seconds, then press the stop button until 5 tones are heard.

7.3. Clean the chamber with chem-wipes.

7.4. Load the samples along with a Si control wafer.

7.5. Select the Process Number: #2 for 3000 Å or #3 for 5000 Å. For this study Process #3 was used.

Parameters for process #3:
Gas flow rate: $200 \text{ cm}^3/\text{min}$
Temperature: 200°C
Power level: 9.0% (100W)
Pressure: 311 mTorr
Time: 20 minutes

7.6. Press the run button on control panel. (NOTE: From this point on, the process is automatic)

7.7. When the chamber opens, unload the samples.

7.8. Clean the chamber.

7.9. To shut down the unit. Press the run button. Once the system has gone into the high vacuum mode, press the stop button, briefly. (NOTE: The thickness of the silicon nitride can be verified using an ellipsometer.)

8.0. To verify the thickness of the silicon nitride layer, a Gaertner Scientific Products Ellipsometer was used. The measurement process was automated by using an Hewlett-Packard computer as a controller. The set-up implemented to determine the nitride thickness is:

8.1. Turn the laser on. Turn the stage motor on.

8.2. Open the shutter to the laser.

8.3. Place the sample on the stage so the laser beam strikes it.

8.4. Look in the collimator and adjust the leveling screws to obtain an alignment.

8.5. With the analyzer switch in the "AS" position, adjust the analyzer ring to obtain a maximum reading on the meter.

8.6. Adjust the "gain" control to obtain a reading of 75 on the meter.

8.7. Put the analyzer switch in the "A" position.

8.8. Pull out the computer drawer and press the "stop" key followed by the "erase" key and then the "execute" key.

8.9. Select the desired program by pressing the "load" key followed by the program number (#) and "execute" key. (Program 0 is for finding a ballpark figure for a film of unknown thickness. Program 4 is for measuring films when the thickness and index of refraction are known.)

8.10. Press the "run" key to start the program. All programs are menu driven.

8.11. To re-run the program, press the "run" key again.

8.12. When finished, slide the computer draw in, turn off the laser power, stage power and collimator light source.

9.0. Exposing only a specified area of the GaAs surface requires the pattern of the mask to be defined in photoresist and the removal of the silicon nitride with a plasma etching unit. The procedures are:

9.1. Clean the samples as described in steps 2.1 through 2.4.

9.2. Place the samples in the oven at 100°C for 5 minutes.

9.3. Place the sample on a spinner and coat the sample with hexamethyl disiloxane (HMDS), an adhesion promoter. Spin at 5000 rpm for 30 seconds.

9.4. Apply Shipely 1450J Positive photoresist to the sample and spin at 5000 rpm for 30 seconds.

9.5.   Place the samples in the oven at 90°C for 30 minutes.

9.6.   Expose the sample with an energy of 12 mW/cm^2, a wavelength of 320 nm for 2.5 minutes. [Karl Suss MJB 3 mask aligner]

9.7.   Develop the sample for 1 minute with a 5:1 dilution of DIW:351 Developer.

9.8.   Rinse it for 15 seconds with DIW.

9.9.   Blow the sample dry with nitrogen for 15 seconds.

9.10. Place the sample in the postbake oven for 30 minutes at 100°C.

10.0. After the pattern has been defined in photoresist, the unwanted silicon nitride was removed so that the GaAs surface was exposed to the etchant. The following parameters were used to remove the silicon nitride layer:

<u>Parameters</u>

Oxygen flow rate:	4.1 cm^3/min
Freon 14 flow rate:	46.0 cm^3/min
Chamber pressure:	0.2500 Torr
Forward RF power setting:	100 W
Repel RF power setting:	5 W
Valve angle:	49.2 degrees
Etch time:	12 minutes

After the etch period, the surface was examined under a microscope to make sure the silicon nitride film was removed.

11.0. Black wax was used to coat the back of the wafer to prevent an undesired GaAs surface from being exposed to the etchant.

11.1. Dissolve a piece of Black (Apezion) wax with Trichloroethylene (TCE) under a fume hood.

87

11.2. When the wax becomes a liquid, immerse the wafer in the wax using a pair of tweezers. Do not to completely submerge the sample.

11.3. Place the sample topside down and allow to dry (approximately 4 hours).

11.4. If the edges of the sample need to be coated with wax, a cotton swab dipped in TCE can be used to dab dissolved wax on the edges.

11.5. Allow the wax to completely dry, then degrease the sample with acetone, methanol, isopropyl alcohol and blow dry with nitrogen, in that order.

11.6. Insure the wax covers the back and edges of the sample. Repeat Step 11.4 as necessary.

12.0. The pH meter was used to determine the pH of the etchants. Before the pH meter was used for measurements, it must be calibrated.

The SA 520 pH meter was calibrated according to the following instructions:

12.1. Slide the power switch to the ON position. Attach the BNC shorting plug to the sensor input (3 in Figure A-1) on rear panel.
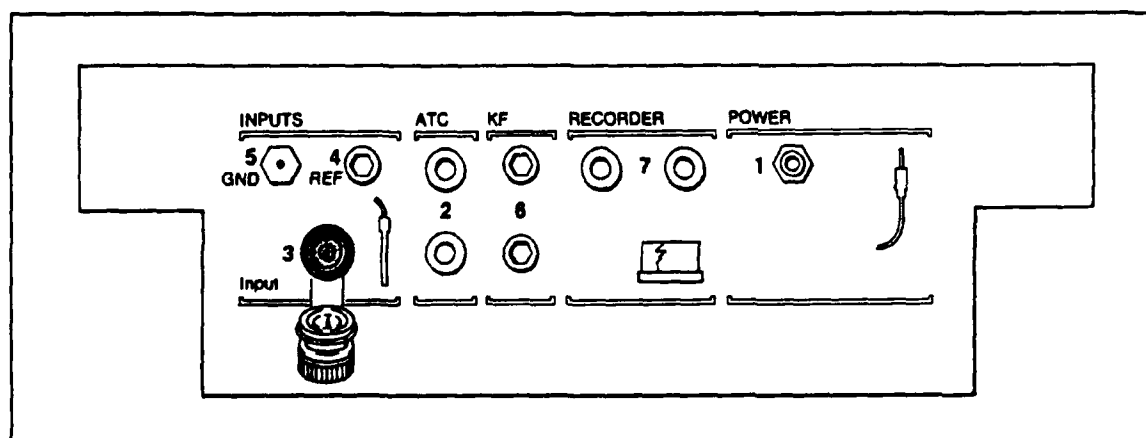
Figure A-1. Arrangement of the Rear Panel of the Orion SA520 pH Meter (36:2).

12.2. If using the AC line converter, connect it to the meter and the appropriate power source.

12.3. If operating on battery power and the LOBAT indicator on the LCD display remains on, replace the batteries or use line power.

12.4. Slide the mode switch to **mV**; the display should read **0 ± 0.3**.

12.5. Slide the mode switch to **temp**; the display should read **25.0** If **25.0** is not displayed, scroll using the ∧ (up) key or the ∨ (down) key until **25.0** is displayed and press **enter**.

12.6. Slide the mode switch to **pH.01**, press **iso**; the display should read the letters **ISO** and then a value of **7.00**. If **7.00** is not displayed, scroll until **7.00** is displayed and press **enter**.

12.7. Press **slope**; the display should read the letters **SLP** and then a value of **100.00**. If **100.00** is not displayed, scroll until **100.00** is displayed and press **enter**.

12.8. Press **sample**. Observe the letters **PH**, then a steady reading of **7.00** should be obtained. If not, press **cal** and scroll until **7.00** is displayed and press **enter**. Press **sample** and observe a reading of **7.00**.

12.9. Remove the shorting plug. After successful completion of steps 1-8, the meter is ready to use with an electrode.

12.10. Connect the pH probe to the rear panel (**3** Figure A-1) of the meter using a BNC connector. The Automatic Temperature Compensation (ATC) probe is connected to the meter on the rear panel (**2** Figure A-1) using banana plugs.

These procedures were taken form the Orion SA 520 Instruction Manual (36:4).

An autocalibration procedure using two buffers allows the pH meter to give accurate readings each time it is used. The procedure is described below.

12.11. Connect the electrodes to the meter. Slide the mode switch to **pH.1** or **pH.01**. Choose either the 4.01 and 7.00 or the 7.00 and 10.01 buffers, whichever will bracket your expected sample range.

12.12. Place electrodes into either the 4.01, 7.00 or 10.01 buffer solutions.

12.13. Press **cal.** The display will alternate between .1. and the pH value of the buffer indicating this is the first buffer and a value has not been entered. Wait for a stable pH display and press **enter.** The display will freeze for 3 seconds and then advance to .2. indicating the meter is ready for the second buffer.

12.14. Rinse the electrodes and place into a second buffer. Wait for a stable pH display and press **enter.** After the second buffer value has been entered the letters **PH** will be displayed. The meter is now calibrated and automatically advances to measure sample solutions.

12.15. Rinse the electrodes and place them into a sample solution. Record the pH directly from meter display. (NOTE: The SA 520 Meter automatically calibrates itself to the correct buffer value using temperature compensation. For the best result, it is recommended that an ATC probe be used.)

This procedure was taken from the SA 520 Orion Instruction Manual (36:5).

If the standard 4.01 or 10.01 buffers are not available, a manual calibration

with two known buffers can be accomplished as presented below.

12.16. Connect the pH electrodes to the meter. Slide the mode switch to **pH.1** or **pH.01.** Choose two buffers that will bracket the expected pH range of the samples.

12.17. Place the electrodes into the first buffer.

12.18. Press **cal.** The display will alternate between .1. and the pH value of the buffer indicating this is the first buffer and a value has not been entered.

12.19. Wait for a stable pH display. Scroll in the correct value, using the ∧ (up), ∨ (down) or **x10** keys and press **enter.** The display will freeze for 3 seconds then advance to .2. indicating the meter is ready for the second buffer.

12.20. Rinse the electrodes and place them into the second buffer. Wait for a stable pH display. Scroll in the correct value and press **enter.** After the second buffer value has been entered the letters **PH** will be

displayed. The meter is now calibrated and automatically advances to measure sample solutions.

12.21. Rinse the electrodes and place them into a sample solution. Record pH directly from meter display.

This procedure was taken from the SA 520 Instruction Manual (36:6).

It is recommended that the pH of the buffer solutions bracket the expected

pH of the sample solution. This calibration should be preformed at the beginning

of the day to measure the drift in the instrument. A one buffer calibration should

be accomplished every two hours to compensate for electrode drift (36:5).

The autocalibration with one buffer procedures are outlined below.

12.22. Verify the slope value by pressing **slope**. If necessary scroll the slope value determined by a calibration with two buffers, and press **enter**. If the slope value is unknown, either enter 100.0 or perform a two buffer calibration. A single buffer calibration does not change the slope value.

12.23. Connect the electrodes to meter. Slide mode switch to **pH.1** or **pH.01**.

12.24. Place electrodes into either a 4.01, 7.00 or 10.01 buffer solution, whichever most closely approximates the expected sample pH.

12.25. Press **cal**. The display will alternate between .1. and the pH value of the buffer, indicating that this is the first buffer and a value has not been entered.

12.26. Wait for a stable pH display and press **enter**. The display will freeze for 3 seconds then advance to .2. indicating the meter is ready for the second buffer. By pressing **sample** the letters **PH** will be displayed indicating the meter is ready for sample measurement.

12.27. Rinse the electrodes and place them into sample. Read the pH directly from the display.

This procedure was taken from the SA 520 Instruction Manual (36:5).

Either the auto or manual calibration was performed before any pH measurements were taken of the test solution. Figure A-2 illustrates the results of a calibration run.
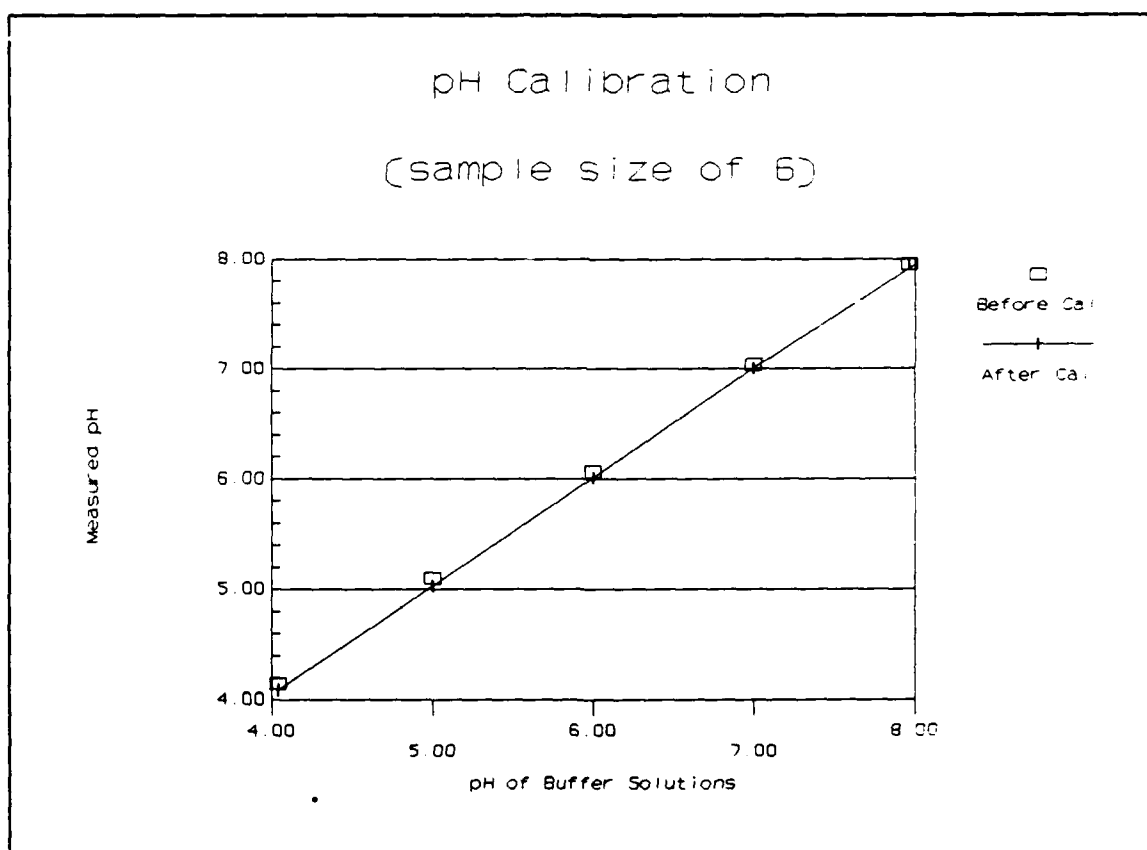
Figure A-2. Calibration of the Orion pH Meter with Standard Buffers.

13.0. The mixing of the solution under study is the next step.

    13.1.   For Gannon's and Nuese's solution, the following procedure was used:

        13.1.1. Measure out 20 ml of NH_4OH and pour it into a 1500 ml Teflon container.

        13.1.2. Measure out 7 ml of H_2O_2 and then pour it into the same Teflon container.

        13.1.3. Measure out 973 ml of DIW and add it to the Teflon container.

        13.1.4. Let the solution stand for one hour, then measure the pH and temperature.

    13.2   The procedure for mixing J. J. LePore's solution with $\gamma = 200$ is:

        13.2.1. Measure out 2 ml of NH_4OH and then pour it into a 1500 ml Teflon container.

        13.2.2. Measure out 400 ml of H_2O_2 and then pour it into the same 1500 ml Teflon container.

        13.2.3. Let the solution stand for one hour, then measure the pH and temperature.

14.0.   While the etching solutions are stabilizing, the samples were weighed to determine their initial weight using a Mettler balance.

    14.1.   Place all the weight knobs to the zero position, empty the pan and close the doors.

    14.2.   Turn the arrest lever counterclockwise to 9 O'clock position, or the *released position*.

    14.3.   Turn the zero knob (on the right hand side of the balance) until the zero line is centered between the bars on the measuring screen.

    14.4.   Put the arrest lever into the arrested (12 O'clock) position.

14.5. Load the pan with a sample and close the doors.

14.6. Turn the arrest lever clockwise to a 3 O'clock or partial release position. Turn the 0.1 g knob (clockwise) until the 1 mg division does not go off scale (> 100 mg).

14.7. Turn the arrest lever to the released position.

14.8. Turn the fine tune adjust knob until a 1 mg division is centered between the bars.

14.9. Read the scale to the nearest 100th of a milligram.

14.10. Turn the arrest lever to the arrested position and remove the sample.

The Mettler balance was calibrated by the Precision Measurement Equipment Laboratory (PMEL) on 15 May 1988. The scale was periodically checked with a class C weight set. The smallest weight available in that set was 20 mg. A calibration run using the class C weights is shown in Figure A-3 below.

15.0. The following steps were used to measure the weight loss of the sample in the etchant.

15.1. Initially weigh the test samples and record their values.

15.2. Place 3 samples in a teflon basket and place it in an etching solution. Start the timer.

15.3. After a period of time, remove the basket from solution, rinse samples in DIW and blow dry with nitrogen. Ensure that no water remains on the sample.

15.4. Reweigh the samples and record their weights.

15.5. Repeat Steps 15.1 through 15.5 as required. At the midpoint and at the end of data collection, remeasure and record the pH of the solution.
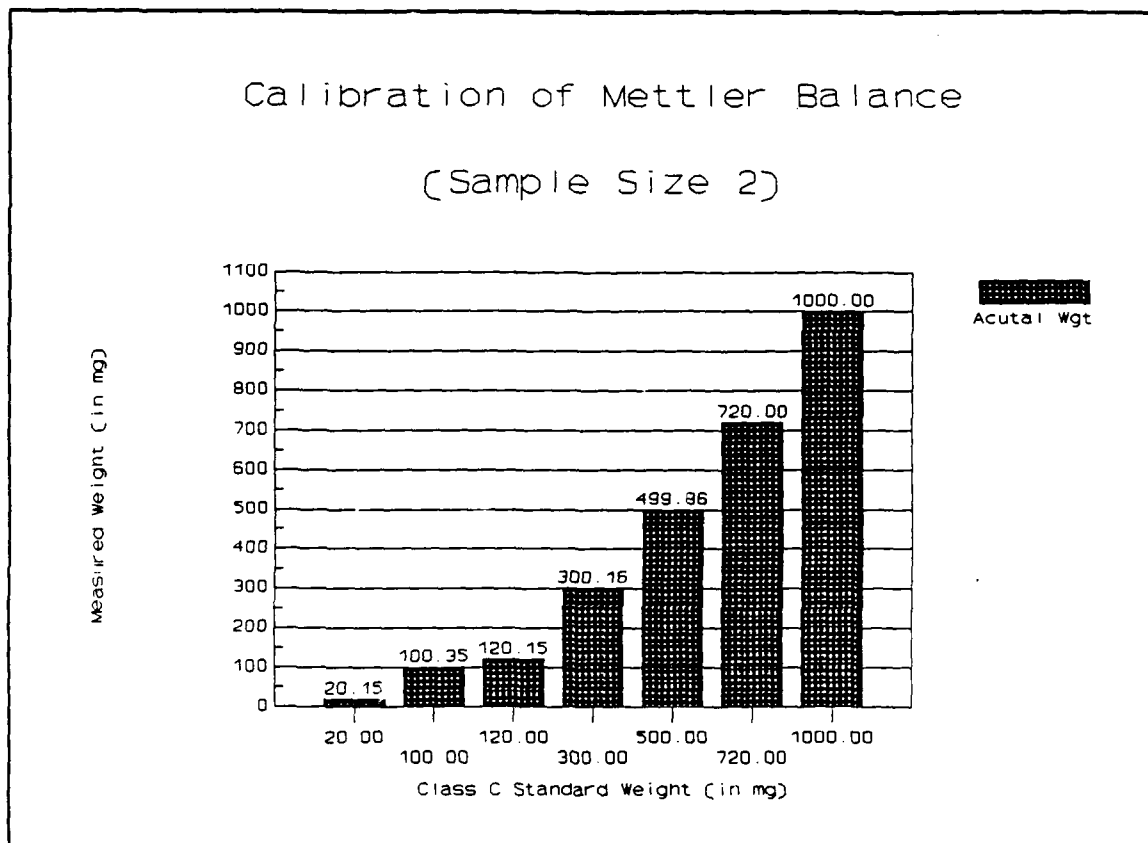
Figure A-3. Calibration of the Mettler Balance with Class C Weights.

16.0. A second method was used to verify the accuracy of the etch rates determined by the weight loss method. This method involved the use of a Sloan Dektak II profilometer to·measure the step height on the sample after a specified period of time in the etchant. The following procedures were used:

16.1. Degrease wafer samples as described in Steps 6.1 - 6.7.

16.2. Follow Steps 9.4 - 9.10 to expose a photoresist pattern on the GaAs surface.

16.3. Prepare the etch solutions as described in Steps 13.1 and 13.2. Measure the pH and temperature of the etchant.

16.4. Place the samples in an etchant for a predetermined time. Remove the samples and rinse in DIW.

95

16.5. Remove the photoresist with a degrease cleaning (Steps 6.1 - 6.4).

16.6. Place the samples on a Sloan Dektak II and measure the step height of the area etched into the GaAs.

Appendix B

Wafer Etching with Fischione Electropolisher

This appendix provides the detailed steps used to etch GaAs and n-$Al_xGa_{1-x}As$ samples with the Fischione Twin-Jet Electropolisher as outlined in Chapter III.

Wafer Preparation

Preparation of the wafer samples for use in the Fischione Electropolisher involved dicing the wafers, dimpling and lapping the samples, measuring the thickness of the samples and finally mounting the samples on a glass microscope slide. The following steps were taken to prepare the samples:

1.0. Larry Callahan, laboratory technician, diced the wafers into 1 cm square chips using the Avionics Laboratory's Wafer saw.

2.0. The diced wafer samples were cleaved in half using a diamond tip cutter.

    2.1.   Place the wafers on table and hold with tweezers.

    2.2.   Gently move the diamond tip stylus across the surface of the sample.

    CAUTION: Do not apply too much pressure to the wafer with the stylus. This may cause the sample to shatter.

    2.3.   Break the sample with the tip of a cotton swab by applying a small amount of pressure.

3.0. The cleaved samples were mechanically dimpled by Scott Apt in the Air Force Materials Laboratory.

4.0. The thickness of the samples were measured using a Bausch & Lomb PR-25B Optical Gauge.

    4.1.   Turn the power to unit on and lower the stylus.

    4.2.   Zero the unit with the zero adjust knob.

    4.3.   Raise the stylus and place the sample to be measured on the stage.

    4.4.   Slowly lower the stylus until it comes in contact with the surface.

    4.5.   Adjust the alignment knob until the cross-hairs line-up.

    4.6.   Read the thickness from the scale. The units accuracy is ± 0.00005 inches.

Three thickness measurements were taken on the sample surface and the dimpled area, then averaged. Table B-1 shows the results of these measurements. In some cases the thickness of the sample at the dimpled area was to large. It would have caused the etching of the sample to take days. (Assuming an etch rate of 30 Å/s and a thickness of 250 μm, the time to etch through the sample would be approximately 24 hours.) If the samples were reduced in thickness the etch time would also be reduced.

5.0. To reduce the thickness of the samples at the dimpled area, they were lapped on the non-dimpled side. The samples were reduced to a thickness of approximately 100 μm at the dimpled area using a 0.3 μm alumina grit and a Speed Lap 12 unit

Table B-1.   Results of Thickness Measurements Made With Bausch & Lomb
             Optical Gauge

Sample	Average* Thickness	Dimple* Thickness	Dimple* Depth
33-04A	433.83	328.93	104.90
33-04B	433.83	322.58	111.25
33-05A	449.33	343.32	106.00
33-05B	449.33	331.05	118.28
33-06A	452.63	340.78	111.84
33-06B	452.63	336.55	116.08
33-07A	430.53	316.65	113.88
33-08A	469.14	340.36	128.78
33-08B	469.14	354.33	114.81
A-03A	497.84	281.94	215.90
A-03B	497.84	272.20	225.64
A-04A	497.84	323.43	174.41
A-04B	497.84	274.32	223.52
A-05B	498.26	268.39	229.87
A-06A	497.84	281.52	216.32
A-06B	498.69	311.57	187.11
A-07A	496.15	251.46	244.69
A-07B	498.26	250.61	247.65
A-08A	499.53	306.49	193.04
A-08B	499.11	283.63	215.48
A-09A	500.80	254.85	245.96
A-09B	501.23	280.67	220.56
A-10A	497.42	140.12	357.29
A-10B	497.84	234.95	262.89
A-11A	497.84	230.29	267.55
A-11B	499.96	229.02	270.93
A-12A	500.38	245.53	254.85
A-12B	497.84	244.69	253.15

* All thickness are in μm

manufactured by Speed Lap Corporation. Using the thicknesses from Table B-1 the amount of material to be removed can be determined, leaving the desired thickness at the dimpled area. The following steps describe the lapping procedure:

5.1. Place a quartz carrier on a hot plate and heat to 300°F.

5.2. Melt a small portion of clear wax on the quartz carrier.

5.3. Place the sample to be lapped (dimple side down) on the carrier.

5.4. Turn off the hot plate and remove the carrier.

5.5. While the wax is still hot, gently press the sample into the wax.

5.6. Allow the sample and carrier to cool; then measure the height of the sample and carrier with a micrometer.

5.7. Set the sample holder to remove the desired height for the mounted samples.

5.8. Mix the 0.3 μm alumina powder with the lapping vehicle to make a slurry solution.

5.9. Position the container so that the slurry drips on the lapping surface.

5.10. Set the timer on the Speed Lap 12 unit for 2 minutes, then start the unit. This action wets the lapping surface.

5.11. Place the sample holder on the lapping surface and set the desired lapping time.

5.12. Start the unit.

5.13. Measure the thickness of the sample after one cycle.

5.14. Repeat Steps 5.8 - 5.12 as needed until the desired thickness is reached.

5.15. Reheat the carrier and the samples on the hot plate in order to remove the samples from the carrier.

5.16. Clean the wax from the samples in acetone, methanol and isopropyl alcohol as described in Appendix A.

5.17. Measure the thickness of the sample as described in Step 4 above.

The results of the measurement after the lapping are presented in Table B-2. The thickness at the dimple was not measured. It was calculated from the difference between the dimple depth and the sample thickness.

6.0. After the thickness of the samples were determined, they were mounted on 8 mm x 12 mm microscope slides (diced by Larry Callahan). The glass slides provide extra support for the dimpled area while in the Fischione Twin-Jet Electropolisher. A trial run using the Fischione Electropolisher on an unlapped (≈ 500 μm thick) GaAs sample demonstrated the sample alone could not withstand the force of the jet spray. The unsupported GaAs sample fractured, before perforation of the sample. The mounting procedure is described below.

6.1. Turn a hot plate on and heat to 300°F.

6.2. Place a diced microscope slide on the hot plate, let it stand for 2 minutes.

6.3. Melt a small amount of clear wax on the slide.

6.4. Place the sample, dimple side down on the slide.

6.5. Remove the slide from the heat and gently press down on the sample.

6.6. Place the sample on a spinner and remove any excess wax with a degrease cleaning as described in Appendix A.

6.7. Dissolve some Apezion black wax with TCE under a fume hood.

6.8. Dab black wax on the undimpled areas to prevent etching on undesired areas of the sample.

Table B-2. Thickness of Samples After Lapping

Sample	Dimple[*] Depth	Thickness[*] After Lapping	Thickness[*] to be Etched
33-04A	104.90	231.99	127.08
33-04B	111.25	235.80	124.54
33-05A	106.00	238.34	132.33
33-05B	118.28	229.87	111.59
33-06A	111.84	288.29	176.45
33-06B	116.08	269.24	153.16
33-07A	113.88	247.23	133.35
33-08A	128.78	274.32	145.54
33-08B	114.81	252.31	137.50
A-03A	215.90	337.82	121.92
A-03B	225.64	321.73	96.10
A-04A	174.41	298.45	124.04
A-04B	223.52	292.95	69.43
A-05B	229.87	241.30	11.43
A-06A	216.32	241.62	25.29
A-06B	187.11	233.68	46.57
A-07A	244.69	327.24	82.55
A-07B	247.65	305.22	57.57
A-08A	193.04	313.27	120.23
A-08B	215.48	321.73	106.26
A-09A	245.96	323.43	77.47
A-09B	220.56	296.33	75.78
A-10A	357.29	493.18	135.89
A-10B	262.89	331.89	69.00
A-11A	267.55	371.69	104.14
A-11B	270.93	373.38	102.45
A-12A	254.85	345.44	90.59
A-12B	253.15	334.01	80.86

[*] All thickness in μm

102

Fischione Electropolisher Set-up and Alignment

7.0. The Fischione Electropolisher must be assembled and aligned before use. The following procedures are provided for set-up and alignment of the Fischione Electropolisher (9):

Set-up

7.1. Plug the connecting cable into the electrical socket on the back of the Power Control unit.

7.2. Insert the motor plug into its socket on the connecting cable. Insure the wires are connected to their corresponding colors.

7.3. Insert the light socket and photocell socket into the respective holder slides.

7.4. Tighten the common cathode leads under the acorn nuts of the jet assemblies.

7.5. Connect the anode lead clip onto the specimen holder rod.

WARNING Shock Hazard: With the power control and the polishing voltage energized, never simultaneously touch the cathode leads and any uninsulated part of the anode lead or specimen holder.

7.6. If required, cooling with tap water is possible by threading the cooling hose fittings into the box.

Alignment Procedure

7.7. To adjust the spacing between the jet assemblies, simply loosen the thumb screws, reposition the jet assemblies then retighten the thumb screws.

7.8. The light conduits are factory adjusted so that the protruding ends are level with the opening in the nozzle of the jet assembly. If readjustment is required, loosen the set screw in the holder slide, reposition the light conduit, then retighten the set screw.

NOTE: Care should be taken when handling the light pipes. Bumping or over-tightening may result in light conduit breakage.

7.9. The position of the specimen holder should be adjusted so that the exposed specimen area is aligned with the jet assemblies and the light conduits. The specimen holder should be perpendicular to the jet assemblies.

7.10. Fill the glass dish with DIW until the level is just above the specimen area and below the top of the specimen holder.

7.11. For a final specimen holder adjustment, immerse the specimen holder into the DIW. Position the polish switch in either AUTO or CONT mode to activate the light source. Move the alarm silent switch to the down position. Remove the photocell socket from its holder slide.

7.12. While looking into the photocell fixture, observe the light transmitted by the light conduits and perform the necessary vertical and lateral adjustments to center the specimen holder.

7.13. With the specimen holder positioned correctly and the photocell detector in place, reduce the sensitivity to a minimum setting so that the alarm is activated when the light is turned on.

7.14. Adjust the pump control to its lowest setting to permit the water to strike the specimen.

The set-up and alignment procedure for the Fischione Electropolisher was taken from the Instruction Manual (9).

8.0. After the Fischione Electropolisher was set-up, it was tested to insure proper operation. First the sensitivity control was adjusted using aluminum samples 2.5 mils thick, and an electrolyte mixture of 300 ml of methanol and 100 ml of nitric acid.

8.1. Align the specimen holder (Steps 7.11 and 7.12).

8.2. Place a 3 mm diameter aluminum sample in the Fischione Electropolisher specimen holder.

8.3. Measure out 300 ml of methanol, and 100 ml of nitric acid; mix the chemicals in the Fischione glass container.

104

8.4. Adjust the sensitivity control to the full clockwise position.

8.5. Place the specimen holder in the solution.

8.6. Move the polishing switch to the AUTO position. Move the pump switch to the AUTO position.

8.7. Adjust the pump setting (Step 7.14).

8.8. Press the reset button to start the unit.

8.9. Adjust the polishing current to read 28-30 mA.

8.10. Remove the specimen holder when alarm sounds and rinse in DIW. If perforation has not occurred, lower the sensitivity setting (turn counter-clockwise) and return to Step 8.8.

Four Al samples were successfully thinned and perforated, to confirm the proper operation of the Fischione Electropolisher. The ability of GaAs to transmit wavelengths in the infrared region complicates the sensitivity adjustment. The following steps were accomplished to insure the proper operation of the Fischione Electropolisher with GaAs samples.

8.11 Undimpled GaAs samples were thinned according to Step 5.0. Five (5.0) μm alumina powder was used.

8.12. Several samples were mounted as in Step 6.0.

8.13. One mounted GaAs sample was placed in the Fischione Electropolisher specimen holder.

8.14. Mix etchant, 3:1:150 ($NH_4OH:H_2O_2:H_2O$ by volume) and let stand for 2 hours.

8.15. Adjust the sensitivity to the full clockwise position.

8.16. Remove the cathode and anode connections.

8.17. Move the polishing switch to the AUTO position. Move the pump switch to the AUTO position. The pump setting should be the same as Step 8.7.

8.18. Press the reset button to start unit.

8.19. Remove the specimen holder when the alarm sounds and rinse it in DIW. If perforation has not occurred, lower the sensitivity setting (turn counter-clockwise) and return to Step 8.16.

Three GaAs samples were successfully etched with this technique. It was found that the highest sensitivity setting was adequate for detection of the perforation. It was noted, that after the alarm sounded, a small perforation occurred in the sample. The GaAs material was completely removed from that area.

9.0. To insure that a precise time was kept from start to finish of the etching process, a Hewlett Packard 5248M Electronic Counter with a plug-in Hewlett Packard 5262A Time Interval Unit was used. The Fischione Electropolisher Digital Power Supply was modified to connect it to the Counter. The modification procedures are covered in Appendix C. Briefly explained, the signal from the reset button on the Power Supply is passed to the Time Interval Unit to activate the Counter; the signal that sounds the alarm is passed to the 5262A to stop the Counter. The display then holds the value until it is reset. The following steps describes the set-up of the Electronic Counter and the Time Interval Unit.

9.1. Insert the plug-in unit and push it firmly into the compartment until front panel of the plug-in is flush with the front panel of the Counter. Turn the retaining latch knob clockwise until it is tight.

9.2. Set the **sensitivity** switch to **plug-in**.

9.3. Set the **level** to **preset**.

106

9.4. Set the **function** switch to **remote** or **time int.**

9.5. Connect the electrical cables to the **start** and **stop** connectors.

9.6. Set the **com-remote-sep** selector to **sep.**

9.7. Set the **time base** switch to 1s.

9.8. Set the **sample rate** to the full clockwise position.

9.9. Set the start channel **slope** to "-" to trigger the timer on the falling edge of the reset signal.

9.10. Adjust the start **multiplier** and **trigger level** controls to set measurement start point at +6 volts.

9.11. Set the stop channel **slope** control to "+" to trigger the timer on the rising edge of the alarm signal.

9.12. Adjust the stop **multiplier** and **trigger level** controls to set the measurement stop point at +6 volts.

9.13. Press **reset** button to clear display. The Unit is now ready to make a time interval measurement.

This set-up procedure was taken from the Instruction Manuals of the Hewlett Packard Timer and Counter (18; 19).

10.0. The etching solution is mixed and allowed to equilibrate to room temperature before the pH and temperature are recorded (see Appendix A Step 13). The composition of the solutions were determined by volume ratios. The pH was adjusted as necessary by using nitric or sulfuric acid or ammonium hydroxide. The pH meter was calibrated before all pH measurements were taken, as described in Appendix A, Step 12.

107

11.0. While the etching solution is cooling, the native oxide is removed from the mounted, dimpled GaAs sample, then the sample is loaded in the specimen holder using the following steps:

11.1. Dip the mounted sample in a 1:1 solution by volume of HCl:DIW for 30 seconds.

11.2. Rinse the sample in DIW until the resistivity of the water is greater than 15 MΩ, as measured by the Blaugh Resistivity meter.

11.3. Dip the mounted sample in a 1:1 solution by volume of buffered oxide etch:DIW for 30 seconds. NOTE: buffered oxide etch is 7:1 ($NH_4F:HF$).

11.4. Rinse the sample in DIW until the resistivity of the water is greater than 15 MΩ.

11.5. Blow the sample dry with nitrogen.

11.6. Place the mounted sample -- glass side towards the platinum wire (anode) -- in the Fischione Electropolisher specimen holder. Ensure the dimpled area is visible through the opening.

11.7. Tighten the specimen holder. NOTE: Do not over tighten the specimen holder, as this action may cause the sample to fracture.

12.0. The actual measurement of the etching time of the GaAs mounted samples is accomplished as follows:

12.1. Place the specimen holder in the etching solution and press the reset button on the Fischione Electropolisher Digital Power Supply. Make sure the counter is operating.

12.2. Align the specimen holder.

12.3. After the alarm has been tripped, record the value of the Counter.

12.4. Remove sample and repeat Steps 9.0 - 12.0 for different solutions and samples.

13.0.   For the etching of the n-Al$_x$Ga$_{1-x}$As epitaxial layers the preparation and mounting of the samples varies slightly. The following steps are used in preparation of the n-Al$_x$Ga$_{1-x}$As samples:

13.1.   The samples were diced then cleaved in half (see Steps 1.0 and 2.0).

13.2.   The samples were then mechanically dimpled to decrease the thickness.

13.3.   The thickness of the samples was measured as described in Step 4.

13.4.   The samples were mounted as described in Step 6.0. The exception to the process is that the samples are place on the glass slide with the dimple side up.

14.0.   The set-up of the Counter and the Fischione Electropolisher are the same except for one step. A No.29 Red Kodak Wratten Gelatin filter is placed in the photocell socket between the photocell and the Light Wire.

15.0.   With the addition of the red filter, the sensitivity control of the Fischione Electropolisher was re-adjusted using the MBE grown n-Al$_x$Ga$_{1-x}$As epitaxial layers. The procedures are the same as Steps 8.11 - 8.17 with a n-Al$_x$Ga$_{1-x}$As/GaAs sample in place of the GaAs sample.

16.0.   The measuring of the etching time is the same as Step 12. The same solution concentrations were used to measure the selectivity of the etchant.

Appendix C

Modifications of the Fischione Twin-Jet Electropolisher

Modifications were made to the Fischione Electropolisher Model 130 Digital Power Control to allow automated measurement of the time required for wafer perforation. Additional modifications were made to enhance the sensitivity of the light detection circuit. This appendix describes these modifications.

Before the modifications are discussed the normal operation of the Digital Power Supply is presented. The Digital Power Control is designed to be used in conjunction with the Fischione Twin-Jet Electropolisher (10). It controls the flow of the electrolyte, the polishing current and voltage, the light source and photo-detection circuitry and the alarms (10). The Pump Select switch and the Polish Select switch, both 3 position switches, determine the mode of operation of the photo-detection circuit.

> With the Pump Select switch in the Auto mode, the photocell circuitry immediately stops the electrolyte flow by latching the internal relay 'Off' at the first sign of light penetration through the specimen. [...] With the Pump Select Switch in the Continuous mode, the pump remains running after the light has penetrated the specimen and the Photocell circuitry has activated the alarms. [10]

The operation of the Polish Select switch is very similar to that of the Pump Select switch. In the Auto mode, the polishing voltage (controlled with a 10 turn potentiometer) is automatically cut off when perforation of the sample is detected

110

by the "Photocell circuitry" (10). While in the Continuous mode the voltage is not cut off when the alarm is triggered. The Polish Select switch also controls the light source, turning it on in either the Auto or Continuous mode (10). A circuit diagram of the Digital Power Control supplied by the manufacturer is shown in Figure C-1.

The modifications allowing automated measurement of the etch time are presented first. When the unit is first turned, on the audio and visual alarms are activated. About twelve (12) volts is present across the audio and visual alarms. Depressing the reset button causes the voltage across the alarms to drop to ground (near switch S-4). As the light penetrates a sample and strikes the photocell, an increased voltage is input to the comparator (LM358). The comparator triggers when the threshold voltage (set by the sensitivity potentiometer) is exceeded. The comparator energizes the relay and the voltage across the alarms goes from ground to 12 volts. This voltage swing activates both alarms.

The voltage swings across the alarms were used as inputs to the Time Interval Unit. When the reset button is depressed, the voltage transitions from 12 to 0 volts and is used as the start signal. The transition of the voltage from 0 to 12 volts, when the alarm is activated, is used as the stop signal. Shielded coaxial cable was soldered into the Digital Power Control Unit. Standard BNC patch cables were used to connect the Time Interval Unit. The actual connection points are shown in Figure C-2.

During the initial calibration of the sensitivity (described in Appendix B), a problem was discovered in the alarm triggering circuit. The alarm would falsely

Figure C-1. Schematic of Model 130 Digital Power Control

sound before the sample was perforated. Upon trouble shooting the unit, it was noted that when the photocell was covered and the pump speed increased the alarm would trigger. This triggering would occur regardless of the sensitivity setting. Examination of the circuit diagram revealed that the DC motor and the photocell shared a common ground. It was suspected that the noise generated by the commutator/brush assembly in the DC motor was interfering with the photo-detection circuitry, thus causing false triggering.

In order to prevent the false triggering, further modification of the Digital Power Control were necessary. In addition to filtering the noise generated by the DC motor several other improvements were made to the Unit. These changes are also shown in Figure C-2 and described in the following paragraphs.

The 0.1 μF capacitors combined with the 1 kΩ resistors, labeled 1a and 1b, respectively are used to filter the triggering signals sent to the Time Interval Unit. The resistors are also current limiting to prevent damage to the circuit in the event a short circuit might occur in the triggering signals. The time delay of the added circuit is sufficiently small ($\approx$ 0.0001 seconds) such that the timing accuracy is not affected.

The 0.1 μF capacitor, labeled 2, filters the noise generated by the DC motor commutator/brush assembly. To further isolate the motor and the photo-detection circuitry, the common ground shared by the motor and the photocell was removed. A shielded lead, 3, from the photocell to the input of the comparator accomplished this. The 0.1 μF capacitor, 4, across the photocell leads filters any residual noise

113
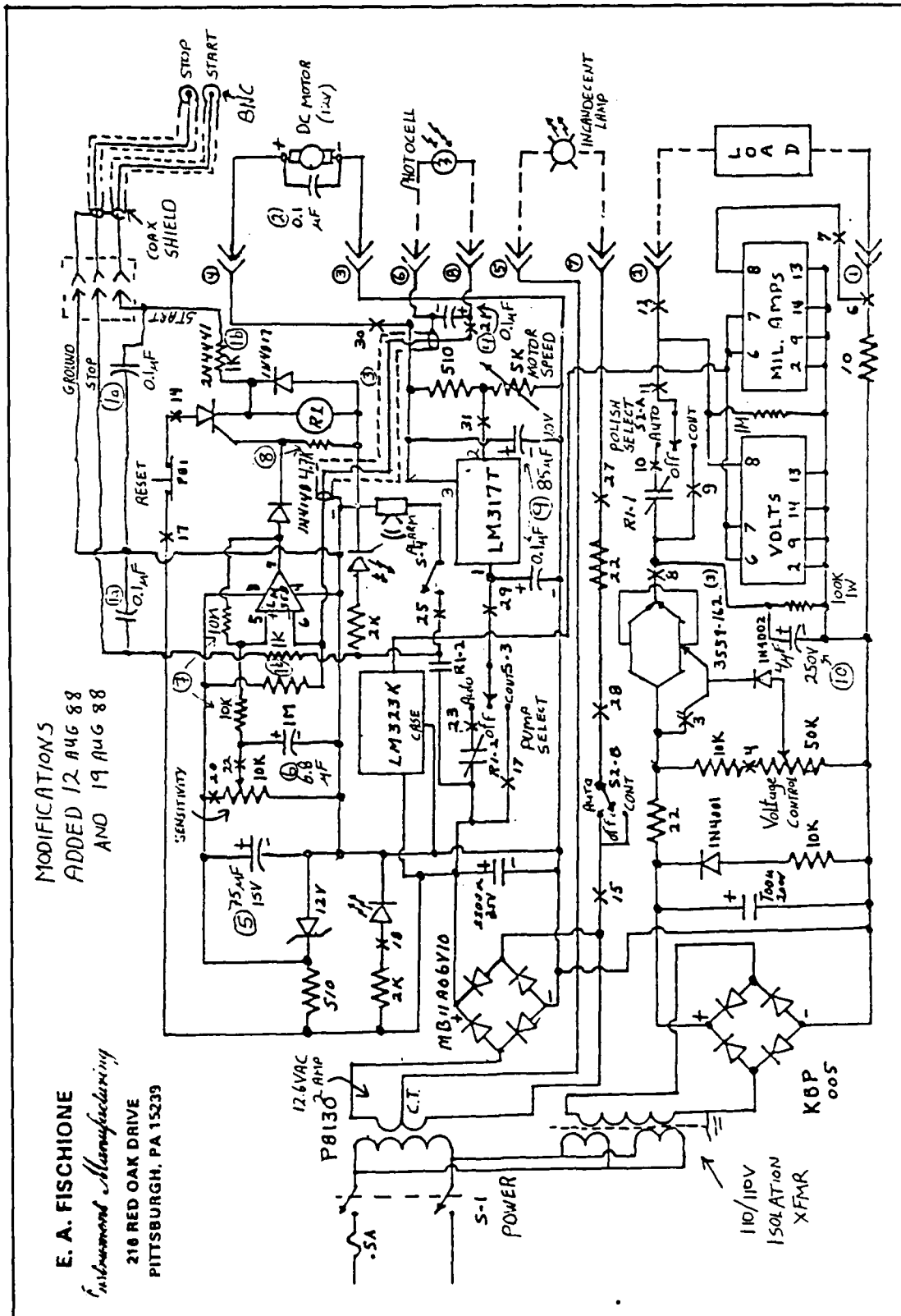
Figure C-2. Modifications Made to the Model 130 Digital Power Control Unit.

114

picked up by the leads. The photocell input circuit has a high input impedance ($\approx$ 1 MΩ) and can receive noise generated from near-by equipment or fluorescent lights. These "AC" noise signals are by-passed to ground while the slowly changing "DC" signal from the photocell is unaffected.

The 75 μF capacitor, 5, filters the noise and voltage transients of the +12 volt regulated supply before reaching the op-amp comparator circuitry. This increases the comparator noise immunity and adds consistency to the trigger-level. The 6.8 μF capacitor, 6, filters the "reference" voltage set by the sensitivity potentiometer. It holds the value steady during any fluctuations of the surrounding circuitry. The 10 kΩ and the 10 MΩ resistors, 7, form a positive feedback loop in the comparator circuit. The positive feedback provides hysteresis for more consistent triggering and better temperature stability.

The 4.7 kΩ resistor, 8, is used as a pull-down resistor to keep the gate lead of the 2N4441 silicon controlled rectifier (SCR) at the same potential as its cathode lead while the driving comparator circuit is in the low (negative or "off") state. It prevents false triggering of the SCR by noise transients or thermal leakage currents.

The 0.1 μF and 85 μF capacitors, 9, are added to the LM317T voltage regulator to improve the regulation under transient conditions. The capacitors smooth the inductive noise spikes generated by the motor operation. The capacitors allow the regulator to monitor a more constant load, thereby resulting in a more consistent motor speed.

115

The 4 μF capacitor and 100 kΩ resistor, 10, shunt residual leakage current from the 3559-162 power transistors, especially at elevated temperatures seen during long periods of operation. They also provide a more stable reading on the voltage display by keeping the transistors off when the voltage output knob is turned to zero.

The modifications were made to the unit and it was retested. With the photocell completely covered the motor speed was increased with no false triggering even with the unit at the highest sensitivity setting. No further problems were encountered with the unit during the experimentation.

Bibliography

1. Adamson, A. W. A Textbook of Physical Chemistry (2nd Ed). New York: Academic Press, 1979.

2. Alferov, S. I. and S. A. Gurevich, M. N. Mizerov and E. L. Portnoi. "Controlled Etching of Epitaxial GaAs Layers and Solid $Al_xGa_{1-x}As$ Solutions and Application in Integrated Optics," Journal of Technical Physics. 45: 2602-2606 (December 1975).

3. Arnold, D. J. and R. Fischer, W. F. Kopp, T. S. Henderson, M. Morkoc. "Microwave Characterization of (Al,Ga)As/GaAs Modulation-Doped FET's: Bias Dependence of Small-Signal Parameters," IEEE Transactions on Electron Devices. ED-31: 1399-1402 (October 1984).

4. Chand, N. and R. Fischer, H. Klem, T. Henderson, P. Pearah, W. T. Masselink, Y. C. Chang, H. Morkoc. "Beryllium and Silicon Doping Studies in $Al_xGa_{1-x}As$ and New Results on Persistent Photoconductivity," Journal of Vacuum Tube Science Technology. 3: 644-648 (March/April 1985).

5. Cooke, H. F. "Microwave Transistors: Theory and Design," Proceedings of the IEEE. 59: 1163-1181 (August 1971).

6. Drummond, T. J. and W. T. Masselink, H. Morkoc. "Modulation-Doped GaAs/(Al,Ga)As Heterojunction Field-Effect Transistor: MODFETs," Proceedings of the IEEE. 74: 773-822 (June 1986).

7. Drummond, T. J. and W. Kopp, R. Fischer, H. Morkoc, R. E. Thorne, A. Y. Cho. "Photoconductivity Effects in Extremely High Mobility Modulation-Doped (Al,Ga)As/GaAs heterostructures," Journal of Applied Physics. 53: 1238-1240 (February 1982).

8. Dyment, J. C. and G. A. Rozgonyi. "Evaluation of a New Polish for Gallium Arsenide Using a Peroxide-Alkaline Solution," Journal of the Electrochemical Society. 118: 1346-1350 (August 1971).

9. E. A. Fischione Instrument Manufacturing. Fischione Twin-Jet Electropolisher Instruction Manual. Fischione Instrument Manufacturing, Pittsburgh, PA, 1988.

10. E. A. Fischione Instrument Manufacturing. Model 130 Digital Power Control, Product Brochure. E. A. Fischione Instrument Manufacturing, Pittsburgh PA, undated.

11. Fischer, R. and T. J. Drummond, J. Klem, W. Kopp, T. S. Henderson, D. Perrachione, and H. Morkoc. "On the Collapse of Drain I-V Characteristics in Modulation-Doped FET's an Cryogenic Temperatures," IEEE Transactions on Electron Devices. ED-31: 1028-1032 (August 1984).

12. Fontana, M. G. and N. D. Greene. Corrosion Engineering. New York: McGraw-Hill, 1967.

13. Gannon, J. J. and C. J. Nuese. "A Chemical Etchant for the Selective Removal of GaAs Through SiO_2 Masks," Journal of the Electrochemical Society. 121: 1215-1219 (September 1974).

14. Gerasimov, YA., Ed. (Translated by G. Leib). Physical Chemistry. Moscow, USSR: Mir Publishers, 1974.

15. Ghandhi, S. K. VLSI Fabrication Principles Silicon and Gallium Arsenide. New York: John Wiley & Sons, 1983.

16. Glasser, L. A. and D. W. Dobberpuhl. The Design and Analysis of VLSI Circuits. Reading, Massachusetts: Addison-Wesley Publishing, 1985.

17. Harrang, J. P. and R. H. Hendel, M. S. R. Heynes, R. Dingle, and H. S. Fuji. Patterning of GaAs and AlGaAs Ultra Submicron Device Structures - Phase I, August 1986 to May 1987. SBIR Contract DAAL01-86-C-0032. Somerville, NJ: GAIN Electronics Corporation, June 1987.

18. Hewlett Packard. Operating and Service Manual with P1 - Time Interval Unit 5262A. Hewlett Packard Company, Santa Clara, CA, September 1972.

19. Hewlett Packard. Operating and Service Manual 5248M. Hewlett Packard Company, Santa Clara, CA, April 1973.

20. Iida, H. and K. Ito. "Selective Etching of Gallium Arsenide Crystals in H_2SO_4 - H_2O_2 - H_2O System," Journal of the Electrochemical Society. 118: 768-771 (May 1971).

21. Kenefick, K. "Selective Etching Characteristics of Peroxide/Ammonium-Hydroxide Solutions for $GaAs/Al_{0.16}Ga_{0.84}As$," Journal of the Electrochemical Society. 129: 2380-2382 (October 1982).

22. Ketterson, A. A. and W. T. Masselink, J. S. Gedymin, J. Klem, C. Peng, W. F. Kopp, H. Morkoc, K. R. Gleason. "Characterization of InGaAs/AlGaAs Pseudomorphic Modulation-Doped Field-Effect Transistors," IEEE Transactions on Electron Devices. ED-33: 564-570 (May 1986).

23. Kittle, C. Introduction to Solid State Physics. New York: John Wiley & Sons, 1986.

24. Klem, J. and W. T. Masselink, D. Arnold, R. Fischer, T. J. Drummond, H. Morkoc. "Persistent Photoconductivity in (Al,Ga)AS/GaAs Modulation Doped Structures: Dependence on Structure and Growth Temperature," Journal of Applied Physics. 54: 5214-5217 (September 1983).

25. Kohn, E. "A Correlation Between Etch Characteristics of GaAs Etch Solutions Containing H_2O_2 and Surface Film Characteristics," Journal of the Electrochemical Society. 127: 505-508 (February 1980).

26. Lee, K. and M. S. Shur, T. J. Drummond, H. Morkoc, "Parasitic MESFET in (Al,Ga)As/GaAs Modulation Doped FET's and MODFET Characterization," IEEE Transaction on Electron Devices. ED-31: 29-35 (January 1984).

27. LePore, J. J. "An Improved Technique for Selective Etching of GaAs and $Ga_{1-x}Al_xAs$," Journal of Applied Physics. 51: 6441-6442 (December 1980).

28. Logan, R. A. and F. K. Reinhart. "Optical Waveguides in GaAs-AlGaAs Epitaxial Layers," Journal of Applied Physics. 44: 4172-4176 (September 1973).

29. Lott, J. A. Characterization of Enhanced Schottky-Barrier $InGaAs/Al_xGa_{1-x}As$ Strained Channel Modulation-Doped Field-Effect Transistors. MS Thesis, AFIT/GE/ENG/87D-38. School of Engineering, Air Force Institute of Technology (AU), Wright-Patterson AFB OH, December 1987.

30. McLaughlin, T. E. Fabrication of AlGaAs/InGaAs Pseudomorphic Modulation Doped Field-Effect Transistors with p-Doped Surface Layers. MS Thesis, AFIT/GE/ENG/86D-11. School of Engineering, Air Force Institute of Technology (AU), Wright-Patterson AFB OH, December 1986.

31. Mori, Y. and N. Watanabe. "A New Etching Solution System, H_3PO_4 - H_2O_2 - H_2O, for GaAs and Its Kinetics," Journal of the Electrochemical Society. 125: 1510-1514 (September 1978).

32. Morkoc, H. and P. M. Solomon. "The HEMT: a Superfast Transistor," IEEE Spectrum. 21: 28-35 (February 1984).

33. Ohata, K. and H. Hida, H. Miyamoto "A Low Noise AlGaAs/GaAs FET with P$^+$-Gate and Selectively Doped Structure," IEEE/MTT-S International Microwave Symposium Digest. 434-436. IEEE Press, New York, 1984.

34. Omega Engineering, INC. Omega 1987 Complete pH and Conductivity Measurement Handbook and Encyclopedia. Omega Engineering, INC, Stamford, CT, 1987.

35. Orion Research Incorporated Laboratory Products Group. Ag/AgCl Glass pH Electrodes Instruction Manual. Orion Research Incorporated, Boston, MA, 1987.

36. Orion Research Incorporated Laboratory Products Group. SA 520 pH Meter Instruction Manual. Orion Research Incorporated, Boston, MA, 1986.

37. Priddy, K. L. and D. R. Kitchen, J. A. Grzyb, C. W. Litton, T. S. Henderson, C. Peng, W. F. Kopp, H. Morkoc. "Design of Enhanced Schottky-Barrier AlGaAs/GaAs MODFETs Using Highly Doped P$^+$ Surface Layers," IEEE Transactions On Electron Devices. ED-34: 175-180 (February 1987).

38. Priddy, K. L. Study and Analysis of AlGaAs/GaAs Modulation Doped Field-Effect Transistors Incorporating P-Type Schottky Gate Barriers. MS Thesis, AFIT/GEO/ENG/85D-1. School of Engineering, Air Force Institute of Technology (AU), Wright-Patterson AFB OH, December 1985.

39. Rosenbaum, E. J. Physical Chemistry. New York: Appleton-Century-Crofts, 1970.

40. Schoone, R. D. and E. A. Fischione. "Automatic Unit for Thinning Transmission Electron Microscopy Specimens of Metals," The Review of Scientific Instruments. 37: 1351-1353 (October 1966).

41. Shannon, J. M. " Control of Schottky Barrier Height Using Highly Doped Surface Layers," Solid-State Electronics. 19: 537-543 (1976).

42. Shockley, W. "The Path to the Conception of the Junction Transistor," IEEE Transaction on Electron Devices. ED-31: 1523-1546 (November 1984).

43. Soares, R., et.al, ed. Applications of GaAs MESFETS. Dedham MA: Artech House, 1983.

44. Solomon, P. M. and H. Morkoc. "Modulation-Doped GaAs/AlGaAs Heterojunction Field-Effect Transistors (MODFET's), Ultrahigh-Speed Device for Supercomputers," IEEE Transactions on Electron Devices. ED-31: 1015-1027 (August 1984).

45. Swanson, A. W. "First Commercial HEMT Challenges GaAs FETs," Microwaves & RF. 24: 107-118 (November 1985).

46. Swanson, A. W. "The Pseudomorphic HEMT," Microwaves & RF. 26: 139-150 (March 1987).

47. Sze, S. M. Physics of Semiconductor Devices (2nd Ed). New York: John Wiley & Sons, 1981.

48. Sze, S. M. Semiconductor Devices Physics and Technology. New York: John Wiley & Sons, 1985.

49. Tarui, Y. and Y. Komiya, Y. Harada. "Preferential Etching and Etched Profile of GaAs," Journal of the Electrochemical Society. 118: 118-122 (January 1971).

50. Techniques of Microphotography. Kodak Publication No. P-52. Eastman Kodak Company, Rochester N.Y., 1967.

51. Teiss, Bill, Engineer for Universal Energy Systems. Personal interview. Air Force Avionics Laboratory, Wright-Patterson Air Force Base, OH, 18 July 1988.

52. Universal Energy Systems. UES Project 207, Project Status Report, 1 February to 29 February 1988. Contract F33615-87-C-1510. Air Force Avionics Laboratory, Wright-Patterson Air Force Base, OH

53. Williams, R. E. Gallium Arsenide Processing Techniques. Dedham, MA: Artech House, 1984.

VITA

Captain Brett F. Mayhew ████████████████████████████████

██

████████████ He received a Bachelor of Science in Electrical Engineering and

his commission in the USAF from the United States Air Force Academy on 30

May 1984. His first assignment was to Aeronautical System Division, Wright-

Patterson Air Force Base where he worked in the F-16 System Program Office,

Engineering Directorate as a lead engineer for cockpit controls and displays.

Captain Mayhew entered the Air Force Institute of Technology May 1987 to obtain

a Master of Science in Electrical Engineering. ████████████████████████

		REPORT DOCUMENTATION PAGE			Form Approved OMB No. 0704-0188

1a. REPORT SECURITY CLASSIFICATION	1b. RESTRICTIVE MARKINGS
UNCLASSIFIED	

2a. SECURITY CLASSIFICATION AUTHORITY	3. DISTRIBUTION/AVAILABILITY OF REPORT
	Approved for public release;
2b. DECLASSIFICATION/DOWNGRADING SCHEDULE	distribution unlimited.

4. PERFORMING ORGANIZATION REPORT NUMBER(S)	5. MONITORING ORGANIZATION REPORT NUMBER(S)
AFIT/GE/ENG/88D-26	

6a. NAME OF PERFORMING ORGANIZATION	6b. OFFICE SYMBOL (If applicable)	7a. NAME OF MONITORING ORGANIZATION
School of Engineering	AFIT/ENG	

6c. ADDRESS (City, State, and ZIP Code)	7b. ADDRESS (City, State, and ZIP Code)
Air Force Institute of Technology Wright-Patterson AFB OH 45433-6583	

8a. NAME OF FUNDING/SPONSORING ORGANIZATION	8b. OFFICE SYMBOL (If applicable)	9. PROCUREMENT INSTRUMENT IDENTIFICATION NUMBER
Electronic Research Branch	AFWAL/AADR	

8c. ADDRESS (City, State, and ZIP Code)	10. SOURCE OF FUNDING NUMBERS			
Air Force Avionics Laboratory Wright-Patterson AFB, OH 45433	PROGRAM ELEMENT NO.	PROJECT NO.	TASK NO	WORK UNIT ACCESSION NO.

11. TITLE (Include Security Classification)

See Box 19

12. PERSONAL AUTHOR(S)
Brett F. Mayhew, B.S.E.E., Captain, USAF

13a. TYPE OF REPORT	13b. TIME COVERED		14. DATE OF REPORT (Year, Month, Day)	15. PAGE COUNT
MS Thesis	FROM _____	TO _____	1988 December	135

16. SUPPLEMENTARY NOTATION

17.	COSATI CODES		18. SUBJECT TERMS (Continue on reverse if necessary and identify by block number)
FIELD	GROUP	SUB-GROUP	Gallium Arsenide, Etching, Semiconductor
09	01		Devices, MODFET, (ES)MODFET

19. ABSTRACT (Continue on reverse if necessary and identify by block number)

Title: CHARACTERIZATION OF SEMICONDUCTOR DEVICE PROCESSING ETCHANT SOLUTIONS FOR GaAs AND p^+ GaAs LAYERS EMPLOYED IN $Al_xGa_{1-x}As$/GaAs MODFETS AND RELATED HETEROJUNCTION DEVICES

Thesis Chairman: Donald R. Kitchen, Major, USAF
Instructor of Electrical Engineering

20. DISTRIBUTION/AVAILABILITY OF ABSTRACT	21. ABSTRACT SECURITY CLASSIFICATION
☐ UNCLASSIFIED/UNLIMITED ☒ SAME AS RPT. ☐ DTIC USERS	UNCLASSIFIED

22a. NAME OF RESPONSIBLE INDIVIDUAL	22b. TELEPHONE (Include Area Code)	22c. OFFICE SYMBOL
Donald R. Kitchen, Major, USAF	(513) 255-3576	AFIT/ENG

DD Form 1473, JUN 86   Previous editions are obsolete.   SECURITY CLASSIFICATION OF THIS PAGE

BLOCK 19:

The purpose of this study was to characterize the etch rate of p^+ GaAs, GaAs, $Al_xGa_{1-x}As$ and $n\text{-}Al_xGa_{1-x}As$ in order to fine a suitable etchant for the last step of the fabrication process of an (ES)MODFET (i.e., removal of the p^+ GaAs layer between the gate-and-drain and the gate-and-source). The effects of solution composition and pH on the etch rates of GaAs, p^+ GaAs, $n\text{-}Al_xGa_{1-x}As$, and $Al_xGa_{1-x}As$ (for $x = 0.30$ and $x = 0.15$) were investigated. Three different techniques were used to measure the etch rates of the material. The first technique used was based upon established procedures for determining the bulk corrosion rates of metals. This technique was applied to etching semiconductor materials. The second method was a variation of a technique used for thinning metals in transmission electron microscopy. It was also applied to etching the semiconductor materials. The third technique, step height measurement with a Sloan Dektak profilometer, was used to verify the results of the first two methods.

The corrosion method of etching gave etch rates as predicted from the literature. For a solution of $NH_4OH:H_2O_2:H_2O$ (20:7:973 by volume) an average etch rate of 16 Å/sec (or 0.10 μm/min) for an (100) GaAs substrate material was measured. This data compares favorable with the published result of 0.12 μm/min (or 20 Å/sec) for (100) GaAs. The Fischione Electropolisher produced an etch rate of 72 Å/sec for a solution composition of $NH_4OH:H_2O_2$ (1:200 by volume); and an etch rate of 17 Å/sec for the $NH_4OH:H_2O_2:H_2O$ (20:7:973 by volume). The Dektak profilometer measured etch rates for the $Al_xGa_{1-x}As$ ($x = 0.15$ and 0.30). For a solution of $NH_4OH:H_2O_2:H_2O$ (1:1:100 by volume) the etch rate for $Al_{0.15}Ga_{0.85}As$ and $Al_{0.3}Ga_{0.7}As$ was 23 Å/sec and 16 Å/sec, respectively. The etch rate for p^+ GaAs in $NH_4OH:H_2O_2$ (1:100 by volume) was 68 Å/sec, approximately 30 times faster than the etch rate for $Al_{0.3}Ga_{0.7}As$ in $NH_4OH:H_2O_2$ (1:100 by volume). This etchant displays the characteristics required for the final fabrication step of an (ES)MODFET.